E949 Technical Note K-073

Analysis of the 1/3 E949 pnn2 data

Joss Ives, Benji Lewis, Dmitri Patalakha,
Zhe Wang, David E. Jaffe, Ilektra Christidi

November 21, 2007

Abstract

The pnn2 analysis of the 1/3 data sample for the E949 exposure of 1.7×10^{12} stopped kaons is described. The signal region has been expanded with respect to the previous pnn2 analyses and divided into nine cells with differing signal-to-background to permit a likelihood-based analysis. The single-event sensitivity and background of the entire signal region is $(0.432 \pm 0.015^{+0.046}_{-0.046}) \times 10^{-9}$ and $0.966 \pm 0.220^{+0.309}_{-0.246}$, respectively, and is $(1.325 \pm 0.389^{+0.141}_{-0.143}) \times 10^{-9}$ and $0.174 \pm 0.068^{+0.152}_{-0.035}$, respectively, in the cleanest cell. Potential observations of 0, 1 or 2 candidates distributed within the signal region have been evaluated and it is expected that the results of this analysis will produce a modest improvement ($\sim$10%) in the precision of the combined E787+E949 measurement of the $K^+ \to \pi^+ \nu \bar{\nu}$ branching fraction.

Contents

List of Figures

List of Tables

Background Component	Entire "Loose"	Cleanest cell "Tight"
$K_{\pi 2}$TT scatter	$0.575 \pm 0.184^{+0.063}_{-0.201}$	$0.115 \pm 0.058^{+0.039}_{-0.022}$
$K_{\pi 2}$RS scatter	-0.0070 ± 0.0042	-0.0031 ± 0.0018
$K_{\pi 2\gamma}$	$0.0500 \pm 0.0084 \pm 0.0030$	$0.013 \pm 0.004 \pm 0.001$
K_{e4}	$0.176 \pm 0.102^{+0.233}_{-0.124}$	$0.034 \pm 0.034^{+0.142}_{-0.026}$
CEX	$0.092 \pm 0.053^{+0.070}_{-0.018}$	$0.0046 \pm 0.0046^{+0.0046}_{-0.0015}$
Muon	0.0281 ± 0.0281	0.00374 ± 0.00374
Two-beam	0.0438 ± 0.0200	0.00317 ± 0.00317
One-beam	0.00157 ± 0.00157	0.00035 ± 0.00035
Total Background	$0.966 \pm 0.220^{+0.309}_{-0.246}$	$0.174 \pm 0.068^{+0.152}_{-0.035}$
Total Acceptance	$(1.841 \pm 0.065^{+0.194}_{-0.194}) \times 10^{-3}$	$(0.600 \pm 0.176^{+0.063}_{-0.064}) \times 10^{-3}$
Single-event sensitivity	$(0.432 \pm 0.015^{+0.046}_{-0.046}) \times 10^{-9}$	$(1.325 \pm 0.389^{+0.141}_{-0.143}) \times 10^{-9}$

Table 1: The estimated backgrounds for the entire signal region, referred to as "loose" elsewhere in the text, and the cleanest cell, referred to as "tight", to be used in the analysis. The first error is the statistical uncertainty; the second error (when present) is the estimated systematic uncertainty. The systematic uncertainties for the K_{e4} and CEX backgrounds are assumed to be fully correlated. The cleanest cell corresponds to the tight settings of the KIN, TD, PV and DELCO cuts. The background due to $K_{\pi 2}$RS scatters is assumed to be negligible and not included in the totals. The bottom rows contains the total acceptance and single event sensitivity of the two regions. The acceptance given in the table does not include the additional factors of $f_S = 0.7740 \pm 0.0011$ and $\epsilon_{T\bullet 2} = 0.9505 \pm 0.0012 \pm 0.0143$.

1 Executive Summary

The E949 pnn2 analysis on the 2002 data benefits from the previous successful analyses of the E787 data [1],[2], the upgrades to the E949 detector and improvements to E949 pnn1 analysis. As a consequence, the size of the E949 pnn2 signal region has been increased and the differential signal acceptance and background rejection within the signal region will be utilized in a likelihood analysis. The total kaon exposure was $KB_{live} = 1.7096 \times 10^{12}$ and is approximately equal to the total exposure of the 1996 [1] and 1997 [2] pnn2 analyses. The results for the background, acceptance and single-event sensitivity are summarized in Table 1 for the entire signal region and the cleanest region within the signal region.

The signal region has been divided into 9 cells with relative signal-to-background varying by $\sim$5. The division is accomplished by variation of four separate cuts:

1. KIN - The limits of the kinematic region are reduced to suppress K_{e4} and $K_{\pi 2}$ background.

2. TD - The requirement on the identification of the $\mu \to e$ decay is removed and the $\pi \to \mu$ identification requirements are loosened with respect to the E949 pnn1 analysis.

3. PV - The photon veto is tightened.

4. DELCO - The delayed coincidence is tightened from 3 ns to 6 ns.

We use the Junk method [3] employed by previous pnn1 analyses to exploit the statistical power of the analysis. All scenarios of potential observations of the 0, 1 or 2 signal candidates have been evaluated with the Junk method using the estimated background in all the cells. For most of the likely outcomes, there is a modest improvement in the precision of $\mathcal{B}(K^+ \to \pi^+\nu\bar{\nu})$ of $\sim 10\%$ when the potential results of this analysis are combined with the previous pnn1 and pnn2 analyses of E787 and E949.

This note is organized as follows. Section 2 briefly describes the philosophy of the note. Sections 3, 4, 5, 6 and 7 describe the improvements and changes to the photon veto, TD, kinematic, delayed coincidence and target cuts, respectively. The skim definitions are provided in Section 8. The estimation of the $K_{\pi2}$-scatter, $K_{\pi2\gamma}$, beam, muon, charge exchange (CEX) and K_{e4} backgrounds are described in Sections 9, 10, 11, 12, 13 and 14, respectively. Section 15 describes the acceptance measuremnts and Section 16 contains the description of the kaon exposure. The investigation of flaws and loopholes with a single-cut-failure study is described in Section 17. The sensitivity of the analysis is evaluated in Section 18 and check on the acceptance via a measurement of the $K_{\pi2}$ branching fraction is described in Section 19.

2 Philosophy

Many cuts tuned and improved by the E949 pnn1 analysis are used in this analysis. In addition cuts devised for the E787 pnn2 analyses, but not required by pnn1, are also used in this analysis. The general philosophy of this note is to only describe cuts or calculations that have been changed from the E949 pnn1 analysis as described in E949 Technotes K-034 [4] and K-038 [5] or the E787 pnn2 analysis described in E787 TN-385, TN-386 [1] or B.Bhuyan's thesis [2].

2.1 Target CCD Fitter

The target CCD fitter received some modifications and bug fixes since its implementation in the E787 PNN2 analysis.
The rest of this section describes and discusses the modifications and fixes that were made. The bug fixes were for the following bugs:

- The fitter was using the raw energy of the pulse as opposed to the normalized energy of the pulse calculated within the fitting routine.
- The flag indicating a saturated pulse was not set properly.

The modifications to the way the fitter functions are summarized as follows:

- Bins with zero counts that were adjacent to bins containing greater than zero counts were included in the minimization of the fit where they were previously excluded.
- The errors associated with the first bin and with bins containing less than ten counts were increased to de-weight these bins in the fit.

- Hold and release fitting for the double-pulse fits. The four-parameter double-pulse fit was changed from a one-stage fit to a two-stage fit. In the first stage, the time for the first pulse was fixed at the time found in the single-pulse fit while the other three parameters were allowed to wander. In the second stage, the values from these three parameters were used as initial guesses and all four parameters were allowed to wander.

- The maximum number of target fibers that were fit was increased to 31 from 15.

2.1.1 Optimizing the fitter

A sample of km2 monitors was used for optimizing the target fitter. For the sample, the following cuts were applied as setup cuts: TGQUALT, DELC, NPITG, TARGET, TGCUT, UTC, RD_TRK, TRKTIM, RDUTM. This left approximately 50,000 events to which CCDBADFIT, CCDPUL and EPIONK were applied. The resulting acceptances of these cuts are shown in Table 2 before applying the following fixes:

Low-Count Error Fix

The errors associated with a specific channel in the fitter having a number of counts N from the E787 PNN2 analysis was given as

- High-gain: Error $= 0.74 + 0.69 \times \sqrt{N}$

- Low-gain: Error $= 1.21 + 0.35 \times \sqrt{N}$

For counts (N) below 10, this function was found to underestimate the error as shown in Figure 1. This was fixed by applying the error corresponding to $N = 10$ counts for all channels having 10 or less counts.

First Bin Error Fix

It was found that for a given pedestal-subtracted pulse that the fit is very sensitive to the first bin. The fitting starts on the first non-zero pulse-height bin and a very low number of counts (such as 1 or 2) counts in this first bin tends to give a very large contribution to the chi-squared of the fit. As shown in Figure 2, a reasonable looking fit can have a large chi-squared contribution due to the first bin. This contribution is reduced by doubling the error associated with the first bin.

Intermediate zero count bins included in the fit

The previous (E787 PNN2) fitter did not include intermediate bins having zero counts in the fit. This was changed so that the fitter first identifies the first and last bins of the pulse are first identified. Then up to the first 30 bins of this pulse are fit with bins having zero counts included. Bins which have been identified as saturated are not included in the fit.

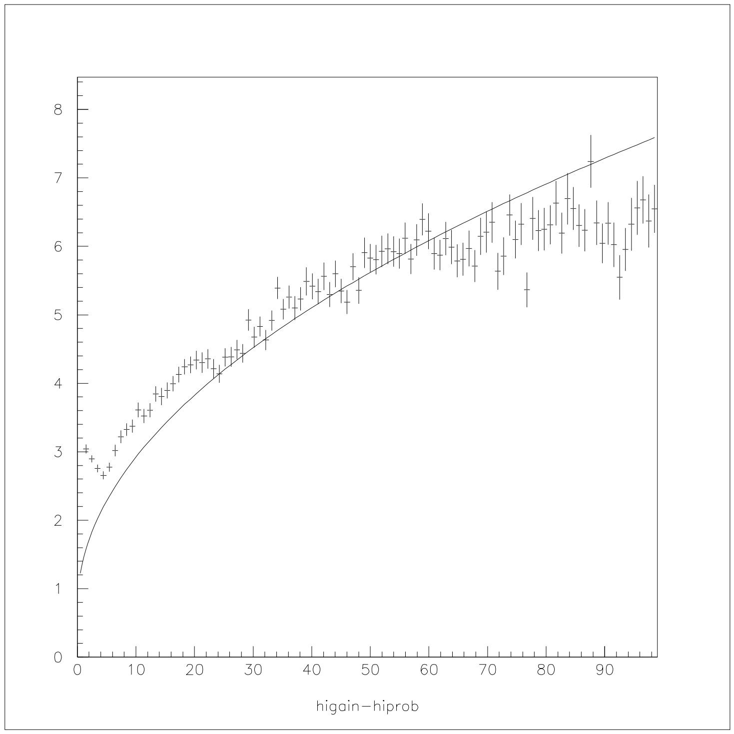

Figure 1: This plot shows the results of leaving the second bin out of the fitter and comparing the actual counts in that bin to those predicted by the fit. The x-axis shows the number of counts in that second bin. The y-axis shows $predicted - counts$ for only positive values of this quantity. The line shows the error for each bin from the equation $0.74 + 0.69 \times \sqrt{\text{counts}}$. For different bins, the turn-up occuring in the data below 5 counts typically occured in the first 5 to 10 bins. Based on these observations, the error applied to all bins having less than 10 counts was fixed at the error associated with 10 counts.

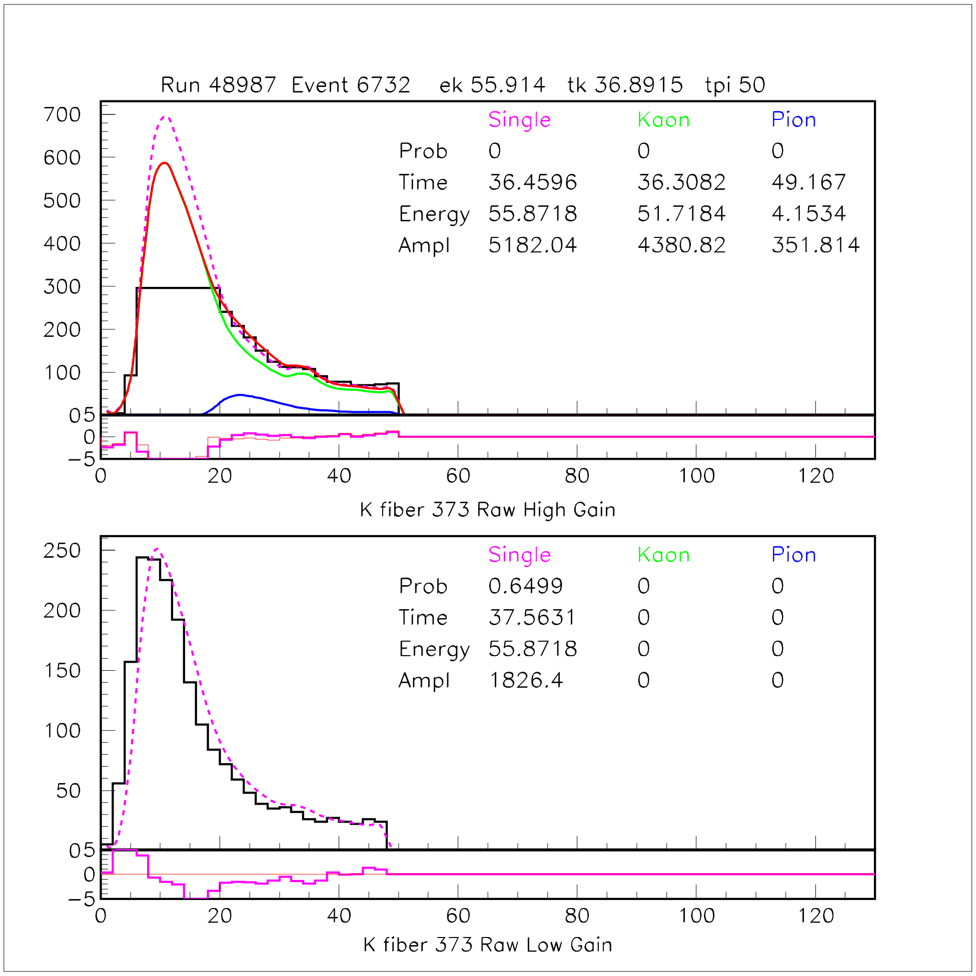

Figure 2: The high-gain single-pulse probability of 0 when the error associated with this bin is treated as usual. This is due to the first bin having only two counts versus the shape of the reference pulse predicting a larger number of counts. Had this bin had a pedestal subtraction that left it with zero counts, the next bin would have been used for the fit and the resulting fit would have been a non-zero probability. To reduce the effect of this sensitivity to the first bin, the errors assigned to the first bin are always doubled. When the fit is performed with this increased first bin error, the single-fit probability for the high-gain is 0.069 instead of the zero probability shown in this figure.

Acceptances for Target Fitter Fixes			
Fix to the fitter	CCDBADFIT	CCDPUL	ALL
No fixes	0.797	0.454	0.362
First bin and low-count error fixes	0.876	0.518	0.453
First bin and low-count error fixes + 0-count bins included	0.881	0.504	0.443

Table 2: The sample used to optimize the target fitter was km2 monitors with the following cuts applied as setup cuts: TGQUALT, DELC, NPITG, TARGET, TGCUT, UTC, RD_TRK, TRKTIM, RDUTM. After these setup cuts have been applied, approximately 50,000 events remained to which CCDBADFIT, CCDPUL and EPIONK were applied. The ALL column shows the combined acceptance of the set of cuts consisting of CCDBADFIT, CCDPUL and EPIONK applied sequentially. The acceptance of the EPIONK cut is 0.999 for all 3 situations so it was not given a column in the table. The row "First bin and low-count error fixes" includes both the first bin error fix (doubling the error for this bin) and the low-count error fix (assigning an error equal to that for 10 counts for all bins having less than 10 counts). The row "First bin and low-count error fixes + 0-count bins included" includes the above fixes in addition to the fix which includes intermediate zero count bins in the fit.

2.1.2 Hold and Release Double-Pulse Fit

The fitter was updated so that the double-pulse fit is a two-stage process. For the first stage of the double-pulse fit process, the first-pulse time is fixed at the time returned from the single-pulse fit. The three other parameters (first-pulse amplitude, second-pulse time and second-pulse time) are allowed to wander in the fit. For the second stage of the double-pulse fit, the values returned from the first stage of the double-pulse fit are used as the guesses.

The sample used to optimize this modification to the fitter was km2 monitors with the following cuts applied: TARGET, TGCUT, UTC, RD_TRK, TRKTIM, RDUTM, TGQUALT, DELC and NPITG. After these cuts were applied, 7021 events remained. With the two-stage fit used instead of the previous one-stage fit the total acceptance of CCDBADFIT and CCDPUL went from 0.402 to 0.451.

3 Photon veto cuts

PVCUTPNN2 removes events with photon activity at track time, t_{RS}, by searching all systems with the ability to detect photons for hits coincident with the track time, but not associated with the charged track. The time window and energy threshold for each category are shown in Table 3. BV, BVL, and RS hits are subdivided based upon the quality of the information from the hit. The acceptance of PVCUTPNN2 is 0.6391 ± 0.0022 as measured by $K_{\mu 2}$ monitor triggers. The tight parameters yield an acceptance of 0.3585 ± 0.0024. Acceptances of the individual photon-detector cuts are listed in Table 47. Acceptance values of 30% and 60% were chosen during cut optimization to give appropriate levels of signal to background in the tight and loose signal region.

3.1 New photon veto cuts

The pnn2 photon veto differs from the E949 pnn1 photon veto in the use of the active degrader (AD), downstream photon veto (DSPV), early BV cut, and the use of TD information to supplement the TDC information for the BVL. In addition, a safety cut, $\mathrm{EARLY_{BVL}}$, described in Sec. 17 and designed to remove events where both photons from π^0 decay in $K_{\pi 2}$ events strike a single BVL counter [6] was added. The precise impact of the use of TD information to supplement the TDC information for the BVL was not evaluated, but we note that it has the potential to move single-ended hits to the more reliable double-ended hit category.

3.1.1 AD photon veto

The active degrader (AD) is a cylindrical, copper-scintillator sandwich-style detector divided into 12 azimuthal sectors [7]. Each sector is equipped with a CCD, TDC and multiplexed into ADCs. The CCDs were used for the PV. The AD was added to improve the PV rejection in the beam region, among other reasons. Extensive studies [8] showed activity coincident with TRS in sectors not traversed by the incident kaon in samples of events enhanced in $K_{\pi 2}$ target scatters identified by "kinks" in the pion trajectory in

Category			60% (Loose)			30% (Tight)		
			Timing (ns)		Energy	Timing (ns)		Energy
			offset	window	(MeV)	offset	window	(MeV)
BV			2.25	7.95	0.20	1.35	8.85	0.70
early BV			-20.70	15.0	30.00	-22.5	15.0	30.0
BVL			3.15	7.55	0.30	3.15	7.55	0.30
RS			0.05	4.30	0.30	2.25	5.55	0.60
EC			1.80	6.15	0.40	1.75	7.75	0.20
EC inner-ring			0.99	4.64	0.20	-2.45	11.55	0.20
EC 2^{nd} pulse			-1.60	4.07	10.60	-1.51	4.19	1.70
TG			-0.25	2.40	2.00	-2.15	4.40	1.40
IC			1.25	3.25	5.00	3.20	6.10	5.00
VC			-2.40	4.15	6.80	-0.20	7.25	6.00
CO			2.90	2.95	0.60	2.15	2.95	1.60
μCO			-1.60	3.90	3.00	-0.60	3.90	0.60
AD			3.00	5.00	0.60	3.00	5.00	0.60
DSPV			2.50	7.50	0.00	2.50	7.50	0.00
$\mathrm{EARLY}_{\mathrm{BVL}}$			3.50	1.50	10.00	3.50	1.50	10.00
Single-end hit categories								
	hit-ends							
	energy	time						
BV	both	single	3.05	15.95	1.00	0.55	13.05	0.40
BV	single	both	4.80	1.50	1.40	4.00	3.10	0.60
BV	single	single	-8.10	8.50	1.60	-8.30	6.90	1.00
BVL	both	single	-5.65	11.80	8.19	-5.65	11.80	8.19
RS	both	single	-2.85	0.70	5.20	0.01	5.36	0.20
RS	single	both	6.60	1.35	0.00	3.70	6.10	0.00
RS	single	single	-6.80	1.22	3.40	-11.54	4.53	0.60

Table 3: 30% and 60% photon cut parameters. The time window is shown in ns and energy threshold in MeV. The BV, BVL, and RS photon cuts require both ends of the detector obtain a result for time and energy. Additional photon cuts are applied when the both-ends requirement in time and energy are not met. *single* refers to a hit in only one end of the detector observed in either *energy* or *time*. *both* means both ends were hit and *no* means a hit was not observed in either end. $|t - t_{RS} - t_{offset}| < t_{window}$ is defined as in coincidence for hit time t.

the target. The cut requires activity within $-2, +8$ ns of TRS and more than 5 ns from TK (to exclude activity from the incident kaon). A rejection in the "kink" sample of 1.95 ± 0.08 was obtained with an acceptance loss of 0.95.

3.1.2 Early BV photon veto cut

The presence of > 30 MeV of energy in the BV due to early accidentals could blind the BV to hits coincident with TRS. Such events were vetoed with little loss of acceptance [8] (Table 47).

3.1.3 Downstream photon veto

The downstream photon veto (DSPV) is a square, lead-scintillator sandwich-style detector with $\sim$7.3 radiation lengths at normal incidence located downstream of the target PMTs along the kaon beam direction [9]. Using the classes defined for the evaluating the PV rejection of $K_{\pi 2}$ target scatters (Table 17), a rejection of 1.125 (18/16) was measured based on any DSPV activity within $-5, +10$ ns of TRS with an acceptance of 0.9999 (20881/20883) [10].

3.2 PV optimization

As performed by Ilektra, discussed in [8] and described in Ref. [4].

4 TDcuts

A study was performed to determine possible acceptance gains from removing EV5 (electron finding) and loosening TDNN ($\pi^+ \rightarrow \mu^+ \rightarrow e^+$ neural-net). The effects on the total background and total acceptance was optimized to give the best performance; muon background was measured directly, while other backgrounds were assumed to scale with increased acceptance based upon background values as reported in [8].

Other TD cuts remained unchanged since E949-PNN1 analysis.

4.1 Electron Finding (EV5)

The cut EV5 was scrutinized to determine if it is possible to remove it from the E949 offline cut-list, to gain the observed 17% acceptance loss.

To determine the effect EV5 has on the muon background, the muon background was measured with and without EV5. Table 4 shows the effect of EV5 on the TD rejection. Table 5 shows the effect of EV5 on the muon background. Note that the muon tail for the PNN2 energy-range box is very high due to limited statistics in rejection measurement. The total muon background is the sum of the muon-band plus the muon-tail measurements.

The acceptance of EV5, when applied last, is 0.83. When EV5 is removed, a gain of 17% acceptance with an increase of the muon background by a factor of 2.0 is observed. The total background will be 0.0260 ± 0.0260 (band+tail) when EV5 is not applied which

Rej & Norm Measurement	with EV5	without EV5
Band All Rejection	357.89 ± 119.13	140.04 ± 29.10
Band ERbox Rejection	423.00 ± 422.50	211.50 ± 149.20
Tail All Rejection	679.00 ± 678.50	679.00 ± 678.50
Tail ERbox Rejection	9.00 ± 8.49	9.00 ± 8.49
Muon Normalization	1.0 ± 1.0	1.0 ± 1.0

Table 4: Rejection and Normalization Summary. Band refers to applying $\overline{RNGMOM}$ to the sample and Tail refers to applying $ptot > 229.$, which will tag the muon-band and muon-tail sample respectively. All (ERbox) refer to applying all setup cuts (all setup cuts plus the PNN2 energy range cut).

Background	with EV5	without EV5
Band All	0.00841 ± 0.00841	0.0216 ± 0.0216
Band ERbox	0.00711 ± 0.00711	0.0143 ± 0.0143
Tail All	0.00442 ± 0.00442	0.00442 ± 0.00442
Tail ERbox	0.37500 ± 0.37500	0.3750 ± 0.3750

Table 5: Muon background summary, scaled to the 3/3 sample. Band refers to applying $\overline{RNGMOM}$ to the sample and Tail refers to applying $ptot > 229$ MeV/c, which will tag the muon-band and muon-tail sample, respectively. All (ERbox) refer to applying all setup cuts (all setup cuts plus the PNN2 energy range cut).

is much less than the expected background from TG-scatters of 0.5 events (at the time of this optimization study).

4.2 TD Neural-Net Cut

TD neural-net cut (TDNN), cuts on one parameter. Therefore, loosening was very easily accomplished. The initial cut parameter is 0.76, set in E949-PNN1 analysis. This parameter was varied from 0.05 to 0.8 in 0.05 increments (16 total values) in an attempt to determine the optimal value for PNN2 analysis. The effects of including and excluding EV5 was done in tandem when optimizing TDNN. In Figures 3-6 black (red) points included (omitted) EV5 in the measurement. Figure 3 shows muon background as a function of the TDNN cut value. Figure 4 shows muon background as a function of *acceptance*.

The acceptances were measured in the Piscat TD acceptance measurement as in Section 15.2 applying TDNN last in the measurement order. The muon-band background was measured by inverting RNGMOM and the muon-tail background was measured by requiring $ptot > 229MeV$. At the time this study was performed it was not known if the muon-tail background would be negligible. Therefore, the muon background in this optimization study included band and tail measurements. There was one event remaining in the normalization branch using the nominal TDNN(0.76) cut; the normalization branch was not measured for the TDNN parameter variations to prevent determining possible location of events within the box. Table 6 lists the background and acceptance values for all TD cut parameter values that were analyzed.

The optimal level for the TDNN's cut parameter can be determined by finding the maximum for the ratio of total acceptance to total background. We assume that all other backgrounds will increase with increased acceptance. All backgrounds (except muon) were measured with EV5 and TDNN(0.76) applied. These backgrounds were scaled with the expected acceptance gain when EV5 and TDNN are loosened. Total background (N_{bkg}) is $\frac{new\ Accept}{orig\ Accept} \times N^*_{bkg} + N_{muon}$. N^*_{bkg} is all backgrounds not including muon background as measured in Ref. [8] and scales directly with acceptance gain. *new Accept* is the acceptance after the changes in TDNN and EV5 and *orig Accept* is the value of the acceptance as measured with the original E949-PNN1 cut levels [4].

Acceptance is normalized to 1.0 when defined as the total acceptance with the TDNN cut parameter being 0.76 and EV5 cut applied (along with all other cuts). The results are plotted in Figure 5. The maximum for the ratio of total acceptance to total background occurs at the maximum tightness for TDNN. Sensitivity is lost at a greater rate starting at TDNN value of 0.3. The muon background at 0.3 is 0.0857 (a factor of 3.3 increase) and the TDNN acceptance increases to 0.9415 (9.6%).

4.3 Conclusions from TD Optimization

The increase in acceptance from loosening TDNN and EV5 was measured to be $\sim 23\%$ with a muon background at a value much smaller than other backgrounds. Not applying EV5 and dramatically loosing TDNN to a cut parameter of 0.3 is an satisfactory method of increasing acceptance since the muon background is very small and continues to be

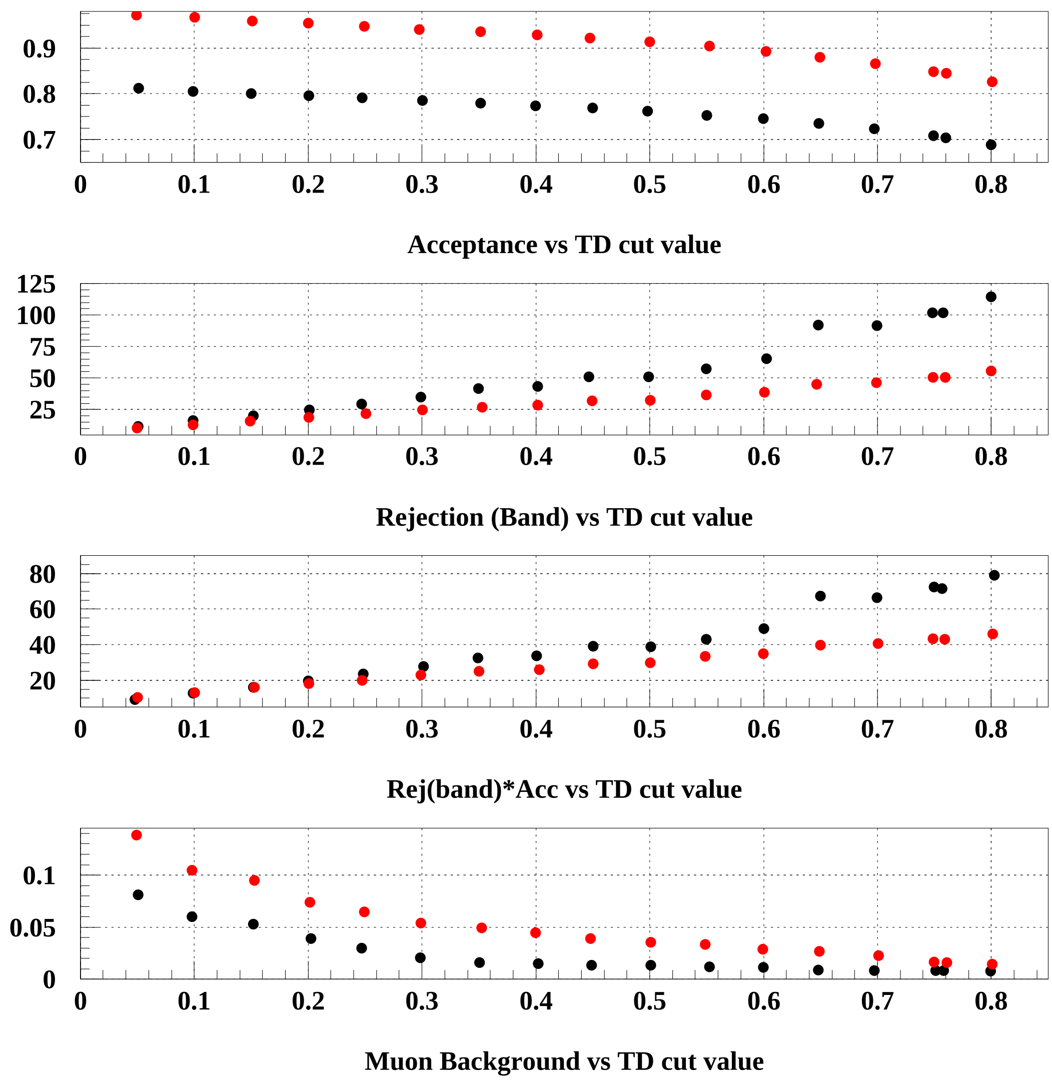

Figure 3: Acceptance, Rejection, and Rejection×Rejection versus TD cut parameter. Black points include EV5 in the calculation, red points have excluded EV5 from the analysis.

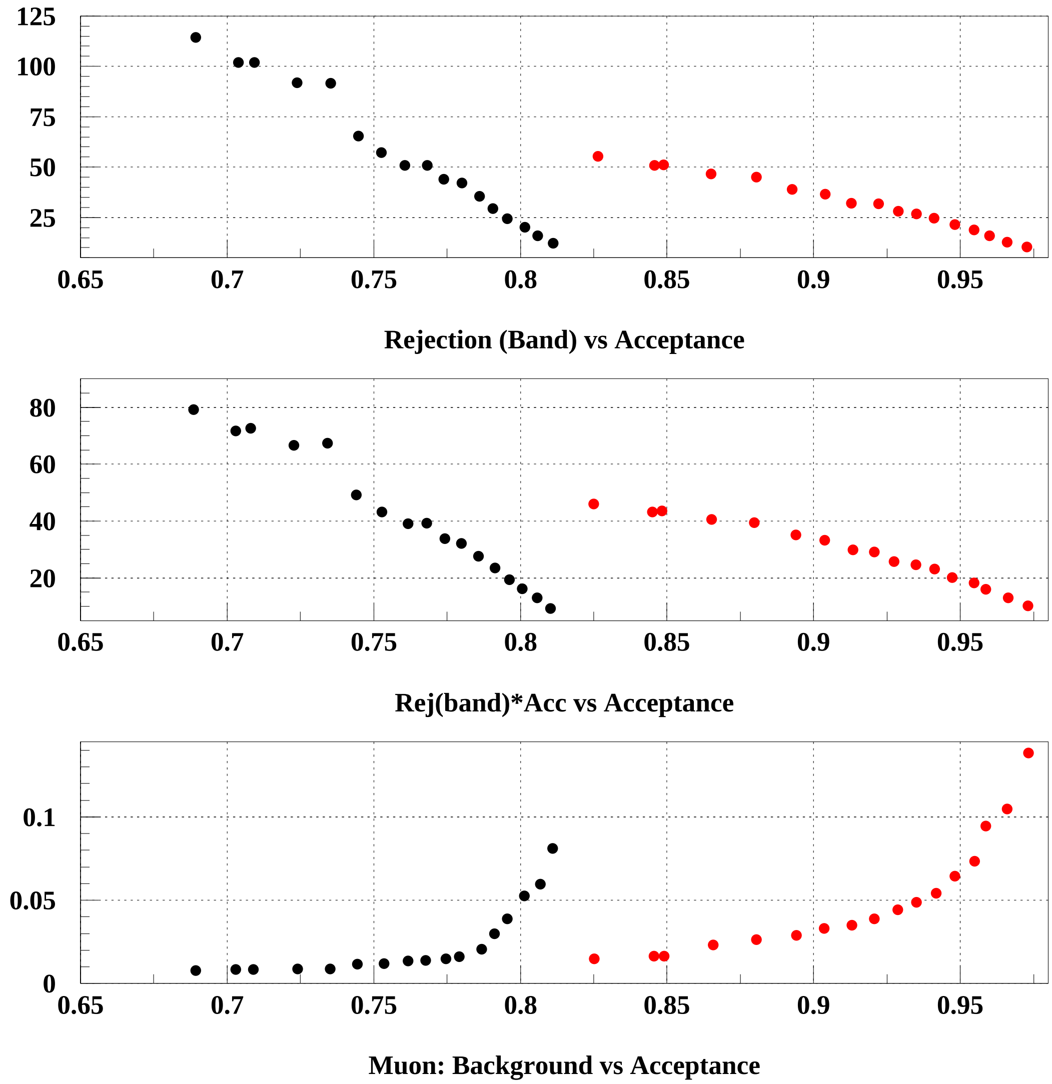

Figure 4: Rejection vs Acceptance with different TDNN cut parameter. Black points include EV5 in the calculation, red points have excluded EV5 from the analysis.

TD cut	with EV5			without EV5		
value	Accept	Band All	Tail All	Accept	Band All	Tail All
0.05	0.9740	0.0470	0.03409	0.9732	0.0689	0.0694
0.10	0.9675	0.0341	0.02545	0.9664	0.0532	0.0516
0.15	0.9612	0.0268	0.02545	0.9602	0.0433	0.0516
0.20	0.9549	0.0220	0.01689	0.9537	0.0366	0.0370
0.25	0.9490	0.0184	0.01123	0.9477	0.0329	0.0312
0.30	**0.9428**	**0.0154**	**0.00560**	**0.9415**	**0.0287**	**0.0255**
0.35	0.9366	0.0130	0.00279	0.9353	0.0262	0.0226
0.40	0.9300	0.0124	0.00279	0.9286	0.0250	0.0197
0.45	0.9224	0.0106	0.00279	0.9211	0.0220	0.0169
0.50	0.9144	0.0106	0.00279	0.9131	0.0214	0.0141
0.55	0.9050	0.00945	0.00279	0.9036	0.0190	0.0141
0.60	0.8939	0.00827	0.00279	0.8928	0.0178	0.0112
0.65	0.8820	0.00590	0.00279	0.8809	0.0154	0.0112
0.70	0.8676	0.00590	0.00279	0.8661	0.0148	0.0084
0.75	0.8511	0.00531	0.00279	0.8495	0.0136	0.00280
0.76	**0.8454**	**0.00531**	**0.00279**	–	**0.0136**	**0.00280**
0.80	0.8270	0.00472	0.00279	0.8253	0.0124	0.00280

Table 6: Muon background at different TD Neural-Net cut parameters. Value is using the 'All' Setup cuts, i.e. ERBox not applied. The bold 0.76 line is the TD cut parameter set at the PNN1 level. Error is 100% on all values, the normalization branch is 1 ± 1 with one event remaining. Any loosening of the TDNN will only reduce the normalization branch to zero, which for us will be the same as the nominal cut value. Scaled to the 3/3 sample.

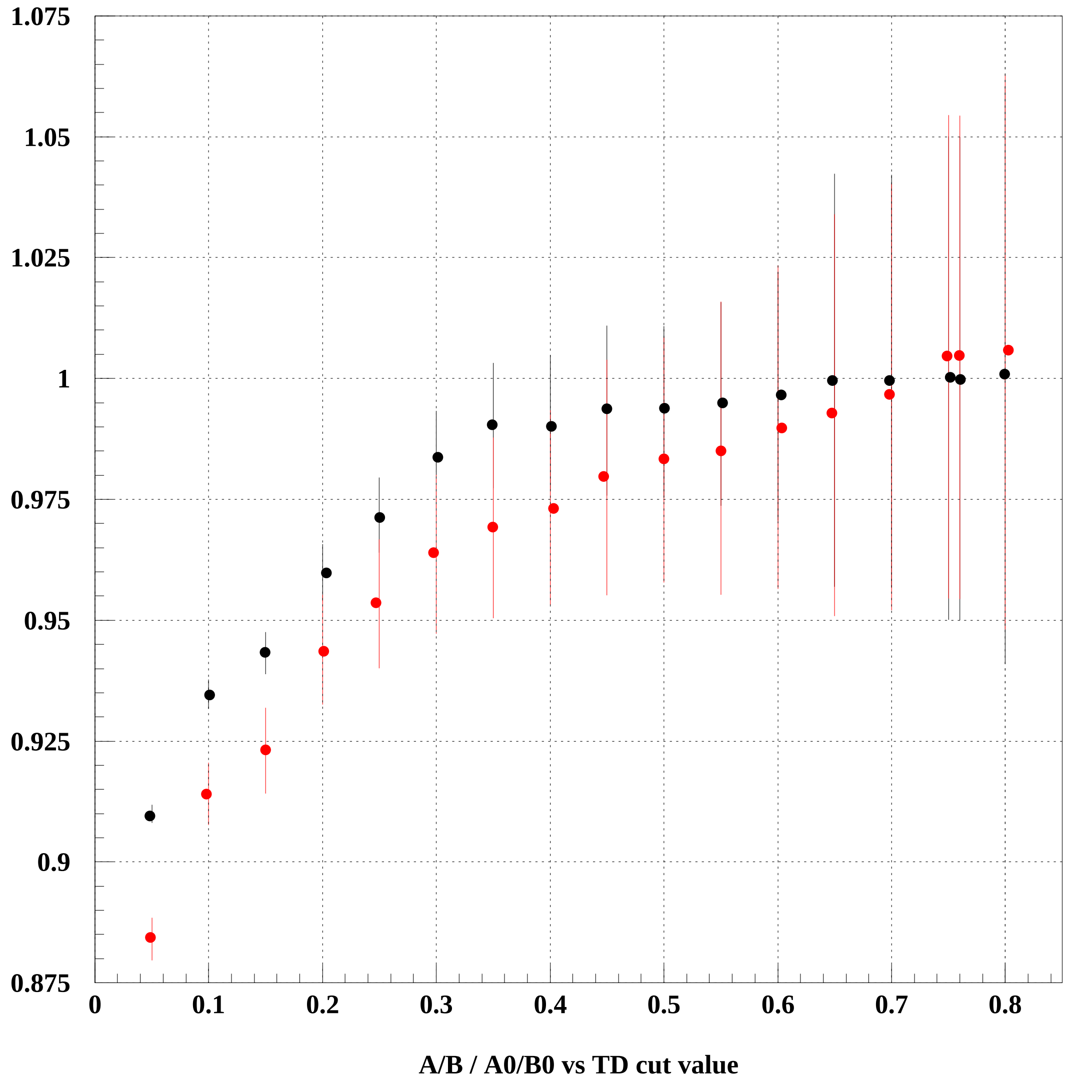

Figure 5: Total Acceptance/Total Background normalized by ratio of the original acceptance-background ratio (cut parameters of TDNN, EV5 at E949-PNN1) A_0/B_0 versus TD cut parameter. Black points include EV5 in the calculation, red points have excluded EV5 from the analysis. Acceptance is normalized to the total acceptance at the tight TD cuts (TDNN(pnn1) and EV5 applied). The total background is approximated from other background + muon background.

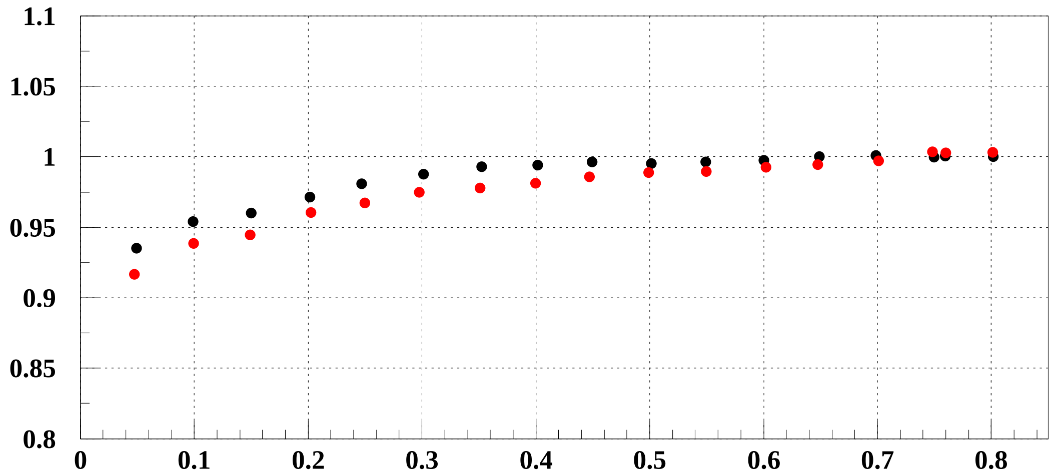

A/(B+1sig) / A0/(B0+1sig) vs TD cut value

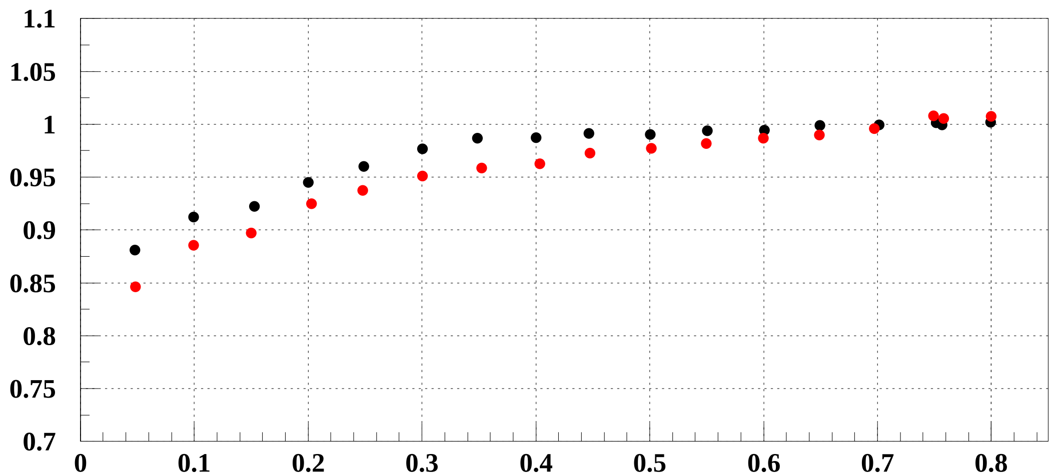

A/(B-1sig) / A0/(B0-1sig) vs TD cut value

Figure 6: Same as Figure 5 except the background value has been varied by 1 sigma. Black points include EV5 in the calculation, red points have excluded EV5 from the analysis. Acceptance is normalized to the total acceptance at the tight TD cuts (TDNN(pnn1) and EV5 applied). The total background is approximated from [8] + Muon Background. This assumes no dependence of the TD cuts on other background or acceptances.

Table 7: E787 and E949 pnn2 kinematic box definitions. The K_{e4}-phobic box is described in Sec. 5.2.

	E787	E949	K_{e4}-phobic box
PTOT (MeV/c)	(140, 195)	(140, 199)	(165, 197)
ETOT (MeV)	(60, 95)	(60, 100.5)	(72,100)
RTOT (cm)	(12, 27)	(12, 28)	(17,28)

much smaller than other background after the cuts were loosened. EV5 and the TDNN, set at the original 0.76, were used to define a much cleaner PNN2 signal region (tight box).

5 Kinematic cuts

5.1 Expand kinematic box

Pions from $K_{\pi 2}$ produce a monochromatic peak in momentum, energy and range. The nominal upper bounds of pnn2 signal box are $2.5 \times \sigma_p$ below the $K_{\pi 2}$ momentum peak, $2.5 \times \sigma_e$ below the energy peak and $2.75 \times \sigma_r$ below the range peak. We exploit the improvements in resolution in momentum, energy and range for E949 [4] to increase the size of the signal region. The definition of the kinematic box is tabulated in Tab. 7. More detailed information can be found in [11].

5.2 K_{e4}-phobic box

Additional kinematic cuts were created to define a low background region inside the "loose" kinematic box (Table 7). This kinematic is dubbed the "K_{e4}-phobic box" because the lower limits are specifically designed to kinematically exclude K_{e4} events. The details of the K_{e4} background study are in Sec. 14.

The momentum of π^+ of K_{e4} events peaks around 160 MeV/c. It is the second largest background of whole pnn2 analysis. Suppression of this background mainly relies on the CCDPUL and TGPV cuts. The CCDPUL cut is a very complicated cut, and the pulse fitting algorithm is not simulated in UMC. The existence of the π^- in the final state also complicates this background estimation. Both these factors contribute to the relative large systematic uncertainty assigned to the K_{e4} background estimate.

Fig. 7 presents the momentum distribution of K_{e4} normalization sample before CCDPUL cuts. It agrees pretty well with the analogous spectrum from the UMC sample (Fig. 8, the middle plot of the first row). A visual scan of the target fibers for the events in Fig. 7 confirms that is composed almost entirely of K_{e4} events. The K_{e4}-phobic box is designed to kinematically suppress K_{e4} background and also reduce the relative systematic uncertainty, so that the likelihood-based pnn2 analysis will contain cells with small and relatively well-determined background.

The $K_{\pi 2}$ scattering background is the largest background for pnn2. The upper bound of the loose pnn2 box is very close to $K_{\pi 2}$ peak. Obviously tightening the upper bound

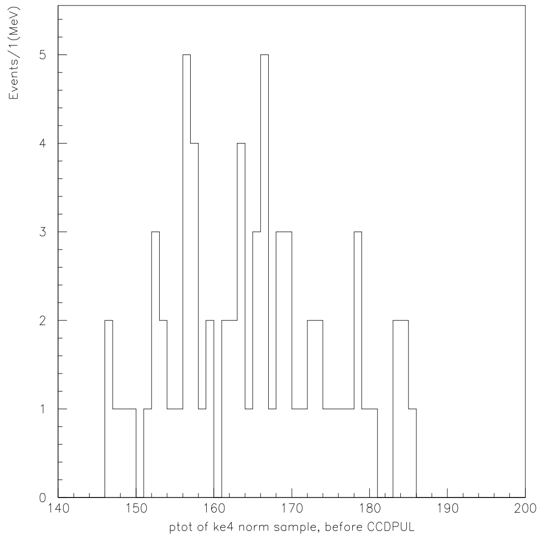

Figure 7: Momentum distribution of K_{e4} normalization sample before CCDPUL cuts.

of kinematic box will also enhance the S/N. Suppression of $K_{\pi 2}$ background guides the upper kinematic limits of the K_{e4}-phobic box.

Three samples are prepared to determine the kinematic limits of the K_{e4}-phobic box. One is UMC pnn2 sample which represents the acceptance sample. The UMC pnn2 sample is required to pass all requirements except the box cuts.

The second sample is a K_{e4} sample. The sample from data has low statistics, Fig. 7, so a UMC sample that passes all possible pass2 cuts except CCDPUL cuts is used. The rejection of CCDPUL cut is assumed to be insensitive to box cuts. The total area is normalized to the K_{e4} background estimate using the loose cuts.

The third sample is for $K_{\pi 2}$. The $K_{\pi 2}$ normalization branch is exploited with the assumption that the rejection of the PVCUTS is insensitive to the kinematic box cuts. Its area is normalized to the actual background measurement for loose cuts. As the other background sources are small and are roughly independent of momentum, their contribution is ignored in this study.

The ptot distribution of these three samples is shown in the first row of Fig. 8. The first step is to find the lower bound of the phobic box by computing the signal acceptance and background contribution of the ptot cut. As shown in the second row of Fig. 8, the acceptance decreases slowly before 170 MeV/c and $K_{\pi 2}$ background is not affected too much. However the K_{e4} background will drop rapidly above after 160 MeV/c. When K_{e4} and $K_{\pi 2}$ are normalized, the acceptance/background has a rather wide maximum at 175 MeV/c (Bottom row of Fig. 8). To keep a higher sensitivity, the lower bound in ptot is set to 165 MeV/c. The etot and rtot lower limits are set to the corresponding values for pions in scintillator.

The second scan is performed for the upper bound with ptot > 170 MeV/c as a setup cut (First row of Fig. 9). The second row of Fig. 9 shows how acceptance and background decrease as the upper ptot cut is tightened. The plot in the third row of Fig. 9 gives the Acc/Bkg as a function of the ptot upper bound cut. The Acc/Bkg ratio is maximize at

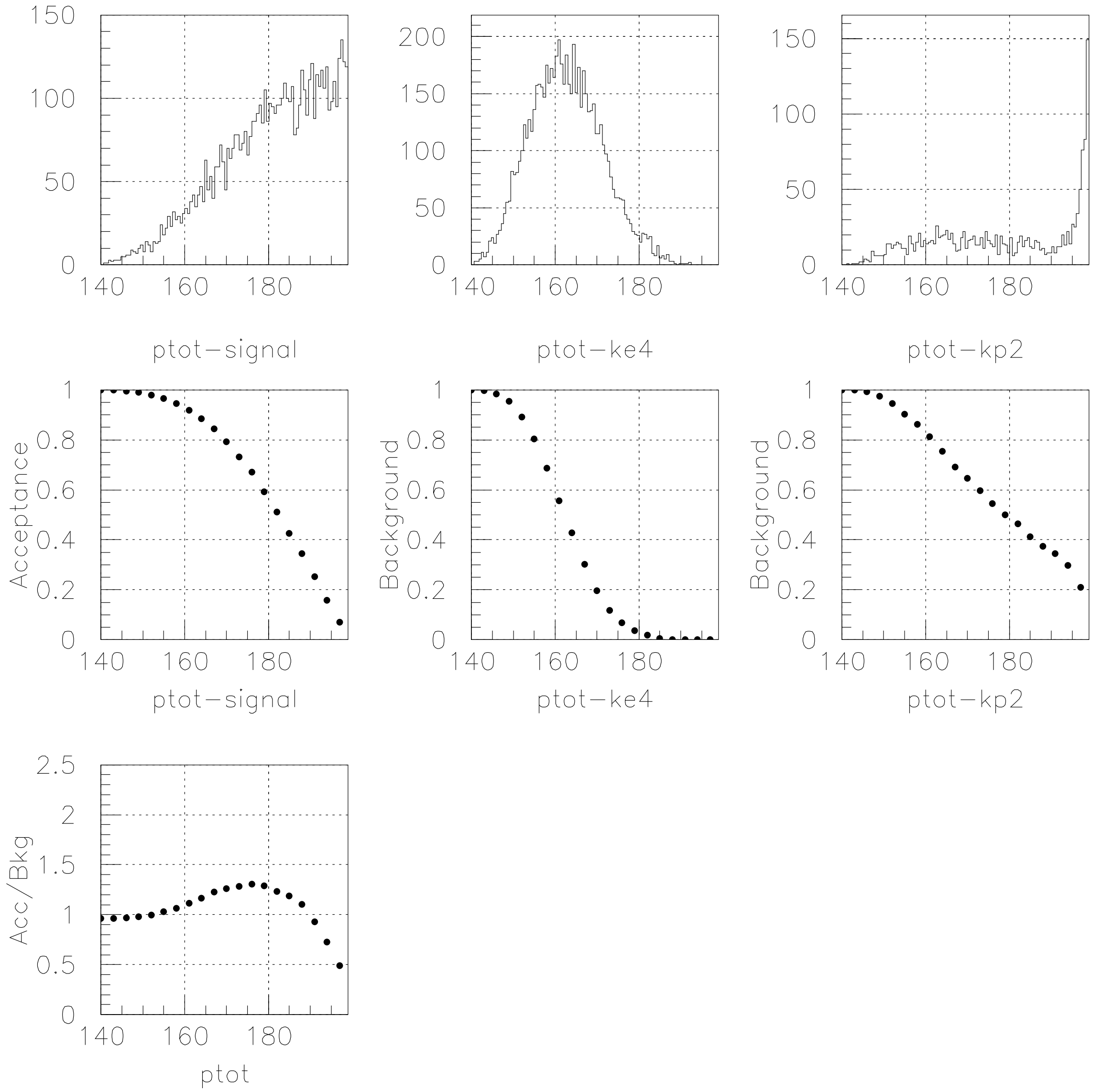

Figure 8: K_{e4}-phobic box lower bound scan. The first row: ptot of UMC acceptance sample, K_{e4} UMC sample and $K_{\pi 2}$ normalization sample. The second row: acceptance loss or background decrease as a function of a ptot lower bound cut for these three samples (normalized to 1.0 for no cut applied). Bottom row: acceptance/background as a function of ptot lower bound cut. Background is the sum of K_{e4} and $K_{\pi 2}$ background, and they are normalized to actual background measurement with loose cuts.

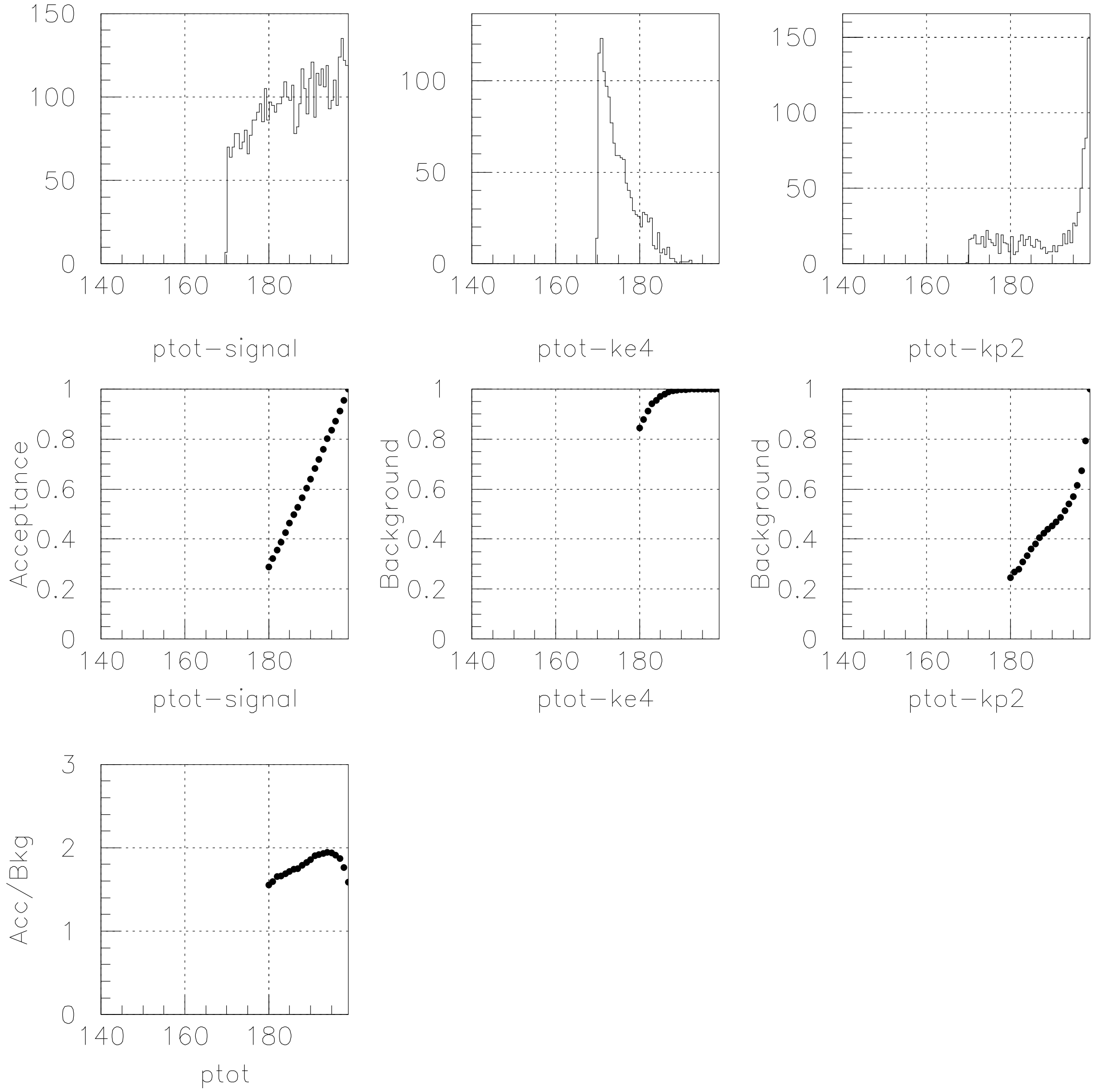

Figure 9: K_{e4}-phobic box upper bound scan. The first row: ptot of UMC acceptance sample, K_{e4} UMC sample and $K_{\pi 2}$ normalization sample where ptot>170 MeV is a setup cut. The second row: acceptance loss or background decrease as a function of a ptot upper bound cut for these three samples (normalized to 1.0 for no cut applied). Bottom row: acceptance/background as a function of ptot upper bound cut. Background is the sum of K_{e4} and $K_{\pi 2}$ background, and they are normalized to actual background measurement with loose cuts.

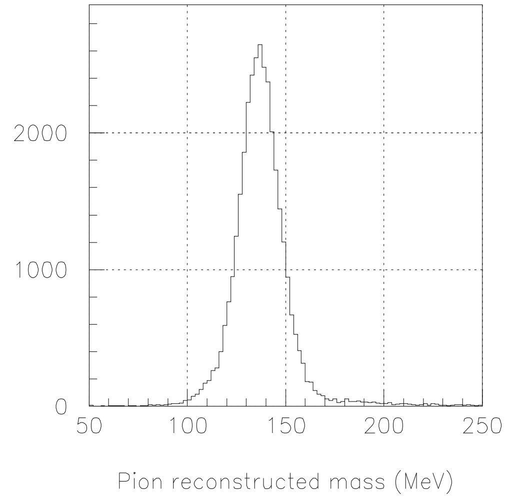

Figure 10: π mass distribution of π_{scat} sample.

$\sim$195 MeV/c. So the upper bound of ptot is set to 197 MeV/c with corresponding etot and rtot cuts.

The procedure was reversed with the upper limit set first and the lower limit second and consistent results were obtained. The kinematic limits of the K_{e4}-phobic box are given in Table 7.

5.3 UTCQUAL

The UTCQUAL cut [4] for the E949 pnn1 analysis was designed to suppress tails in the $K_{\pi 2}$ momentum distribution by rejecting events in which the charged track has a poor UTC fit. Poor UTC fitting is associated with fewer x-y hits, fewer z hits, some overlapping hits, etc. and is generally accompanied by worse momentum resolution.

The acceptance of the pnn1 UTCQUAL cut was found to decrease from $\sim$94% [12] at the $K_{\pi 2}$ peak and dropt to $\sim$87% [8] in the pnn2 region. The momentum dependence was examined and it is found that many good track were unnecessarily removed the the pnn1 UTCQUAL cut.

To clearly see this phenomenon, a π_{scat} sample is selected. The setup cuts are quite like to that used in π_{scat}-based acceptance study. A clean π mass plot from this sample is shown in Fig. 10. The gradually dropping acceptance with momentum is shown in Fig.11.

With this sample some further study is done with UTCQUAL cut. For charged tracks, the E949 detector provides range and energy measurements almost independent of the momentum measurement With energy and range information, the momentum of a track can be estimated. Fortunately this method yields a very good momentum resolution of $\sigma(P_{dc} - P_{exp}) \approx 3.01$ MeV where P_{dc} is the momentum measured directly by the UTC and P_{exp} is momentum estimated from energy and range.) This gives an opportunity to tune UTCQUAL cut independent of momentum.

There are 10 failure modes identified as part of UTCQUAL cut. Some of them are

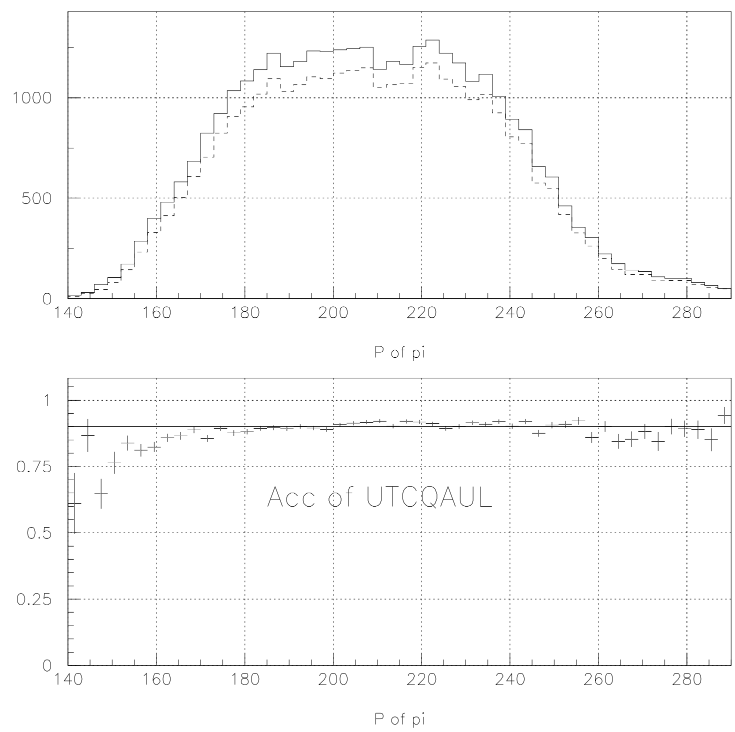

Figure 11: Upper:momentum of pion, the solid line represents all events and the daashed line represents the events pass pnn1 UTCQUAL; Lower: acceptance of UTCQUAL with momentum, the horizontal solid line is at 90%, and the error are statistical only.

based on probabilities of χ^2 of components of the fit and the others cut on specific cases such as number of hits, etc. If a failure mode removes mainly good tracks, based on the agreement of P_{dc} and P_{exp}, then the component of the cut based on this failure mode is loosened. For instance, as shown in Fig. 12, the cuts for modes 4 and 7 are loosened, whilst obviously a mode 10 cut is very effective at reducing tails. Fig.13 shows the result before and after the tuning for UTCQUAL. A lot of good tracks were recovered. with an acceptance improvement from 87% to 95%.

5.4 PRRF

The PRRF cut as used in the pnn1 analysis [4] had 4 components:

1. $PRRF$ = the probability of χ^2 of the RS track (TRKRNG) fit [1]

2. PRRFZ1 = probability of χ^2 of the match of the UTC track extrapolation to the z position determined from the RSSC information,

3. PRRFZ2 = probability of χ^2 of the match of the UTC track extrapolation to the z position determined from the RS timing, and

4. PRRFXY = probability of χ^2 for the match between the UTC track extrapolation and the RSSC and RS (sector-crossings) xy position measurements.

Use of the pnn1 version of the PRRF cut had a $\sim 30\%$ acceptance loss in tracks that stopped before the first RSSC layer. Since pnn2 accepts shorter range tracks by definition, changes in the PRRF cut were made. The PRRFXY requirement of the PRRF cut was removed for pnn2 because a significant fraction of pnn2 signal events have no RSSC hits or RS sector-crossings. Tracks with no RSSC information or sector-crossings are accepted, otherwise $PRRF$ is required to be greater than 0.01. The PRRFZ1 or PRRFZ2 requirements are imposed only when RSSC information or RS timing information is available. The resulting rejection of the PRRF cut is $\sim$1.15 with the PRRFZ2 contributing a rejection of $\sim$1.11.

5.5 RSDEDX

In the E949 pnn1 analysis [4], the cut on the probability of χ^2 of the RS counter energy measurements was dependent upon whether the largest deviation in the (expected-measured) energy in a RS counter was positive or negative. This innovation of an asymmetric cut lead to a $\sim$10% increase in muon rejection and a $\sim$2% increase in acceptance of pnn1. It was found that the calibration for the expected energy deposit for the shorter range tracks of pnn2 was not sufficiently robust for the asymmetric cut to be exploited. In addition since the muon background is much less troublesome for pnn2, we reverted to a cut on the probability of χ^2 of > 0.04 independent of the largest deviation.

[1] In this section we denote the probability cut as $PRRF$ and the composite cut with all components as PRRF.

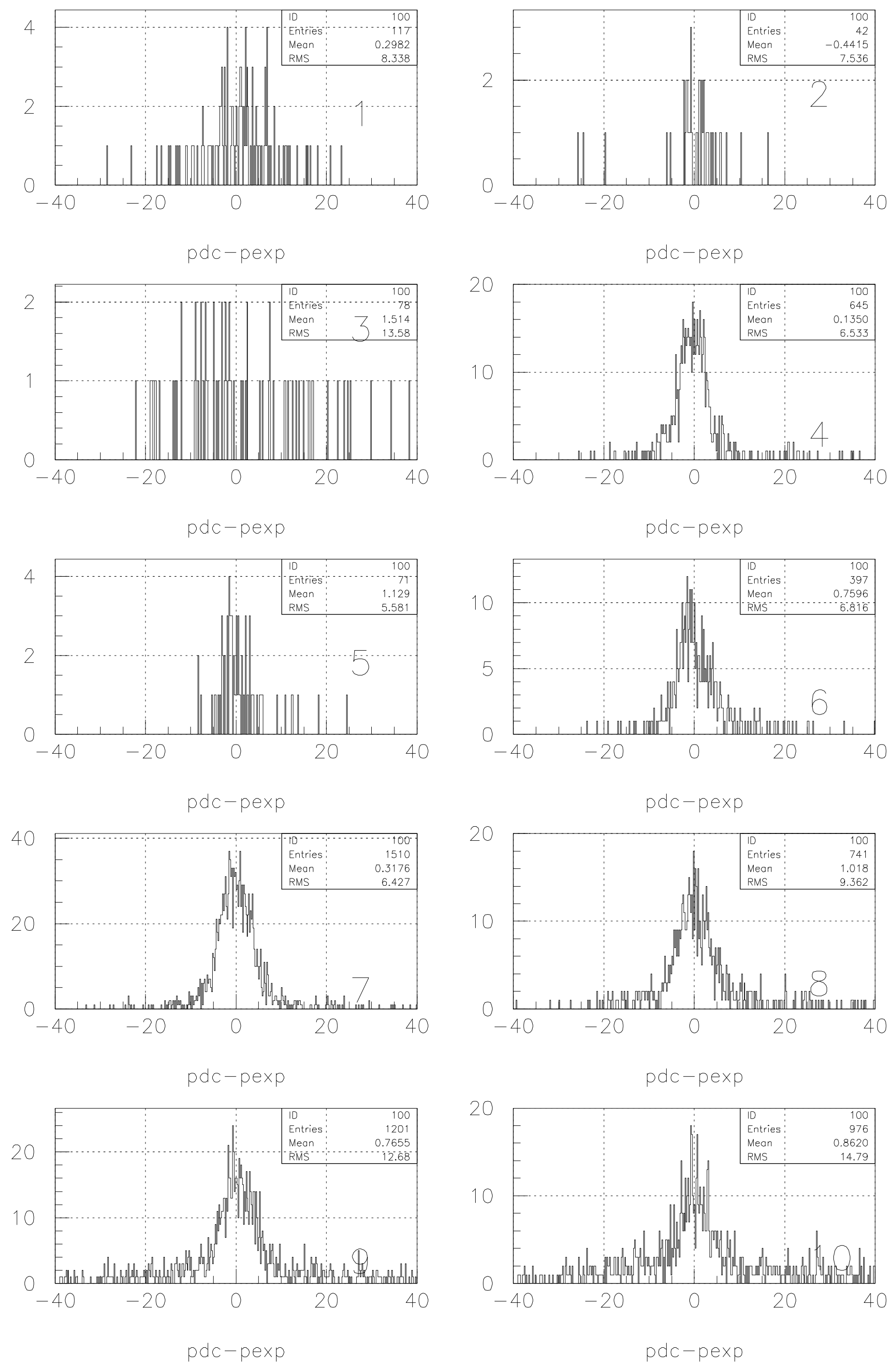

Figure 12: $P_{dc} - P_{exp}$ for events failing pnn1 UTCQUAL for the 10 ten failure modes.

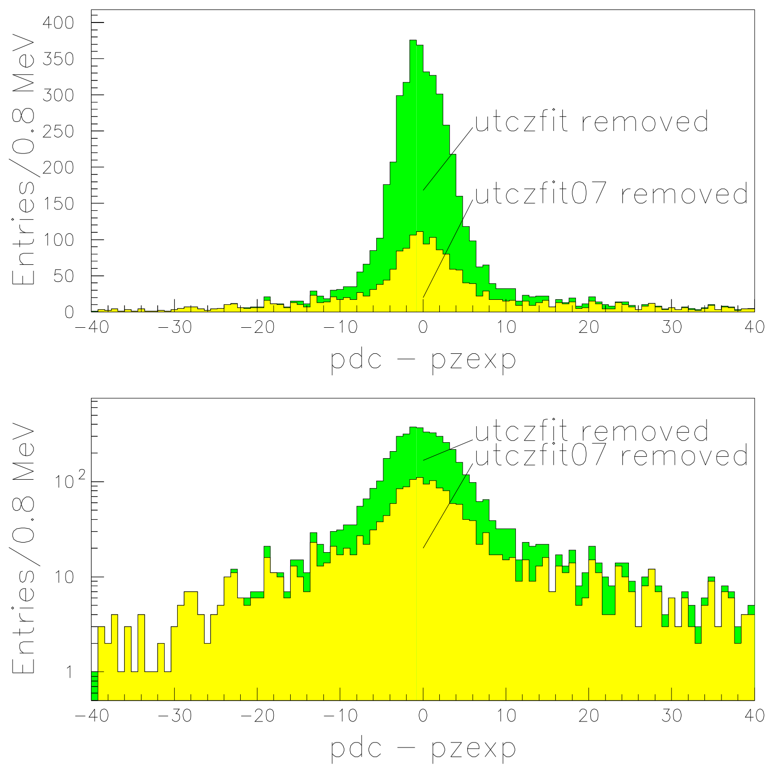

Figure 13: $P_{dc} - P_{exp}$ for events that *failed* the UTCQUAL cut before (green) and after (yellow) tuning. UTCQUAL07 is the cut after tuning. The upper one is in linear scale, the lower one is in log scale.

6 Delayed-coincidence cuts

6.1 K^+ Stop Requirement: Delayed Coincidence (DELC3)

Determining that the incoming K^+ stops within the TG is accomplished by observing a delay in the outgoing charged track which is presumed to be a K^+-decay product. This requirement will remove beam-π^+ scattering events and K^+ decay-in-flight events. DELC3 requires a delay of at least 3.0 ns between the target π^+ time, t_π, and the target K^+ time, t_K,($tpi - tk \geq 3.0$ ns). Additionally, DELC3 requires the constraints defined in the conditional delco function, *delc*, described below. $K_{\mu 2}$ monitors are used to measure an acceptance of 0.8569 ± 0.00020 when DELC3 is applied first and an acceptance of 0.9669 ± 0.00023 when DELC3 is applied last. Note that DELC3 and DELCO3 are two names for the same cut.

6.2 Tight Delayed Coincidence (DELC6)

A tighter delayed coincidence cut is employed for the use in a signal region with reduced background. This is accomplished by a 6.0 ns delayed concidence requirement ($tpi - tk \geq 6.0$ ns). The acceptance of DELC6 when applied first is 0.7044 ± 0.00026 and 0.8804 ± 0.00043 when applied last. Note that DELC6 and DELCO6 are two names for the same cut.

6.3 Delayed Coincidence Function (*delc*)

This function tightens the delay coincidence when the timing consistency between detectors are degraded [4]. Events are rejected if $t_\pi - t_K < delc_{thres}$. The cut threshold, $delc_{thres}$ is the maximum of the following conditions ($delc_{thres}$ minimum is 2.0 ns).

- $delc_{thres} = 5.0$ ns if the discrepancy between the TG K^+ time and B4 hit time is greater than 1.0 ns.
- $delc_{thres} = 6.0$ ns if the discrepancy between the TG π^+ time and track time is greater than 1.5 ns.
- $delc_{thres} = 5.0$ ns if t_π is obtained from the time of the I-Counter hit, not from the TG π^+ fiber hits.
- $delc_{thres} = 4.0$ ns if the energy deposit of a K^+ in the TG is less than or equal to $50MeV$.
- $delc_{thres} = 3.0$ ns if there are less than four TG π^+ fibers found.
- $delc_{thres} = 3.0$ ns if the beam likelihood value is less than 200 (to be explained in the Pathology Cuts section).
- $delc_{thres} = 4.0$ ns if the discrepancy between any of the individual K^+ fiber times and the average K^+ time is greater than 2.0 ns.

- $delc_{thres}$ = 4.0 ns if the discrepancy between any of the individual π^+ fiber times and the average π^+ time is greater than 3.5 ns.

7 Target cuts

7.1 TIMKF

This cut is a refined version of TGKTIM. The times of the kaon fibers are checked for consistency with the energies and positions of the kaon fibers. The times of the kaon fibers are tabulated against the distance of the kaon fiber from the vertex in the X-Y view. They are also tabulated against the range of the kaon. The range is computed from the kaon energy in the target fibers up to the vertex fiber. We use standard range tables to compute the range with the appropriate corrections for saturation. Both the times versus the distances to the vertex, and the times versus the ranges are fit to linear functions. The slopes of the linear functions are the inverse of the velocity (called *velk* and *velkz*) of the kaon toward the vertex and the intercept is the time of the kaon stop (*tkprm* and *tkzprm*). The probability of the fits (xprob1 and xprob2) is computed from the chi-squared of the fits assuming the number of degrees of freedom to be Nfibers-2. If the number of kaon fibers is less than 3, the probability is set to 1.

This cut was designed to eliminate hits that are classified as kaon hits due to pion scatters for events with small DELCO (the difference between global pion and kaon times).

The fixes to TIMKF are as follows:

- It was found that a small fraction of the events (5 of 16000 in an early study) were passing identical values to linfit for the y-array. This resulted in an infinite slope being determined by linfit. The code was modified so that this type of information was flagged, the fit never performed, and the event automatically failing the TIMKF cut.

- The ccd rise times associated with the variable ccdrk have changed from the E787 to the E949 analyses. One of the fail conditions for TIMKF is when either of the probability distributions xprob1 or xprob2 have a value of less that 0.03. The change in ccd rise times resulted in non-flat probability distributions for these two probability variables. To flatten these probability distributions, the errors in the y-array passed to linfit (the variable tres) was multiplied by 0.8.

- It was found that approximately 1% of the events passing the target cut study setup cuts retained their initialization values (equal to -8) in the variables xin, yin, x_b4sw and y_b4sw. As TIMKF uses these distances in some of its calculations, events with variables still containing this initialization data are now rejected.

- To allow late kaons, the cut failing conditions based on the y-intercept (tkzprm) of the linear slope of the times versus the ranges were removed.

Note that these fixes were primarily bug fixes or modifications to explicitly allow late kaon events and studies in the change in performance of the cut in terms of acceptance versus rejection were not performed.

An event can fail the TIMKF cut under any of the following conditions:

- $abs(velzk + 0.063).gt.0.75$
- $xprob1.lt.0.05$ - Low consistency of kaon fiber times to their distance to the vertex.
- $xprob2.lt.0.05$ - Low consistency of kaon fiber times to their range determined from the range-energy lookup table.
- Either of the linear fits used to determine xprob1 or xprob2 returns an infinite slope
- Events containing stale data in either x_b4sw and y_b4sw (discussed above).

7.2 CCDPUL

The former CCDPUL cut as it was used in the E787 PNN2 analysis was actually two cuts in one. An event could fail the cut if any of the target fibers failed either the "Pion energy" or the "Bad pulse fit" conditions. This cut has since been split into two cuts. The first is a safety cut called CCDBADFIT to deal with the "Bad pulse fit" condition. The second keeps the name CCDPUL and deals with the "Pion energy" condition.

7.2.1 Description of CCDPUL

The CCDPUL cut removes events that have kaon fibers with second pulse energies above a certain threshold (1.25 MeV) at a time that is consistent with the global pion time, *tpi*. As each fiber has two gain channels (low-gain and high-gain), before checking for the time and energy conditions for a target fiber the CCDPUL algorithm needs to determine which CCD data is used: the low-gain, the high-gain. This cut is a three stage process.

CCDPUL - The First Stage

Separately the results of the fits from the low-gain and high-gain target CCDs are considered. The high-gain channel data is not passed onto the second stage if any of the following conditions are met:

- The single fit probability is greater than 0.25 as the double-pulse fit is only performed if the single fit probability is less than or equal to 0.25.
- The number of bins in the second pulse with non-zero amplitude less than 3.
- The double fit probability is equal to 0.

The same conditions as above were applied to the low-gain channels with one additional condition. If the fiber is found to be multiplexed with other fibers having activity within ± 5 ns of the global pion time *tpi*, the energy within that time window from those other fibers is subtracted from the second pulse energy of the fiber being examined.

CCDPUL - The Second Stage

During the second stage of CCDPUL, an algorithm decides which CCD data is used: the low-gain, the high-gain, or a weighted average of the two. If only the high-gain or low-gain CCD data for this fiber has been passed on from the first stage, that is what will be used. If the first stage passed on both the high-gain and the low-gain CCD data the decision of how to use these data was based on the following conditions which are checked **in sequence**:

- An average of the the high-gain and low-gain will be used if the fiber energy as determined by ADC is between 10 MeV and 30 MeV and the fractional error in the second-pulse amplitude for both the low-gain and high-gain CCD channels is greater than 0.05. A typical pulse will start to saturate at around 25 MeV so the fiber energy condition includes high-gain fibers that show small amounts of saturation. The second-pulse energy and relative time between the first and second pulses are the quantities which are determined via the weighted average. For the rest of the quantities passed onto the third stage, the information from the high-gain channel is used. The following equations show how the weighed average is determined for a quantity x:

$$w_{hi} = \frac{dA_{hi}^2}{dA_{hi}^2 + dA_{lo}^2}$$

$$w_{lo} = \frac{dA_{lo}^2}{dA_{hi}^2 + dA_{lo}^2}$$

$$x = x_{hi}w_{hi} + x_{lo}w_{lo}$$

  where dA_{lo} and dA_{hi} are the errors on the second-pulse amplitudes of the low-gain and high-gain double pulse fits respectively.

- Use high-gain if it has not saturated.

- Use low-gain if high-gain has saturated and the energy in the fiber as determined by ADC is greater than 40 MeV. The low-gain channel will typically start to saturate at around 40 MeV.

- Choose the better fit based on the fiber energy E_k (from ADC) and the time difference between the global pion time tpi and the global kaon time tk. High gain is used if either of these conditions are met:

$$15 < E_k < 25 \text{ .AND. } tpi - tk > 12$$

$$25 < E_k < 40 \text{ .AND. } tpi - tk > 20$$

  Low gain is used if either of these conditions are met:

$$15 < E_k < 25 \text{ .AND. } tpi - tk < 12$$

$$25 < E_k < 40 \text{ .AND. } tpi - tk < 20$$

This information is then passed onto the third stage.

CCDPUL - The Third Stage

All fibers passed onto stage 3 are checked for second-pulse energy above a certain threshold where the timing of the second pulse is consistent with the global pion time *tpi*. The event fails if any fiber in stage 3 meets both of the following conditions:

- The second-pulse energy is above 1.25 MeV
- The quantity *deltat* falls between -7.5 and 10 ns inclusive. The quantity *deltat* is a measure of consistency between the global pion (*tpi*) and kaon (*tk*) times and the first (t_1) and second (t_2) pulse times from the fit for that kaon fiber:

$$deltat = (t_2 - t_1) - (tpi - tk)$$

7.2.2 Description of CCDBADFIT

The CCDBADFIT safety cut removes events that have kaon fibers where it can be concluded that the fitter was unable to make a successful fit on that fiber. This occurs when the probabilities for both the single and double-pulse fits are equal to zero. As with CCDPUL, the two gain channels (low-gain and high-gain) for each fiber are considered when determining that the fitter was unable to make a successful fit. As with CCDPUL, this cut is a three-stage process.

CCDBADFIT - The First Stage

Separately the results of the fits from the low-gain and high-gain target CCDs are considered. The high-gain channel data is not passed onto the second stage if any of the following conditions are met:

- The single fit probability is greater than 0.25 as the double-pulse fit is only performed if the single fit probability is less than or equal to 0.25.
- The number of bins in the second pulse with non-zero amplitude less than 3 when the double fit probability is greater than 0.
- The double fit probability is equal to 0 when the single fit probability is greater than 0.

The same conditions as above were applied to the low-gain channels.

CCDBADFIT - The Second Stage

During the second stage of CCDBADFIT, a similar decision making process is used as CCDPUL to determine which CCD data is used: the low-gain or the high-gain. The difference is that a weighted average of the low-gain and high-gain is never used, but the rest of the decision making sequence is the same.

CCDBADFIT - The Third Stage

All fibers passed onto stage 3 are checked for probabilities equal to zero for both the single and double-pulse fits. If this condition is met and the fiber energy as determined by the ADC is greater than 1.25 MeV, the event fails the CCDBADFIT cut.

7.2.3 CCDBADFIT and CCDPUL Coding Changes

As was discussed previously in this section, the CCDPUL cut was split into two cuts: CCDBADFIT which deals with unfitable pulses and CCDPUL which deals with rejecting events showing appropriate second pulse activity.

Due to the method in which fibers are passed from the second to third stages of CCDPUL or CCDBADFIT, it is possible for up to 62 fibers to be passed onto the third stage of CCDPUL or CCDBADFIT. The target fitter treats the low-gain and high-gain CCD data separately and makes no correspondence between the low-gain and high-gain data of a given channel. There is a maximum of 31 low-gain and 31 high-gain channels which can be fit, but it is entirely possible that due to some fibers missing data in either the high-gain or low-gain channels, there could be more than 31 different fibers which have been fit. This possibility was not accounted for in CCDPUL (or CCDBADFIT) and we saw a few events where the number of fibers being passed from the second to third stages of CCDPUL and CCDBADFIT exceeded 31 and caused an "array out of bounds" error. This was corrected by changing the maximum number of fibers which could be passed on from stage two to stage three of these cuts from 31 to 62.

The condition that only target fibers identified as kaon fibers was added. Previously, any fiber fit by the target CCD fitter could cause the event to fail CCDPUL.

An additional safety condition was added to CCDBADFIT. Due to changes in the fitter that only allows the first 30 bins (60 ns) to be fit, second pulses for very large DELCOs cannot be found by the fitter. As a result, the condition that an event with a DELCO (difference between global pion and kaon times) larger than 60 ns fails the cut was added to CCDBADFIT.

7.2.4 CCDBADFIT Optimization

From a combination of optimization and observation of many pulse fits, the classification for unfitable pulses (CCDBADFIT) was changed from pulses having both single and double-fit probabilities lower than 0.01 to both these fits having probabilities equal to 0. Due to the ntuple granularity, target fitting probabilities equal to 0 in the ntuple correspond to probabilities less than $10^{-}5$. Additionally, the condition that CCDBADFIT could only cut a fiber having more ADC energy than the CCDPUL energy threshold was added. It doesn't matter if there fitter couldn't find a solution if there isn't enough energy in the fiber that it could possibly fail CCDPUL.

7.2.5 CCDPUL Optimization

For the E787 pnn2 analyses [2], the energy threshold above which second pulses would cause an event to be rejected by CCDPUL was set to 1.5 MeV for the 1997 data set and 1.0 MeV for the 1996 data set. The second pulse needed to be within ± 10 ns of pion time.

From the optimization, the second-pulse threshold energy was set to 1.25 MeV. The timing window was made asymmetric and the the quantity *deltat* had to fall between -7.5 and 10 ns inclusive for a second pulse above the energy threshold to fail the cut. The quantity *deltat* is a measure of consistency between the global pion (tpi) and kaon (tk) times and the first (t_1) and second (t_2) pulse times from the fit for that kaon fiber given by $deltat = (t_2 - t_1) - (tpi - tk)$.

It is important to note that this optimization was performed before the fixes to the fitter seen in the final reprocessing and using a version of CCDPUL which had many of the bugs described above. The optimized values were verified on the reprocessed data using the up-to-date CCDPUL as can be seen in Table 8

The samples used for studying and optimizing CCDPUL and the safety cuts CCDBADFIT, CCDBADTIM and CCD31FIB are shown in Tables 9 and 10.

7.2.6 CCDBADTIM

This cut is a safety cut designed to remove events with time values returned from the double-pulse fit in the target fitter which have been observed to be consistent with incorrect solutions. The ntuple stores the single and double-pulse times from the fit over only a limited range. Times that are smaller than a certain minimum value are stored in the ntuple as this minimum value. For example, any first-pulse times less than or equal to -9.9939 are stored as -9.9939 in the ntuple. This number is not exactly -10 due to the ntuple binning. As there is no way to determine the exact time of any value stored in this -9.9939 bin, the event has to be rejected due to incomplete timing information.

The first stage for CCDBADTIM is the same as for CCDPUL. The second stage for CCDBADTIM is the same as for CCDBADFIT. In the third stage of CCDBADTIM each fiber is checked to see if the fiber energy as determined by the ADC is greater than 1.25 MeV. If the energy is above threshold and any of the following conditions are met, the event fails the cut.

- The first-pulse time from the double-pulse fit is less than -9.98 This is the minimum value stored in the ntuple for the first-pulse times from the double-pulse fits.

- The second-pulse time from the double-pulse fit is less than -4.99. This is the minimum value stored in the ntuple for the second-pulse times from the double-pulse fits.

- The first-pulse time from the double-pulse fit (t_1) is not consistent with the global kaon time tk. The failing conditions are $t_1 - tk < -6$ or $t_1 - tk > 7$. Figure 14 discusses this choice of cutting parameters.

The acceptance loss and rejection of the CCDBADTIM cut are shown in Table 11.

$T_{lo} = -10$ns, $T_{hi} = 10$ns			
E_{pion} (MeV)	Acceptance	Rejection	Acceptance × Rejection
0.75	0.299	9.764	2.917
0.875	0.324	9.079	2.944
1.0	0.353	8.625	3.041
1.125	0.384	7.916	3.037
1.25	0.415	7.289	3.025
1.375	0.447	6.561	2.935
1.5	0.479	6.097	2.923
1.75	0.538	5.287	2.847
2.0	0.591	4.585	2.708

$E_{pion} = 1.25$MeV, $T_{hi} = 10$ns			
T_{lo} (ns)	Acceptance	Rejection	Acceptance × Rejection
-6	0.475	6.142	2.918
-7	0.453	6.592	2.988
-7.5	0.445	6.787	3.017
-8	0.437	6.877	3.005
-9	0.425	7.126	3.025
-10	0.415	7.289	3.025
-12	0.401	7.486	3.001
-15	0.388	7.638	2.966
-18	0.382	7.709	2.946

$E_{pion} = 1.25$MeV, $T_{lo} = -10$ns			
T_{hi} (ns)	Acceptance	Rejection	Acceptance × Rejection
6	0.434	6.809	2.952
7	0.428	6.946	2.971
7.5	0.425	7.005	2.979
8	0.423	7.077	2.993
9	0.419	7.163	2.998
10	0.415	7.289	3.025
12	0.409	7.514	3.070
15	0.402	7.782	3.128
18	0.397	7.977	3.169

Table 8: The three tables show the acceptance and rejection results for the combined group of cuts CCDPUL, CCDBADFIT and EPIONK. for scanning the three main cut parameters as described in Section 7.2.5. Note that CCDBADFIT and EPIONK are only affected by the the changes to E_{pion}. These are the same samples as described in Tables 9 and 10 Each table show one of the three parameters being scanned while the other two are held constant. These optimized parameters had previously been chosen before fixes to the target fitter and CCDPUL so this optimization was performed to check that the set of parameters were still appropriate. Although it can be seen that there are values for E_{pion}, T_{lo} and T_{hi} which would result in very slight gains in overall Acceptance × Rejection performance, it was determined that the values from the previous optimization continued to be reasonable so they were not changed.

CUT	Events	Acceptance
START	5439378	1.000
BAD_RUN	5361618	0.986
FIX_ALL	5361618	1.000
PSCUT	4755957	0.887
TGCUT	4433507	0.932
RDUTM	4199585	0.947
RANGE1	4199585	1.000
RD_TRK	4199585	1.000
TRKTIM	4199585	1.000
TARGET	4199479	1.000
UTC	4199479	1.000
TGQUALT0	4199479	1.000
UTCQUAL	3903640	0.930
PTOT_229_245	3423191	0.877
ERS_120_150	890047	0.260
COS3D	804036	0.903
ZUTOUT	802037	0.998
PCUTS	616602	0.769
B4EKZ	547954	0.889
TGZFOOL	541237	0.988
EPIMAXK	499031	0.922
TGER	498503	0.999
TARGF	482833	0.969
DTGTTP	482833	1.000
RTDIF	476842	0.988
DRP	476470	0.999
TGKTIM	456855	0.959
EIC	442796	0.969
TIC	442796	1.000
TGEDGE	438653	0.991
TGENR	433483	0.988
PIGAP	428442	0.988
TGLIKE	418881	0.978
TGB4	389600	0.930
PHIVTX	375160	0.963
NPITG	375160	1.000
DELC + DELCO3	338480	0.902
TIMKF	301400	0.890
VERRNG	279400	0.927
ANGLI	279386	1.000
KIC	277754	0.994
PV_noBV	166278	0.599
EPITG	158646	0.954
TGFITALLK	153126	0.965
DECAYV	153126	1.000
CCDBADFIT	136263	0.890
CCDPUL	68355	0.502
EPIONK	68153	0.997

Table 9: The acceptance sample for CCDPUL studies is a km21 monitor sample. The 'Events' column shows the number of events remaining after that cut has been applied. The cut 'PV_noBV' is the regular photon excluding all barrel veto, barrel veto liner and early barrel veto subsystems. The cut 'PTOT_229_245' only accepts events having *ptot* between 229 and 245. The cut 'ERS_120_150' only accepts events having *ers* between 120 and 150.

CUT	Events	Rejection
COUNT	0.1308653E+08	1.000
BAD_RUN	0.1282168E+08	1.021
FIX_ALL	0.1282168E+08	1.000
TGQUALT0	0.1213954E+08	1.056
TARGET	0.1213954E+08	1.000
TGCUT	0.1213858E+08	1.000
UTC	0.1213858E+08	1.000
RD_TRK	0.1213858E+08	1.000
TRKTIM	0.1213858E+08	1.000
RDUTM	0.1213858E+08	1.000
PSCUT	9043844	1.342
PRESCALE3	9043844	1.000
TGPVCUT	7999455	1.131
STLAY	7999218	1.000
BOX2	9182930	8.711
PV_noTG	700773.0	1.310
LAYV4	7007720	1.000
ICODEL14	7007680	1.000
FIDUCIAL	6577930	1.065
UTCQUAL	6026540	1.091
B4DEDX	5899260	1.022
BWTRS	4876780	1.210
B4TRS	4609650	1.058
B4ETCON	4550730	1.013
B4CCD	4495680	1.012
CPITRS	4434930	1.014
CPITAIL	4432940	1.000
CKTRS	2529640	1.752
CKTAIL	2322150	1.089
TIMCON	2281810	1.018
TGTCON	1958300	1.165
DELC	1495930	1.309
TGGEO	99608	1.502
RVUPV	97761	1.019
B4EKZ	76843	1.272
TGZFOOL	75562	1.017
EPITG	56281	1.343
EPIMAXK	56281	1.000
TARGF	51328	1.096
DTGTTP	51327	1.000
RTDIF	50929	1.008
DRP	50439	1.010
TGKTIM	49767	1.014
EIC	48730	1.021
TIC	48730	1.000
TGEDGE	48165	1.012
TGDEDX	45419	1.060
TGENR	44590	1.019
PIGAP	44115	1.011
TGB4	40832	1.080
PHIVTX	35708	1.143
OPSVETO	33283	1.073
TGER	33283	1.000
NPITG	33283	1.000
TGLIKE	31562	1.055
TPICS	31550	1.000
CHI567	26873	1.174
VERRNG	24207	1.110
CHI5MAX	22472	1.077
ANGLI	22429	1.002
KIC	22420	1.000
RSDEDX	16414	1.366
RNGMOM	5826	2.817
PRRF	5345	1.090
TGFITALLK	5062	1.056
TIMKF	4133	1.225
DECAYV	4133	1.000
CCDBADFIT	3692	1.120
CCDPUL	610.	6.052
EPIONK	609.	1.002

Table 10: The rejection sample for CCDPUL studies uses the pnn2 data with an inverted photon veto. This photon veto, indicated as 'PV_noTG', excludes the target subsystem. The 'Events' column shows the number of events remaining after that cut has been applied.

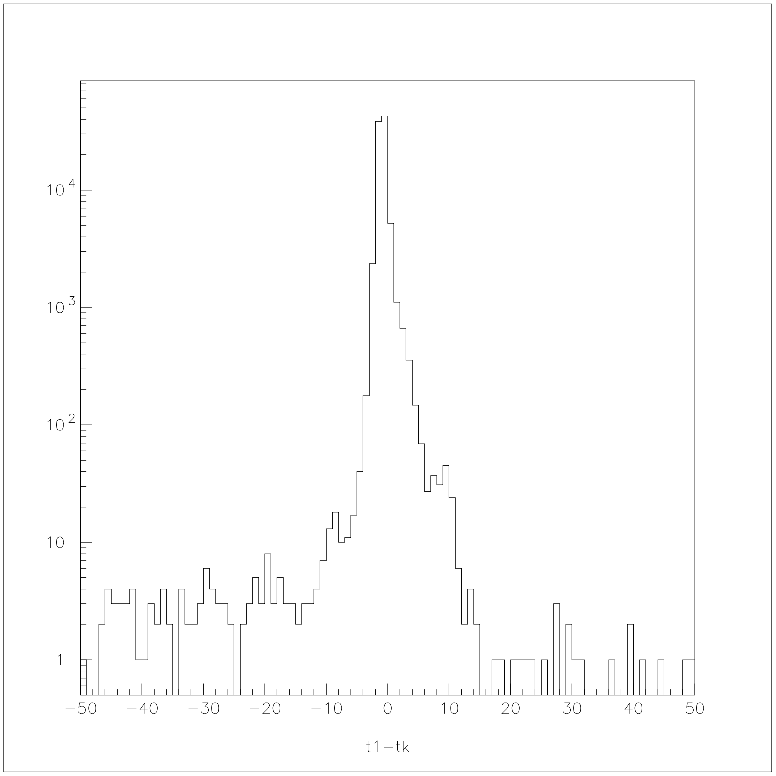

Figure 14: This plot shows the distribution of the difference between the first-pulse time t_1 from the target double-pulse fitter and the global kaon time tk. This is for the same acceptance sample as described in Table 11. This plot shows the difference in the quantities described for all fibers being considered in the third stage of CCDBADTIM with these additional conditions applied: the first-pulse time from the double-pulse fit is greater than -9.98 and the second-pulse time from the double-pulse fit is greater than -4.99. The bounds for the cut were set to $t_1 - tk < -6$ and $t_1 - tk > 7$ which corresponds to beyond the valleys on either side of the peak. Visual observation of many events past these bounds confirms that these times are consistent with fits that did not converge on the appropriate solution for the double-pulse fit.

CUT	Acceptance	Rejection	Acceptance $\times$ Rejection
SETUP	134763	3917	
CCD31FIB	134761 (1.000±0.000)	3917 (1.000±0.000)	1.000±0.000
CCDBADFIT	120008 (0.891±0.001)	3495 (1.121±0.006)	0.999±0.007
CCDPUL	60185 (0.502±0.001)	590 (5.924±0.222)	2.974±0.118
EPIONK	59889 (0.995±0.000)	587 (1.005±0.003)	1.000±0.003
CCDBADTIM	59513 (0.994±0.000)	569 (1.032±0.008)	1.026±0.008

Table 11: Acceptance and rejection for the safety cuts CCDBADTIM and CCD31FIB. The data and setup cuts are the same as used for the CCDPUL samples shown in Tables 9 and 10. The acceptance and rejections show the number of events after the cut has been applied with the acceptance or rejection in brackets. The right column shows the product of the acceptance and rejection.

7.2.7 CCD31FIB

The CCD31FIB cut is a safety cut created to deal with a mistake in the target fitter that was not discovered until after the final reprocessing of the data. There are a maximum of 31 fibers that can be fit for each of the low-gain and high-gain CCDs by the target fitter. For the 31st fit fiber of either high-gain or low-gain having single-pulse fit probabilities lower than 0.25, the subsequent double-pulse fit values were not stored in the ntuple properly. Any event meeting the conditions described above fail this cut as the information needed to apply CCDPUL is not present. The acceptance loss and rejection of the CCD31FIB cut are shown in Table 11.

7.3 TGdEdX

7.3.1 Cut Description

$\frac{dE}{dX}$ (in scintillator) of π^+'s in the PNN2 momentum region, 140 MeV/c $\leq P_{\pi^+} \leq$ 195 MeV/c, changes from 3.08 MeV/cm to 2.47 MeV/cm. Therefore, any cut based upon $\frac{dE}{dX}$ which does not account for the momentum dependence of the outgoing π^+ within the Target will wastefully lose acceptance.

TGDEDX calculates the likelihood that the charged track in the TG was due to a π^+. The $\frac{dE}{dX}$-likelihood ($like_{tgdedx}$), Eq. (1), was determined using the measured momentum ($ptot$), target range (rtg), target energy, (etg[2]), and expected rtg (rtg_{exp}) based upon the observed $ptot$ and etg.

$$like_{tgdedx} = \frac{1}{2} \cdot \left(1 + erf\left(\frac{rtg - rtg_{exp}(etg, ptot)}{\sigma_{exp}(etg, ptot)} \right) \right) \tag{1}$$

Over small bands in momentum $\frac{dE}{dX}_{\pi^+}$ will only change slightly. With this assumption, $ptot$ was quantized in five momentum "bins" (<170 MeV/c, $170-180$, $180-188$, $188-$

[2] As will be discussed shortly, this was not always the nominal etg.

199.53, > 199.53) and *etg* was quantized into 15 bins ($0-2MeV$, $2-4$,..., $26-28$). The value of the 15^{th} bin was defined equal to the value of the 14^{th} bin; effectively cutting very large energy deposits in the TG, since TGDEDX uses extrapolation of adjacent values to extract the expected *rtg* value for a given *etg* and *ptot*.

Events were cut by TGDEDX if $like_{tgdedx} < 0.05$ (setting the 0.05 threshold value is discussed later). That is, TGDEDX cut events when the measured target range was much smaller than the expected target range of a signal π^+.

7.3.2 Coding Changes

In E787-PNN2, *swathccd* does not allow π^+ hits to occur in K^+ flagged fibers; this was allowed in E949 when $t_\pi - t_K > 15$ ns. These K^+/π^+ fibers do not occur in π_{scat} samples, due to the large delayed-coincidence requirement. Since the π_{scat} sample was chosen to calibrate TGDEDX, due to the large π^+-momentum spectrum in π_{scat}'s, TGDEDX was modified to use a corrected *etg* which excluded π^+ energy from a K^+ flagged fiber (this was a local change to *etg*, specific for this cut only). No *rtg* modification was needed, since the decay vertex is not effected in comparing a signal sample to a π_{scat} sample, in this regard. Hence, all references to *etg* in Section 7.3 refers to the "corrected" π^+ TG energy.

7.3.3 TGdEdX Calibration

The expected target range, rtg_{exp} requires precise calibration to maximize the efficiency of TGDEDX. A fit of the *rtg* distribution for each *ptot*-*etg* bin (i.e. *ptot*-*etg* spectrum-slice) yielded a mean (rtg_{exp}) and sigma (σ_{exp}) which was utilized by Eq. (1). The calibration process used $\pi_{scatter}$ monitors in the π^+-band region. The cuts used to determine the final calibration sample are shown in Table 12. This sample is created by applying cuts which will yield events with only one well reconstructed π^+ track.

$Kpiang > \theta$ selects events which undergo a scatter in the x-y plane; the angle, θ, was determined by the following points: (1) K^+-entering position, (2) "decay vertex" (i.e. scattering vertex), and (3) the position where the π^+ left the TG. The angle θ was set at 35° and 55° in an attempt to construct a clean calibration sample. A π_{scat} event's reconstructed decay vertex would be close to the scattering vertex, but the lack of a delayed coincidence makes the reconstruction process fraught with peril. However, $\pi_{scatter}$ events with a large θ have improved decay-vertex determination by the TG-reconstruction algorithm due to geometrical information available in x-y scattered events (a precise decay-vertex measurement was the key determination to reliable target range). A further sample was created by applying the tighter (30% acceptance) PV cut; to avoid bias the TG photon-veto was excluded. Ultimately these (ideally) better samples contained insufficient statistics for proper calibration. However, studies were performed employing these improved samples to validate the use of the high-statistics sample used to determine all $(2\times5\times15)$ rtg_{exp} and σ_{exp} parameters. The parameter values are plotted in Figures 15-17.

The kumacs used to produce the calibration values and plots seen in this note are stored at `~benjil/bkg/studies/tgdedx/calib/`. The calibration histograms were created from histograms embedded in the piscat acceptance study, see `~/bkg/src/piscatacc.f` and

`~/bkg/src/special_plots.f`. The acceptance measurement on TGDEDX was done using Kpi2 monitors, see `~/bkg/src/kp2acc.f`.

A Piscat sample with a better determination of the decay vertex was obtained by making a cut a *kpiang*, the angle made from the Kaon entering position, decay vertex, and the exiting value of the Pion. An angle of 55° was required in this sample. An additional sample was created by applying the 30% acceptance PV cut, instead of the 60%. The calibration parameters, for TGDEDX, were determined and we measured the effect on the Kpi2 monitor sample. Figure 22 shows that there is no difference between the E949 calibration and the tighter PV sample.

A small difference is observed between the E949 and the calibration with $kpiang > 55°$ required. Figure 19 show that there is no noticeable dependence on *etg* for the different calibration sets (most relevant points in Figure 19 are *ptot bin 5*).

Cut name	Events remaining (Acc)
$BADRUN$	5859925 (-)
$RDTRK\ TRKTIM$	5856748 (-)
$TARGET\ STLAY$	4949979 (-)
$UTC\ PDC\ RDUTM$	2833580 (-)
$ICbit$,$b4abm2 < 1.3MeV$	1986916 (-)
$\lvert t_\pi - t_{RS}\rvert \geq 5$	1881543 (-)
$\lvert ictime - t_{RS}\rvert \geq 5$	1847951 (-)
$TGCUT\ BADSTC$	1508139 (-)
$tgqualt$,$npitg$	1435572 (0.951883)
$timcon$	1430524 (0.996484)
$tgtcon$	1390018 (0.971685)
$b4etcon$	1360826 (0.978999)
$targf$	1278186 (0.939272)
$dtgttp$	1278117 (0.999946)
$rtdif$	1181683 (0.92455)
$eiccon$	1149627 (0.972873)
$ticcon$	1149616 (0.99999)
$pigap$	1034138 (0.899551)
$tgdb4$	886404 (0.857143)
$tgdb4tip$	561715 (0.633701)
$tgdvxtip$	466019 (0.829636)
$tgdvxpi$	427166 (0.916628)
$phivtx1$	315481 (0.738544)
$pv(not\ tg)$ 60%	87063 (0.275969)
$cos3d$	76823 (0.882384)
$utcqual$	72564 (0.944561)
$rngmom$	65767 (0.906331)
$rsdedxmax$,$rsdedxcl$	41896 (0.637037)
$rslike$	41429 (0.988853)
$tgz > -10.$	41244 (0.995535)
Final E949 calibration used this sample.	
The following are cleaner “decay vertex” samples	
$Kpiang > 35°$	23662 (0.573708)
$Kpiang > 55°$	**14323** (0.605317)

Table 12: Generated $\pi_{scatter}$ sample for TGDEDX calibration. Numbers in parenthesis are acceptances of that cut.

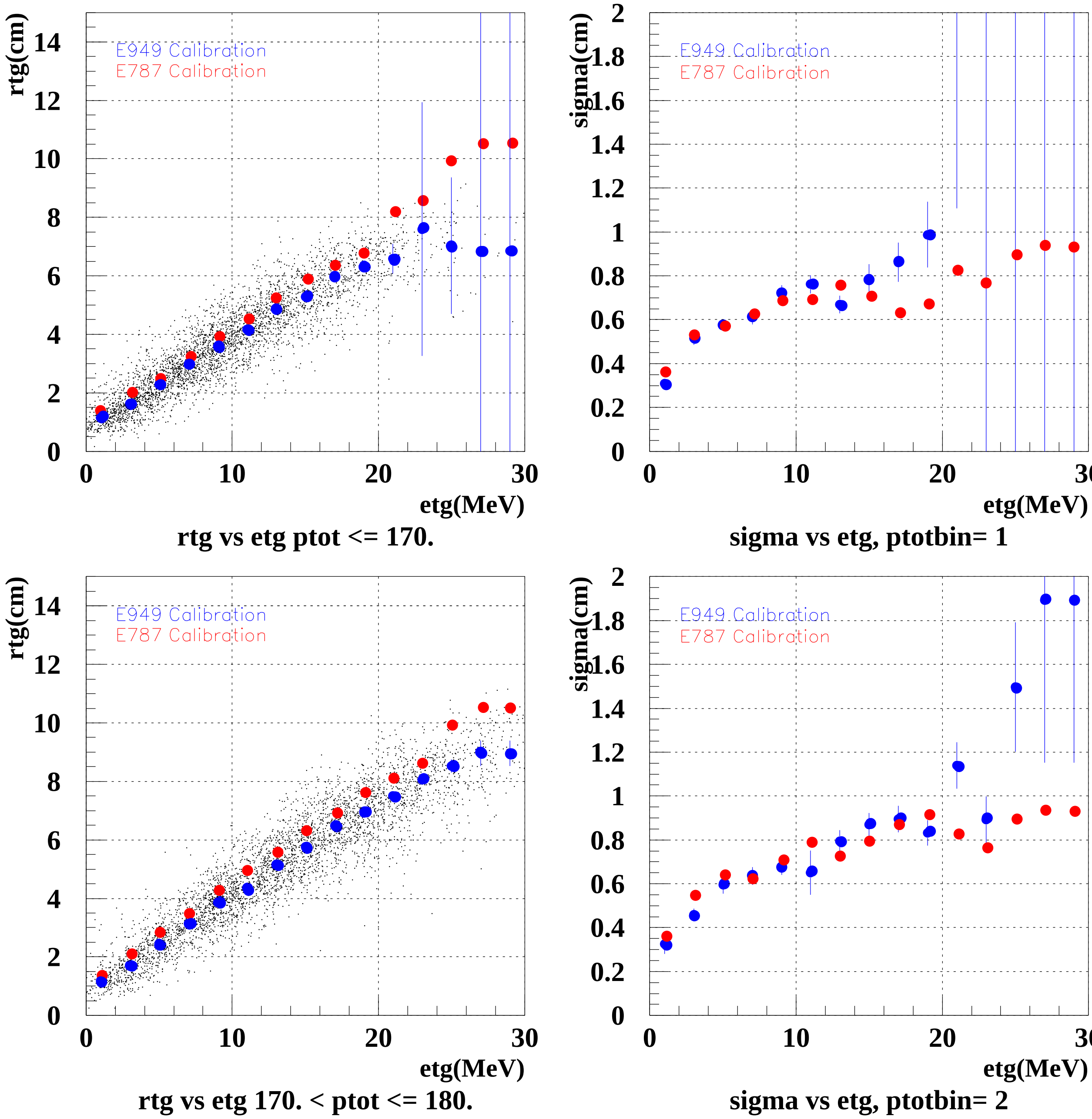

Figure 15: Calibration of new rtg_{exp} (left) and σ_{exp} (right) values for $ptot$ bins 1 (top) and 2 (bottom). Red (blue) points are the E787 (E949) parameter values. The errors shown are the uncertainty on the fitted parameter from a gaussian fit. Black points are the calibration sample.

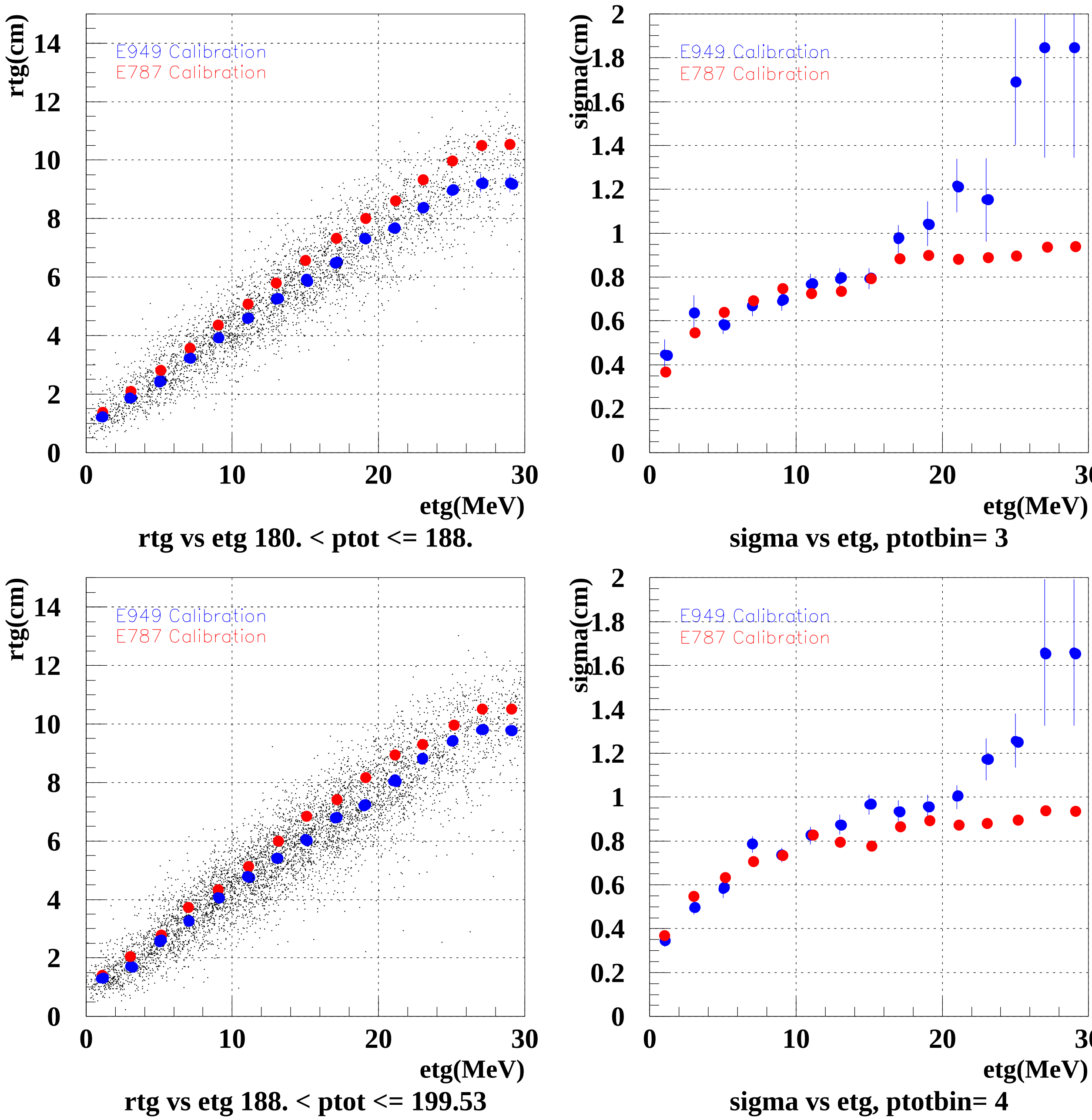

Figure 16: Calibration of new rtg_{exp} (left) and σ_{exp} (right) values for $ptot$ bins 3 (top) and 4 (bottom). Red (blue) points are the E787 (E949) parameter values. The errors shown are the uncertainty on the fitted parameter from a gaussian fit. Black points are the calibration sample.

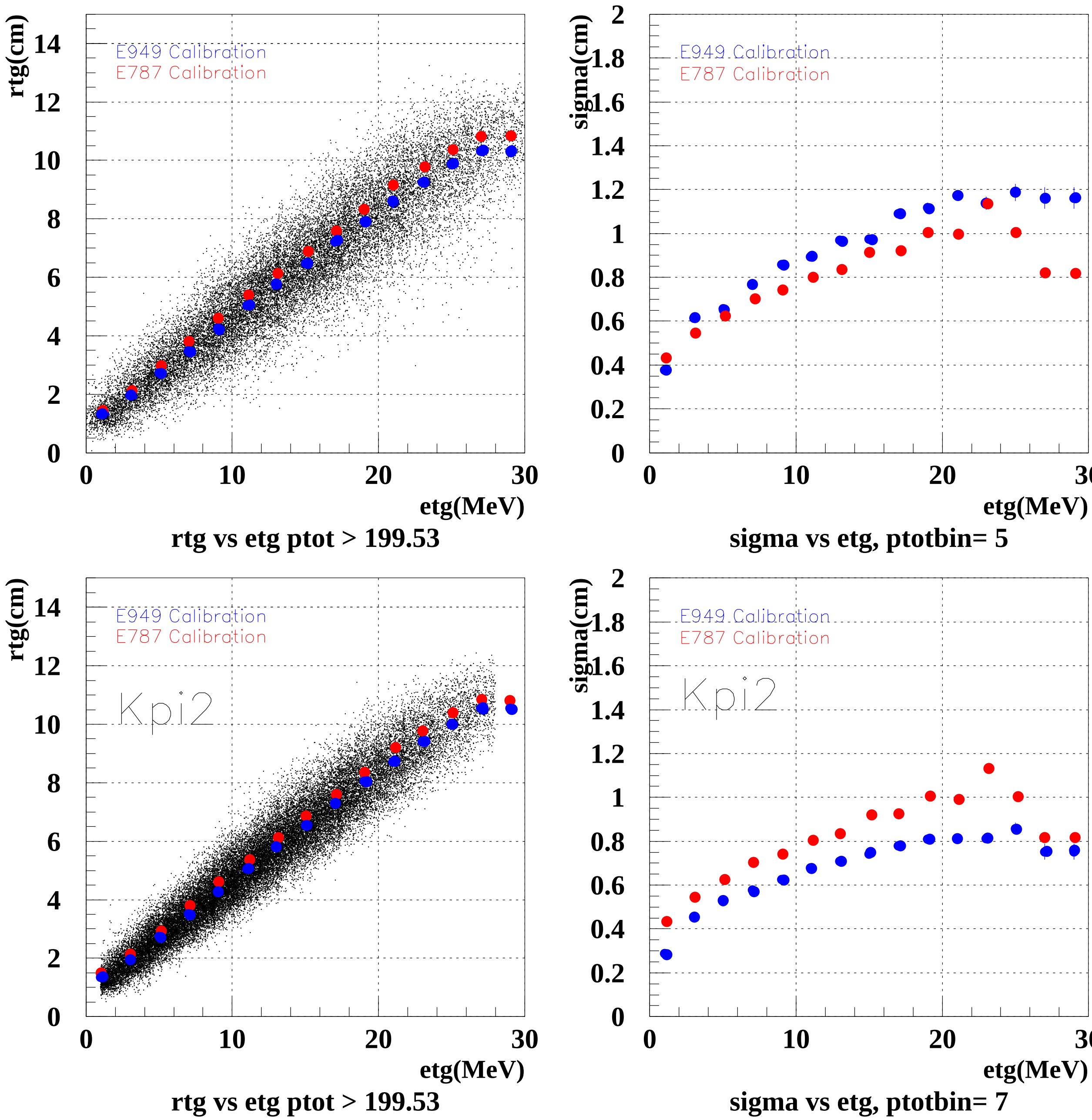

Figure 17: Calibration of new rtg_{exp} (left) and σ_{exp} (right) for $ptot$ bin 5 (top). The bottom plots, labeled "ptotbin = 7", were from the calibration process on $K_{\pi 2}(1)$ monitors; only used as a check. Red (blue) points are the E787 (E949) parameter values. The errors shown are the uncertainty on the fitted parameter from a gaussian fit. Black points are the calibration sample.

7.3.4 Parameters

The rtg_{exp} and σ_{exp} values are listed below in the five $ptot$ bins, rtg^N_{exp}, σ^N_{exp} such that

- $N = 1:$ $ptot < 170$ MeV/c
- $N = 2:$ 170 MeV/c $< ptot \leq 180$ MeV/c
- $N = 3:$ 180 MeV/c $< ptot \leq 188$ MeV/c
- $N = 4:$ 188 MeV/c $< ptot \leq 199.53$ MeV/c
- $N = 5:$ $ptot > 199.53$ MeV/c

The 15 numbers in each of the following lines are for $etg = 1MeV$,$3MeV$,..., $29MeV$.

7.3.5 E787 Parameters

rtg^1_{exp} = 1.41,1.99,2.51,3.28,3.92,4.56,5.23,5.88,6.30,6.77,8.2,8.6,9.95,10.5,10.5
σ^1_{exp} = 0.36,0.53,0.57,0.62,0.69,0.70,0.76,0.71,0.64,0.67,0.83,0.77,0.90,0.93,0.93
rtg^2_{exp} = 1.41,2.09,2.82,3.50,4.29,5.02,5.62,6.31,6.96,7.60,8.17,8.58,9.95,10.5,10.5
σ^2_{exp} = 0.36,0.54,0.64,0.62,0.71,0.79,0.72,0.79,0.88,0.91,0.83,0.77,0.90,0.93,0.93
rtg^3_{exp} = 1.41,2.09,2.82,3.53,4.36,5.05,5.83,6.60,7.29,7.99,8.61,9.33,9.95,10.5,10.5
σ^3_{exp} = 0.36,0.54,0.64,0.70,0.74,0.72,0.73,0.79,0.89,0.90,0.87,0.89,0.90,0.93,0.93
rtg^4_{exp} = 1.41,2.09,2.82,3.72,4.28,5.17,6.06,6.83,7.39,8.17,8.93,9.33,9.95,10.5,10.5
σ^4_{exp} = 0.36,0.54,0.64,0.71,0.73,0.83,0.79,0.78,0.86,0.90,0.87,0.89,0.90,0.93,0.93
rtg^5_{exp} = 1.48,2.15,2.97,3.75,4.58,5.37,6.10,6.84,7.64,8.36,9.16,9.77,10.38,10.83,10.83
σ^5_{exp} = 0.44,0.54,0.62,0.71,0.74,0.80,0.84,0.91,0.92,1.0,0.99,1.14,1.0,0.81,0.81

7.3.6 New E949 Parameters

rtg^1_{exp} = 1.15,1.64,2.27,2.96,3.59,4.16,4.83,5.29,5.95,6.35,6.58,7.,7.5,8.0,8.0
σ^1_{exp} = 0.31,0.52,0.57,0.61,0.72,0.76,0.67,0.79,0.86,0.99,1.04,1.28,1.28,1.28,1.28
rtg^2_{exp} = 1.17,1.69,2.45,3.15,3.86,4.35,5.17,5.77,6.49,6.91,7.50,8.05,8.53,8.96,8.96
σ^2_{exp} = 0.33,0.46,0.60,0.64,0.68,0.65,0.79,0.87,0.90,0.83,1.14,0.89,1.50,1.89,1.89
rtg^3_{exp} = 1.20,1.87,2.46,3.23,3.91,4.59,5.29,5.91,6.50,7.34,7.67,8.35,8.95,9.21,9.21
σ^3_{exp} = 0.45,0.64,0.59,0.67,0.69,0.77,0.79,0.79,0.97,1.04,1.22,1.15,1.69,1.85,1.85
rtg^4_{exp} = 1.29,1.71,2.61,3.29,4.08,4.77,5.43,6.07,6.76,7.27,8.04,8.78,9.40,9.80,9.80
σ^4_{exp} = 0.35,0.49,0.58,0.78,0.74,0.82,0.87,0.97,0.94,0.96,1.00,1.17,1.26,1.66,1.66
rtg^5_{exp} = 1.32,1.96,2.74,3.50,4.27,5.04,5.76,6.47,7.21,7.91,8.59,9.25,9.88,10.30,10.30
σ^5_{exp} = 0.38,0.61,0.66,0.77,0.86,0.89,0.97,0.97,1.09,1.12,1.17,1.14,1.19,1.16,1.16

7.3.7 Manual changes

The fit for $ptot < 170$ MeV/c and $etg > 20MeV$ was very poor due to lack of statistics. Therefore, the rtg_{exp}'s were set by visual inspection of this sample with consideration given to the linear nature of the rtg_{exp} with respect to etg. Five bins corresponding to the largest etg values were set by this visual inspection method. These last four σ_{exp} values were determined by combining the events from the last four bins, $20\text{MeV} < etg < 30\text{MeV}$ (to create a sample with sufficient statistics). The σ_{exp} for the $etg = 19\text{MeV}$ bin was determined by extending the etg-slice to $17\text{MeV} < etg < 21\text{MeV}$.

From fits,
rtg^1_{exp} = 1.15,1.64,2.27,2.96,3.59,4.16,4.83,5.29,5.95,6.35,6.58,7.60,7.03,6.84,6.84
σ^1_{exp} = 0.31,0.52,0.57,0.61,0.72,0.76,0.67,0.79,0.86,0.99,2.02,3.64,3.84,12.70,12.70
were changed by visual inspection to the following:
rtg^1_{exp} = 1.15,1.64,2.27,2.96,3.59,4.16,4.83,5.29,5.95,6.35,6.58,7.,7.5,8.0,8.0
σ^1_{exp} = 0.31,0.52,0.57,0.61,0.72,0.76,0.67,0.79,0.86,0.99,1.04,1.28,1.28,1.28,1.28

7.4 Calibration Validity

To determine if the calibration removed an observed energy (etg) dependence, plots of rtg_{exp} from various samples, such as E787, E949, $kpiang > \theta$, PV_{tight}, were performed. The flat distributions (except for the low momentum bin, "ptot bin 1") in Fig. 18 indicates that TGDEDX acceptance no longer has an energy dependence. Also, Fig. 19 shows that there was no noticeable dependence on etg for the different calibration samples; most relevant set of points in Fig. 19 is "*ptot*-bin 5".

Fig. 20 shows the difference in $like_{tgdedx}$ values before and after calibration. By matching distributions from Fig. 20 to the different hypothetical samples shown in Fig. 21 two things are evident:

- The top plot of Fig. 20 and the "$Mean < 0.0$" (light blue), from Fig. 21, distribution appear similar in overall shape. Thus, E787 parameters appears to have an offset in the mean, which is also shown in Figures 15-17 as a systematic vertical displacement of the E787 parameters compared to the newly calibrated values.

- The bottom plot of Fig. 20 and the "$Sigma < 0.0$" (dark blue), from Fig. 21, distribution appear similar in shape. This implies that the calibration sample (π_{scat}) had worse resolution than the acceptance sample ($K_{\pi 2}$), an expected effect from better determination of the decay vertex in $K_{\pi 2}$ events. A plot of $like_{tgdedx}$ for π_{scat}'s using the updated calibration parameters, not shown, yielded a flat distribution (as it should). Since calibration of TGDEDX employed the entire π_{scat} sample, the acceptance measurement of TGDEDX (Section 15) has to be performed on $K_{\pi 2}$ monitors, otherwise a bias would occur.

Obtaining consistent results on an independent sample, such as $K_{\pi 2}$, would validate that the calibration sample used was a proper sample. Thus, distributions associated with TGDEDX were measured on a $K_{\pi 2}$ monitor sample for the (updated) E949 calibration. Fig. 22 shows no difference discernible between the calibration sample and the cleaner sample with the tight PVPNN2 applied. As shown in Fig. 22(a), a small difference at large $like_{tgdedx}$ was observed between the calibration sample and the calibration sample with $kpiang > 55°$ requirement. Again, this was expected due to $kpiang > 55°$ having better resolution in rtg due to better decay-vertex finding.

Figure 21, created by `~benjil/bkg/studies/tgdedx/calib/error_function.kumac` , shows the shape of the distribution for different offsets in the mean and sigma of the gaussian fit.

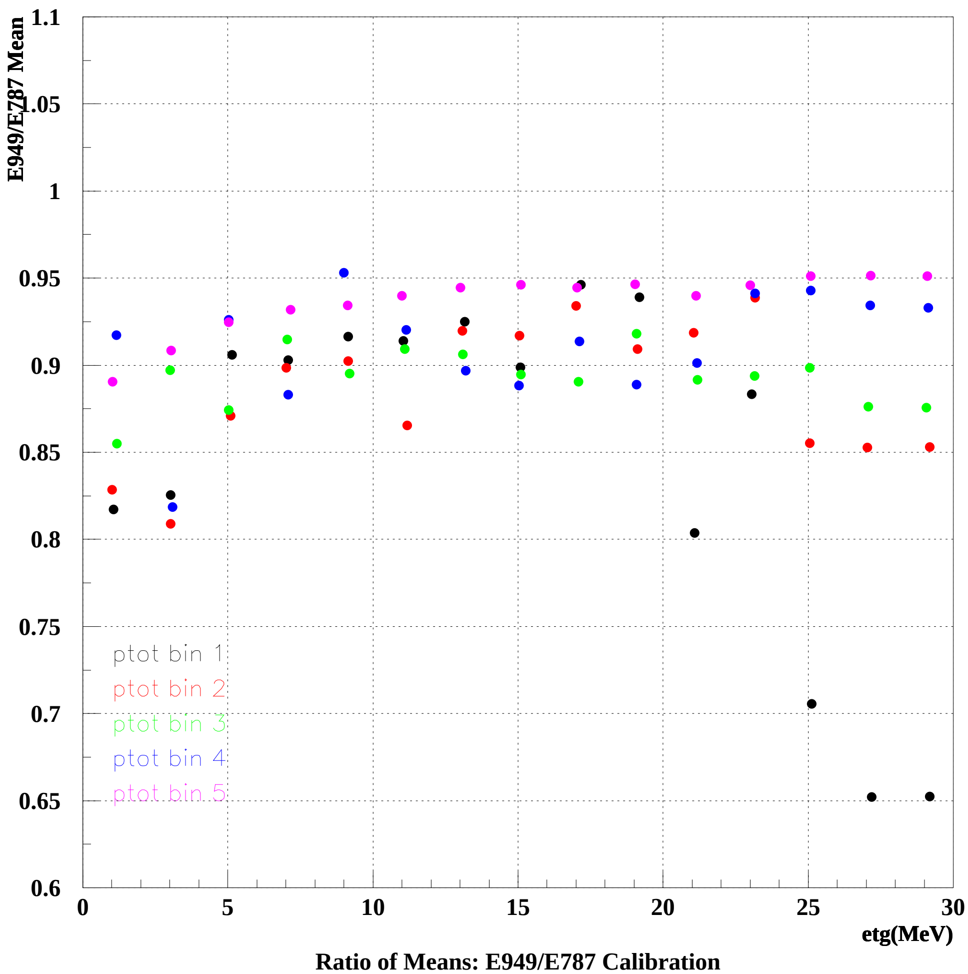

Figure 18: Ratios of the rtg_{exp} E949 to E787 parameters. The points on the lower right ("ptot bin 1" with large *etg*) have low statistics and the E949 values for these parameters were later changed by visual inspection.

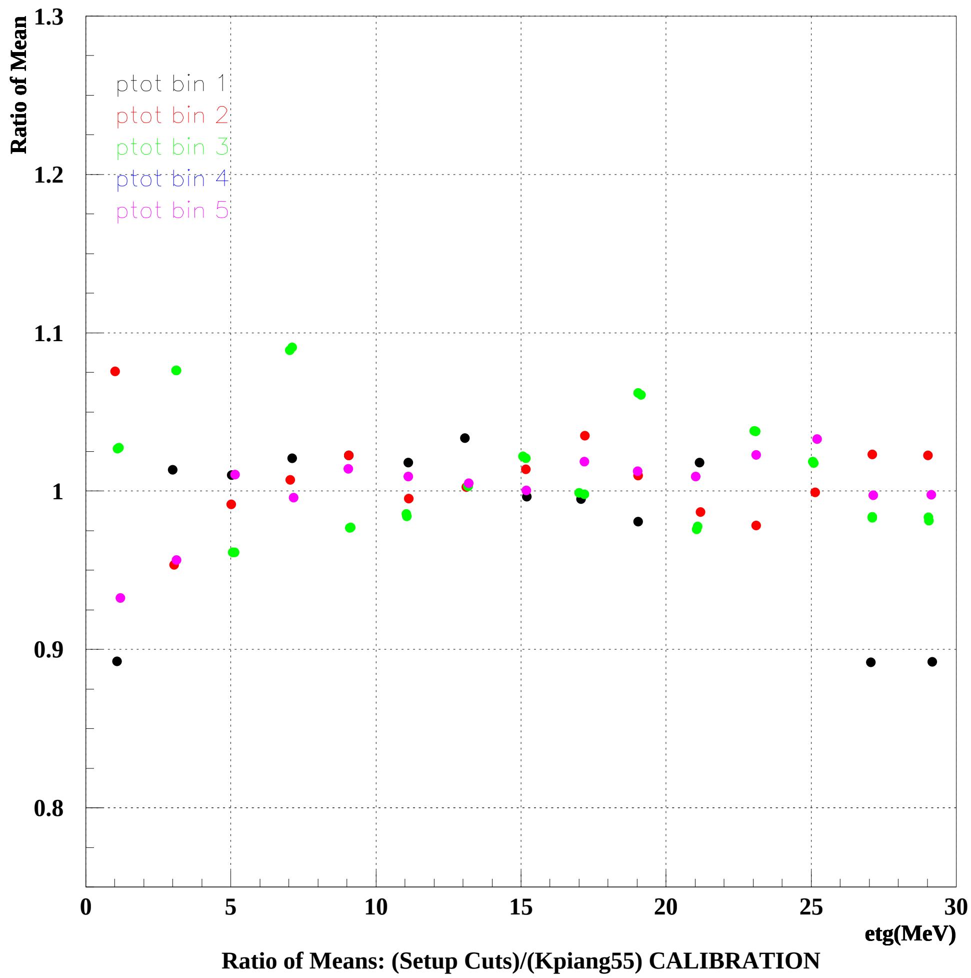

Figure 19: Ratio of rtg_{exp} (Means) determined by the sample chosen (Setup cuts) and the enhanced decay-vertex sample ($kpiang > 55$).

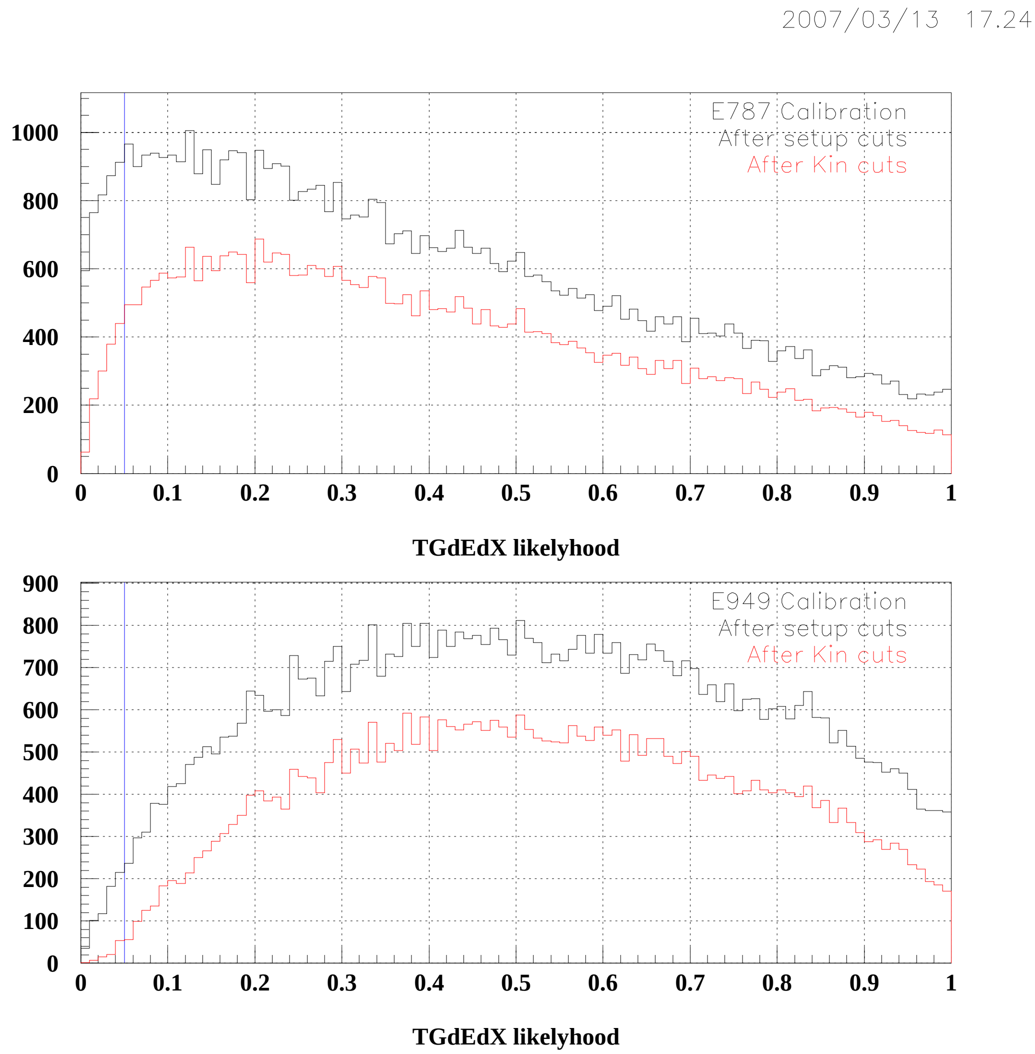

Figure 20: $like_{tgdedx}$ distributions before and after calibration ("E787 Calibration" means before calibration). "Setup cuts" are cuts applied before TGDEDX cut was applied, as seen in Table 60. The "Kin cuts" are all cuts in the acceptance study except for TGDEDX (i.e. TGDEDX applied last). Events left of the blue line (0.05) are removed by TGDEDX.

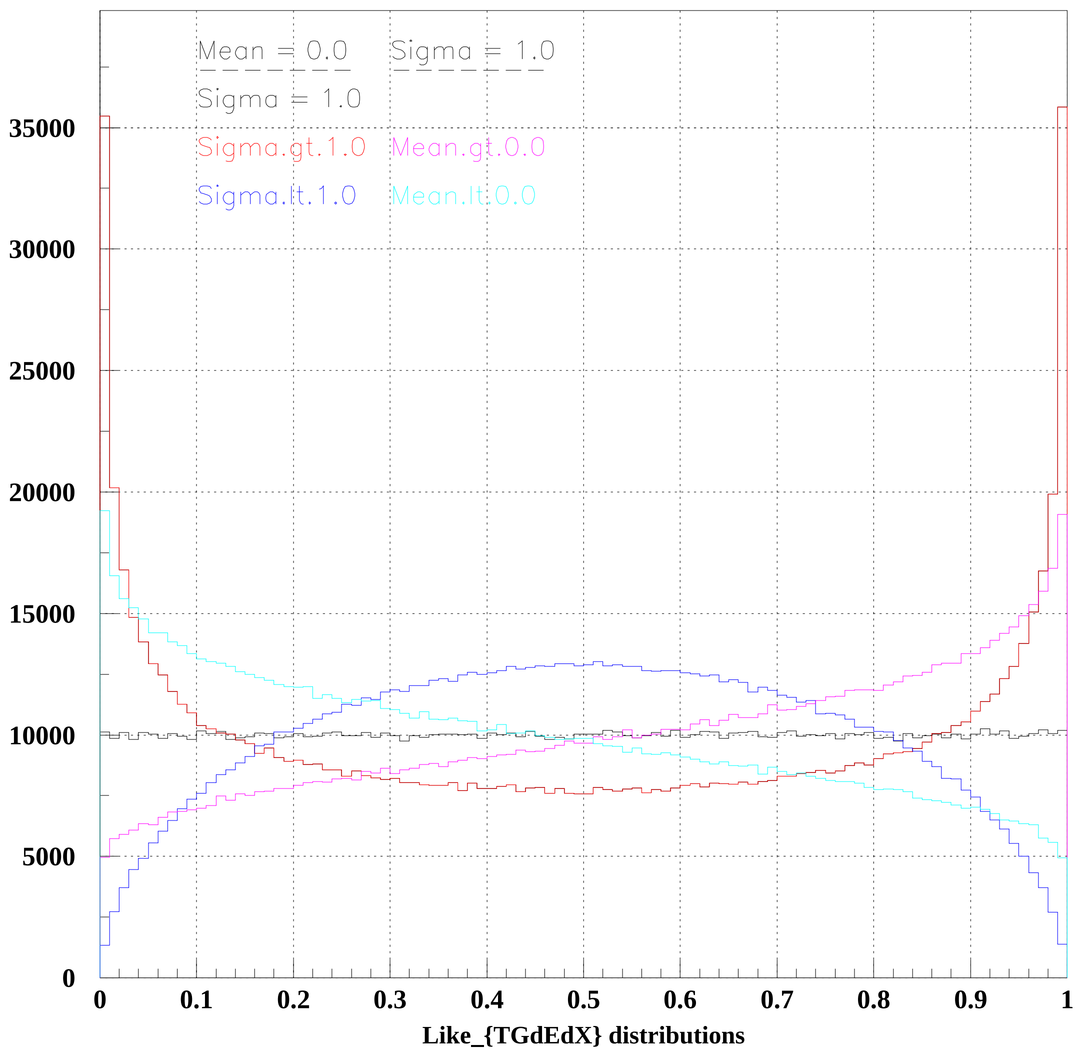

Figure 21: Expected $like_{tgdedx}$ distributions for different "improperly" calibrated parameters (in colors) and properly calibrated parameters (in black). $Mean = rtg_{measured} - rtg_{exp}$ and $Sigma = \sigma_{exp}/\sigma_{true}$. $Mean = 0$ for the $Sigma = 1$ (black, flat curve), $Sigma > 1$ (red U-shaped), and $Sigma < 1$ (dark blue, upside-down U-shaped) curves. $Sigma = 1.0$ for the $Mean > 0.$ (magenta,/-shaped) and $Mean < 0.$ (light blue,\-shaped) curves.

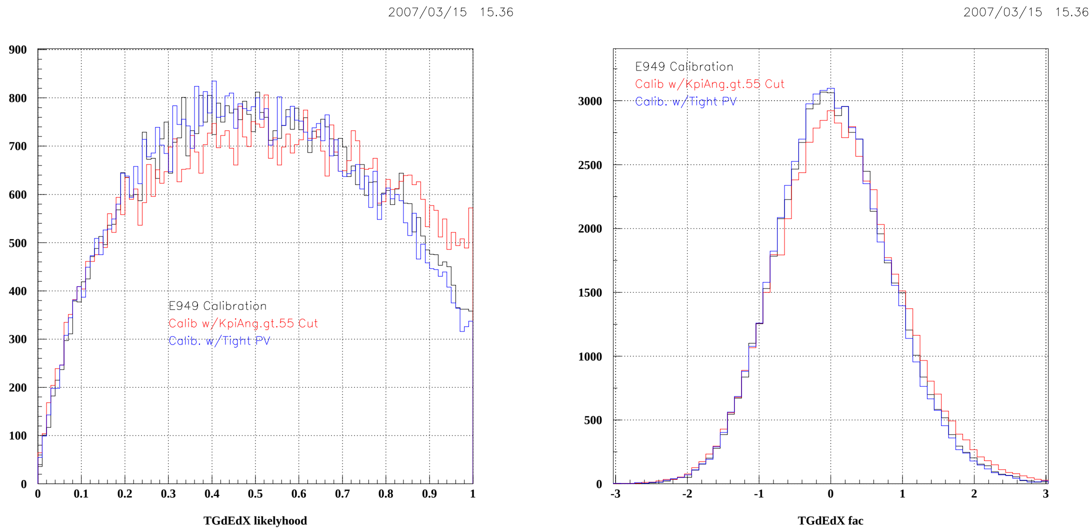

(a) $like_{tgdedx}$ (b) $\frac{rtg-rtg_{exp}(etg,ptot)}{\sigma_{exp}(etg,ptot)}$

Figure 22: Comparison of the possible calibration samples. Plot (a) is TGDEDX's likelihood value, $like_{tgdedx}$, after different calibration samples were used. Plot (b) is the value given to the error function as indicated in Eq. (1). The "E949 Calibration", in black, is the high-statistics sample chosen for the final calibration. The red (blue) distribution is for the better-determined-decay-vertex (tight photon-veto) sample.

If we plot $Like_{TGdEdX}$ for piscats using the updated calibration parameters then we would see a flat distribution. When we measure $Like_{TGdEdX}$ on Kpi2's, Figure 22, we observe a symmetric distribution with a slight offset to larger values.

This implies that our calibration sample has worse resolution that our acceptance sample. This is most likely due to a better determination of the decay vertex in Kpi2's.; Measurement of the decay vertex is the key determination of the target range (rtg).

To determine if the calibration removes the energy (etg) dependence, I plotted the ratio of the E949 calibration means to the E787 calibration means. Figure 18, indicates that we are calibrating out any energy (etg) dependence.

7.4.1 TGdEdX Acceptance Sample

E787-PNN2 measured TGDEDX acceptance of 0.9858. The TGDEDX acceptance measurement employed in this calibration was the same used in Section 15.5. Using E787-PNN2 calibration parameters on E949 data yielded an acceptance of 0.9339. The newly calibrated TGDEDX acceptance was measured to be 0.9893 ± 0.00042 (see Section 15.5), which is consistent with the E787-PNN2 measured value.

Cut Applied	Events remaining (Acc)
SetupOPS	62149 (-)
opsveto	60535 (-)
TGPVCUT	**59882** (-)
TGDEDX	59231 (0.989129)
tger	59215 (0.99973)
tgenr	57283 (0.967373)
*tglike*1	56252 (0.982002)
*tglike*2	55351 (0.983983)
TGLIKE	55351 (1)
epitg	49614 (0.896352)
epimaxk	49614 (1)
tgedge	49348 (0.994639)
drp	49263 (0.998278)
*chi*567 *Loose*	42369 (0.860057)
chi5max	**39447** (0.931034)
Total Acc.	0.658746 ± 0.00269197

Table 13: Kpi2 TG-kinematic Acceptance

7.4.2 TGdEdX Rejection Sample

E787 tuned the cut to $Rej_{TGDEDX} = 1.44$; however, due to correlation with CHI567, TGDEDX had no rejection after all cuts in E787. Table 14 shows the sample selection for measuring Rej_{TGDEDX} in E949. $TGDEDX_{uncorr}$, denoted in red, shows a rejection of 1.35 before uncorrelated cuts are applied. After applying the correlated cuts (EPITG, EPIMAXK, CHI567, CHI5MAX), a rejection of 1.07 was measured. The $like_{tgdedx}$ distributions for the acceptance and rejection samples are shown in Fig. 23.

Cut Applied	Events remaining (Rej)
$BADRUN$	30408052 (0.00)
$DUPEV$	30408048 (1.00)
$TRIGGER$	15232707 (2.00)
$ICbit$	15232564 (1.00)
$lhex$	15232564 (1.00)
DC	15232516 (1.00)
$Lev11$	15232516 (1.00)
RD_TRK	15232515 (1.00)
$TRKTIM$	15232515 (1.00)
$TARGET$	15232515 (1.00)
$STLAY$	15232515 (1.00)
UTC	15232515 (1.00)
$RDUTM$	15232515 (1.00)
BAD_STC	15232515 (1.00)
PDC	15232515 (1.00)
$pv(not\ tg)\ Loose60$	12954315 (1.18)
$TGCUT$	7142934 (1.81)
$tgqualt$	6765533 (1.06)
$npitg$	6765533 (1.00)
$timcon$	6685429 (1.01)
$tgtcon$	6316877 (1.06)
$b4etcon$	6184009 (1.02)
$DCBIT$	6184009 (1.00)
$DELCO$	4280023 (1.44)
$Delc\ Loose$	3595811 (1.19)
$PSCUT$	2185154 (1.65)
$b4dedx$	2169877 (1.01)
$bwtrs$	1799849 (1.21)
$cpitrs$	1797020 (1.00)
$cpitail$	1796540 (1.00)
$cktrs$	1781679 (1.01)
$cktail$	1762093 (1.01)
$b4trs$	1674587 (1.05)
$b4ccd$	1650344 (1.01)
$upvtrs$	1623531 (1.02)
$rvtrs$	1615563 (1.00)
$tggeo$	1060126 (1.52)
$b4ekz$	886102 (1.20)

continued on next page

Cut Applied	Events remaining (Rej)
tgzfool	870567 (1.02)
targf	826789 (1.05)
dtgttp	826779 (1.00)
rtdif	819240 (1.01)
tgktim	811136 (1.01)
eiccon	792084 (1.02)
ticcon	792075 (1.00)
pigap	774063 (1.02)
tgdb4	760772 (1.02)
tgdb4tip	752741 (1.01)
tgdvxtip	746892 (1.01)
tgdvxpi	729199 (1.02)
TGB4	729199 (1.00)
phivtx1	672405 (1.08)
ccdpul	166933 (4.03)
timkf	149649 (1.12)
verrng	135863 (1.10)
angli	135717 (1.00)
ALLKfit	133136 (1.02)
tpics	133047 (1.00)
kic	133004 (1.00)
epionk	132901 (1.00)
BOX Loose	12503 (10.63)
icodel14	12503 (1.00)
cos3d	12181 (1.03)
layv4	12181 (1.00)
zfrf	12158 (1.00)
zutout	12134 (1.00)
FIDUCIAL	12134 (1.00)
utcqual Loose	11226 (1.08)
prrf1	10855 (1.03)
prrfz	9906 (1.10)
PRRF	9906 (1.00)
rsdedxmax	9406 (1.05)
rsdedxcl	6725 (1.40)
rslike	6725 (1.00)
RSDEDX	6725 (1.00)
rngmom	1016 (6.62)
tgdb4	1016 (1.00)
tgdb4tip	1016 (1.00)
tgdvxtip	1016 (1.00)
tgdvxpi	1016 (1.00)
TGB4	1016 (1.00)
piflg	990 (1.03)
elveto	924 (1.07)
tdfool	920 (1.00)
tdvarnn02 Loose	849 (1.08)
TD *Loose*	**849** (1.00)
TGDEDX	**629** (1.35)
epitg	551 (1.54)
epimaxk	551 (1.00)
chi567 Loose	415 (1.33)
chi5max	389 (1.07)
TGDEDX	**365** (1.07)

Table 14: TGDEDX Rejection Table. The red TGDEDX was the value before correlated cuts were applied, and the black TGDEDX(last line) is the rejection after all cuts are applied.

7.4.3 TGdEdX Results

The numbers outlined in Section 7.3.6 were officially utilized by the cut due to low statistics limitations in the other samples (*kpiang* $> 55°$, PV(not TG) 30%). Comparisons of the cleaner samples to the high-statistics sample (the sample ultimately chosen) did not show any significant differences in TGDEDX variables, see Figures 22-19. In addition, the *kpiang* $> 55°$, PV(not TG) 30% samples were lacking statistics in the lower-momentum bins. The consistency with E787's measured value indicates the calibration was done successfully. Table 15 shows that TGDEDX is capable of removing backgrounds after all other cuts are applied; as opposed to E787, in which TGDEDX remained in the analysis as a safety cut.

Determining TGDEDX's cut threshold, or cut value, (nominal value was 0.05) is shown

Experiment	*Acc*	*Rej*	*Acc* × *Rej*
E787	0.9858	1.44	1.42
E949	0.989	1.35	1.34
After all cuts			
E787	0.9858	1.00	0.986
E949	0.989	1.07	1.06

Table 15: TGDEDX *Acceptance* × *Rejection*. The TGDEDX cut is $like_{tgdedx} < 0.05$.

in Fig. 24. The *acceptance*, $rejection$, and *acceptance*×$rejection$ was plotted as a function of the cut value. The lower plot, *acceptance* × $rejection$, indicates that improvement in signal-to-background by tightening this cut (to a larger threshold). However, due to the lack of an inflection point in the *acceptance*×$rejection$ versus *cut value* shape leads to the conclusion that setting the threshold to 0.05 gives the benefit of keeping the acceptance loss small. Therefore, the threshold was left at the E787 value of 0.05.

7.5 Target Gap between K^+ and Pion Fibers (TARGF)

Require the identified K^+ cluster to be contiguous with π^+ fibers by rejecting events with the minimum distance between K^+ and π^+ fibers greater than 0.6 cm (i.e. more than one fiber). $K_{\mu 2}$ monitors are used to measure an acceptance of 0.9678 ± 0.00013 and an acceptance of 0.9705 ± 0.00022 after all correlated cuts are applied.

7.6 Tag Gaps between K^+ and Charged Track (KPIGAP)

KPIGAP is a specialized function used to tag events where the π^+ track does not emerge from the K^+ fibers in the TG. TARGF will do this in ideal situations. However, the *swathccd* algorithm has limitations placed upon the energy of the charged track. This limitation can mask possible K^+ decays where the charged track emerges from the K^+ identified stopping position. TG π^+ scatters have this quality. *swathccd* will likely reconstruct high-energy scatter pion-fiber hits as photon hits. KPIGAP searches for coincident photon fibers (within 3.0 ns of t_{RS}) that can fill the gap. If the gap between the K^+ and π^+ fibers are bridged with coincident photon fibers, then do not tag the event. KPIGAP is used only in the beam and CEX background measurements to tag a cleaner, compared to previous analyses, sample. In past analysis, $\overline{TARGF}$ was used to tag the background samples used in 2-beam and CEX backgrounds. This cut is not applied in normalization branches of backgrounds or the final signal box, so no acceptance was measured.

7.7 CHI567

The track fitter of charged pion in the target gathers the energy deposit and position information of all possible pion fibers considers whether they agree with the UTC track curvature and momentum. A detailed description can be found in [2]. CHI567 is one of output this fitter. A cut on CHI567 may remove target scattering background. (CHI567 is the sum of the 5^{th}, 6^{th} and 7^{th} terms in the χ^2 of the fitter.) CHI5 tells whether the energy deposit in each fiber agrees with that expected from dE/dx for the energy resolution of the target fiber. CHI6 and CHI7 are penalty terms in the fitter corresponding to the case of a fiber without energy but the track is projected to traverse the fiber and the case of a fiber with energy, but the track is not projected to traverse it, respectively.

Just like the rest of us, target fibers have to face an aging problem. This is thought to induce a dramatic lowering of the acceptance of the CHI567 cut. From an independent calibration for target fibers done by Benji and from a direct tuning of the probability of CHI567, a degradation of more than 20% in energy resolution is found with respect to E787. A correction factor, 1.621, is introduced to redefine the CHI5 contribution to CHI567,

$$CHI567 = CHI5/1.621 + CHI6 + CHI7 \ .$$

After this redefinition and optimization, the cut on the probability of CHI567 is set at 0.015.

A bug in this target fitter was also rectified for the E949 pnn2 analysis. MINUIT is used in this fitter. The last action it takes is to vary the fitted parameters and find out the errors on these parameters. The best estimation of these parameters are kept by MINUIT. However, if some quantities are extracted from these parameters, one must remember to use the final fitted result, and not those still in fitting process. In principle it is supposed to affect every event and also affect all CHI567 related cuts, such as CHI5MAX, ANGLI, etc. But only for some events this correction will show significant changes. Correction of this bug did not have a significant effect on either the global acceptance and rejection.

7.8 B4EKZ

B4EKZ is a likelihood based on the consistency of the the B4 energy, EK and TGZ. As this cut was found to have some rejection as $K_{\pi 2}$ scatters in the target, we use the tighter cut of B4EKZ > 10 as recommended by previous pnn2 analysis [1] instead of the the pnn1 level of B4EKZ > 2.

7.9 TGZFOOL

The TGZFOOL cut requires the reconstructed z of the kaon decay (TGZ) to be in the fiducial volume of the target, TGZ > -5 cm. This cut eliminates $K_{\pi 2}$ scatters in the target as well as beam pions that scatter in B4 [1]. In E949 pnn1, this requirement had been loosened to > -15 cm.

7.10 EPIONK

The target reconstruction by SWATHCCD is capable of finding a second pulse from a pion in kaon fiber for large decay times and/or a small kaon energy deposit in the fiber. The EPIONK cut is a requirement that the energy of the second pulse be less than a certain value (1.5 MeV for E787 pnn2 [2]). Modifications to the CCDPUL fitter for E949 moved some events that had been subjected to the CCDPUL cut to be subjected to the

EPIONK cut instead. To ensure consistency, the EPIONK cut was set to the same value as the CCDPUL cut of 1.25 MeV.

7.11 Discarded Cuts

We briefly explain why target cuts used the E787 pnn2 or E949 pnn1 analysis were discarded for this analysis.

7.11.1 B4TIM

The B4TIM cut rejects events when the B4 strobe time differs from the kaon time in the target by more than 2 ns [2]. This cut was required to enable the CCDPUL fit algorithm to be reliable for the E787 pnn2 analyses. With the modifications described in this note, the B4TIM cut was no longer needed for CCDPUL reliability. Since B4TIM has a $\sim$3% acceptance loss and does not suppress background, it was discarded for E949. Extensive studies showed that background rejection on the "late kaons" admitted by removing this cut was consistent with the overall background rejection.

7.11.2 PBG

Since the lead glass detector in the beam was replaced by the active degrader, we discarded PBG, the cut based on the lead glass detector.

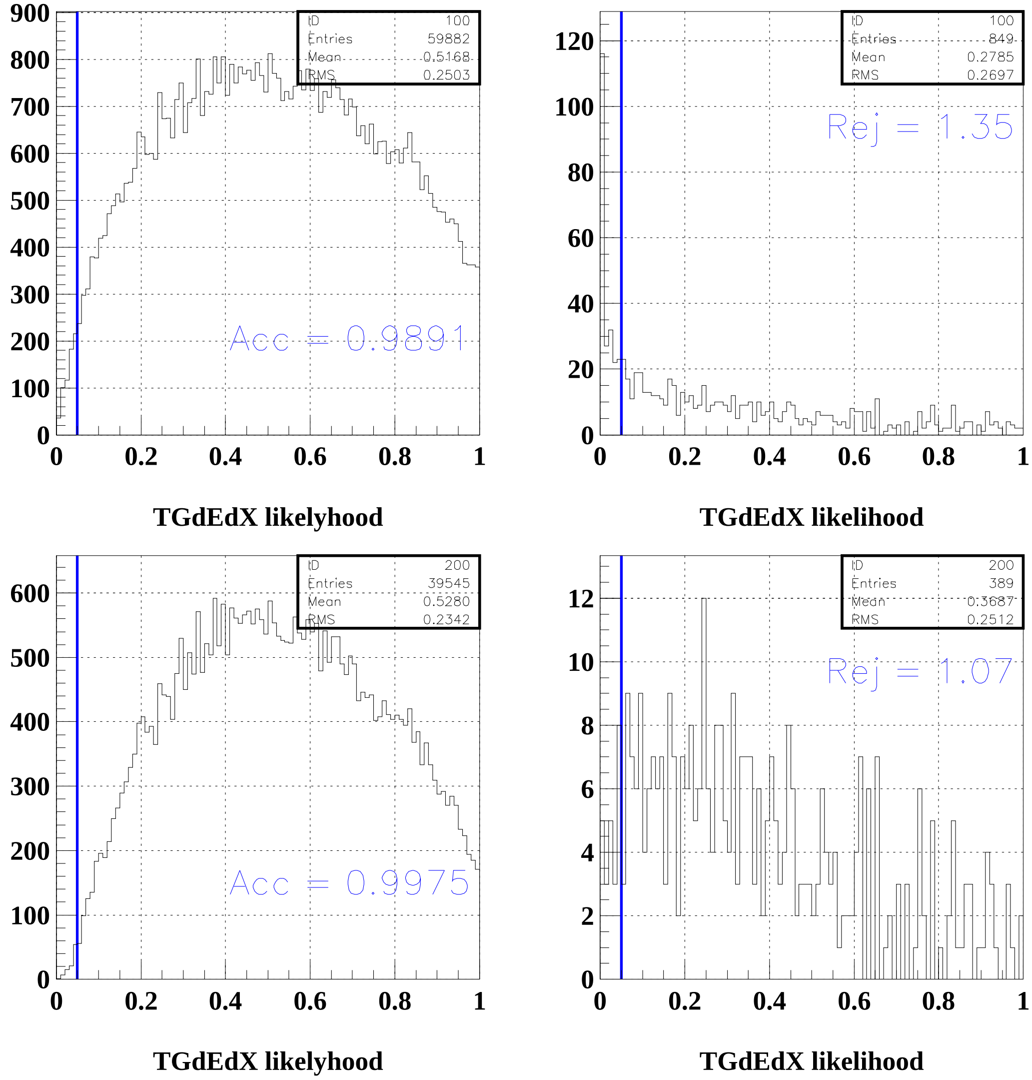

Figure 23: $like_{tgdedx}$ distributions of the acceptace (left) and rejection (right) samples. The top (bottom) plots are sample without (with) correlated cuts applied. The blue line is the cut threshold value of 0.05 (events on the left of the line are considered possible background). E787 had a acceptance (rejection) of 0.9858 (1.44) and no rejection after all cuts were applied.

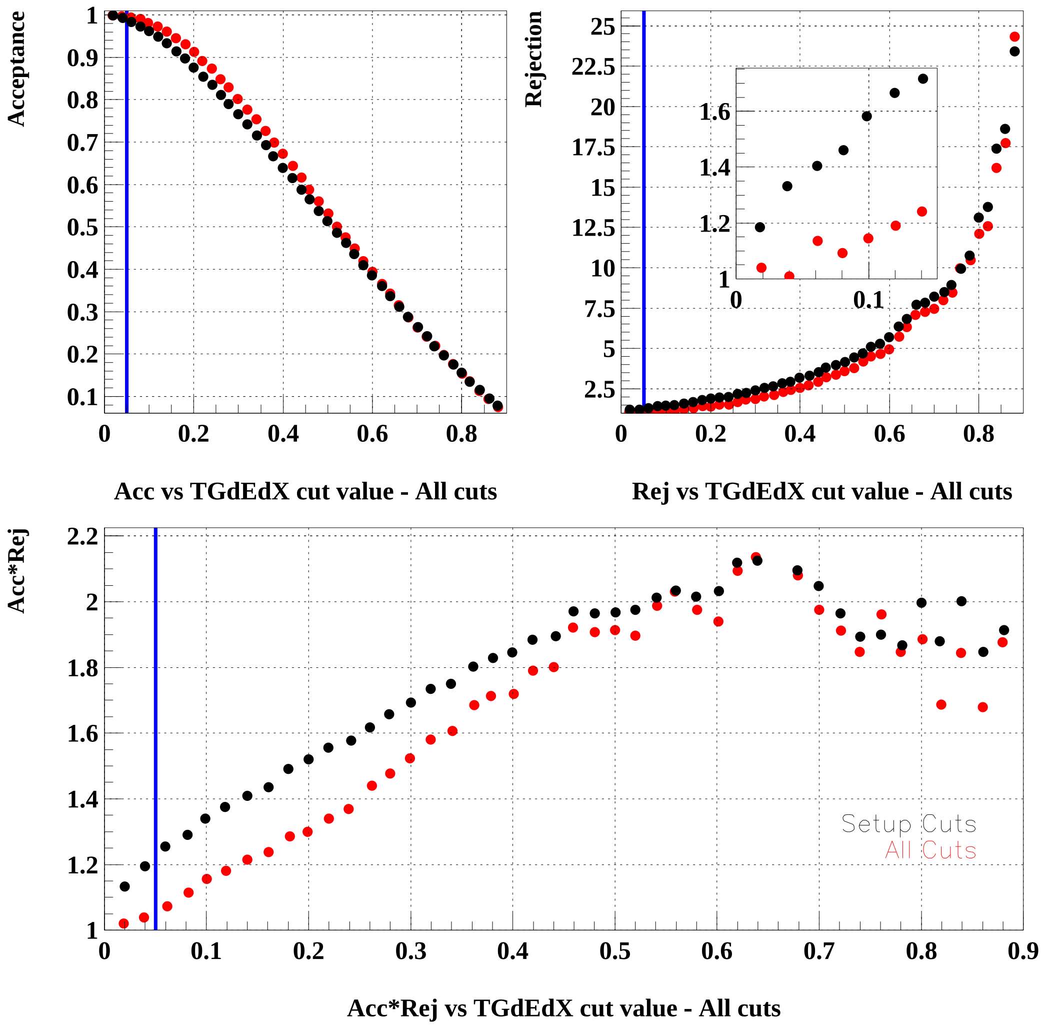

Figure 24: Acceptance and Rejection versus TGDEDX cut threshold. The TGDEDX cut is $like_{tgdedx} < cut\ value$. The blue line is the nominal cut value of 0.05. The red (black) points are after (before) correlated cuts are applied.

8 Skim Definitions

List of setup cuts, PASS1, which were applied before processing of the event continued.

- PRESCALE (1/3 or 2/3) DUPEV PASS1 TRBIT 1.0 2.0 LEV11 LEV12 RD_TRK STLAY BAD_STC RSHEX TRKTIM UTC RDUTM PDC LAY14 UTC1 RANGE1 RSHEX2.

Table 16 lists the cuts which compose the eight skims employed by the analysis. Skims 5-7 (1/3 sample) were used for optimization of cuts and initial background evaluation. Skims 1-3 (2/3 sample) will be used for background evaluation. Skim 4 and 8 (3/3 kink sample) were used in PV optimization.

skim	Data Sample	Cuts
1 (5)	1/3 (2/3) $K_{\pi 2}$	TGCUT, PSCUT, TDCUT, TGPVCUT
2 (6)	1/3 (2/3) $K_{\mu 2}$	TGCUT, PSCUT, PVCUT, TGPVCUT, DELCO
3 (7)	1/3 (2/3) $\pi_{scatter}$	TGCUT, TDCUT, PVCUT
4 (8)	1/3 (2/3) kinks	GOODKINK

Table 16: Definition of skims. Each skim is an enhanced background sample, as denoted in the *Data Sample* column. The union of skim 1-3 (5-7) comprise the 1/3 (2/3) signal sample. The "kinks" are TG-scatters in the x-y plane identifed with the algorithm described in Ref. [13].

9 $K_{\pi 2}$-Scatter background

9.1 $K^+ \to \pi^+ \pi^o$ Target Scatters

The $K_{\pi 2}$ decay, where the π^+ scatters in the target, is the dominant background for the $\pi\nu\overline{\nu}(2)$ analysis [1]. As it has been shown with Monte Carlo simulations [14] , the photon distribution from the π^o decay is more uniform in polar angle for events where the π^+ has scattered in the target, than for unscattered ones. Therefore, the PV rejection for TG scatter events is expected to be different than that for $K_{\pi 2}$ events in the peak. The π^+ kinematics cannot be used in the bifurcation study, since the PV rejection has to be measured inside the $\pi\nu\overline{\nu}(2)$ kinematic box.

9.1.1 Rejection Branch

The other set of cuts used to suppress this background are the target quality cuts (TGCUT06). These eliminate events with evidence of a scattered pion in the target, either the scatter occurred outside the Kaon fibers (scatters visible in xy, or "xy-scatters") or inside them (events where the π^+ started in the beam direction and then scattered into the detector acceptance, or "z-scatters"). The two categories are not mutually exclusive. By inverting some of these cuts and applying others, samples with varying mixtures of xy-

CLASS	TGCUTS
1	All cuts, KP2BOX
2	$\overline{CCDPUL}$, $\overline{EPIONK}$
3	$\overline{CCDPUL}$, $\overline{EPIONK}$, all others
4	CCDPUL, EPIONK, TGZFOOL, EIC, OPSVETO, $\overline{OTHERS}$
5	$\overline{CCDPUL}$, $\overline{EPIONK}$, $\overline{CHI567}$, $\overline{VERRNG}$
6	$\overline{CCDPUL}$, $\overline{EPIONK}$, $\overline{CHI567}$, $\overline{VERRNG}$, all others
7	$\overline{CHI567}$, $\overline{VERRNG}$
8	$\overline{CHI567}$, $\overline{VERRNG}$, all others
9	$\overline{CCDPUL}$, $\overline{EPIONK}$, $\overline{CHI567}$, $\overline{VERRNG}$, KIC, PIGAP, TARGF, TPICS
10	$\overline{B4EKZ}$
11	$\overline{B4EKZ}$, all others
12	$\overline{CCDPUL}$, $\overline{EPIONK}$, $\overline{B4EKZ}$
13	$\overline{CCDPUL}$, $\overline{EPIONK}$, $\overline{B4EKZ}$, all others

Table 17: Definition of the classes of events (2-13) used to measure the PV rejection in the $\pi\nu\overline{\nu}(2)$ kinematic box. Class 1 events have passed all the TG quality cuts, therefore they are required to be in the $K_{\pi 2}$ kinematic box as to not look in the signal region. All Classes that have either CCDPUL applied or CCDPUL inverted have the three associated safety cuts (CCDBADFIT, CCDBADTIM and CCD31FIB) applied. The nomenclature $\overline{CCDPUL}$, $\overline{EPIONK}$ means $\overline{CCDPUL + EPIONK}$.

and z-scatters can be created for the rejection branch. These samples will be contaminated to an extent with K_{e4}, $K_{\pi 2\gamma}$ and Charge Exchange background, but the contamination is shown to be small [8]. Thirteen such "classes" were used, described in Table 17, and the PV rejection was measured on them in the $\pi\nu\overline{\nu}(2)$ kinematic box (Table 18) . The Class 1 rejection is for the $K_{\pi 2}$ peak and is given for comparison. The PV rejections measured for different classes are consistent with each other within statistical uncertainties. For the final PV rejection, class 12 was used, because it had adequate statistics and it is expected to be the richest in z-scatters, since the cuts that mainly attack them are inverted: CCDPUL and EPIONK cut events with large pulses in the kaon fibers at trs, and B4EKZ rejects events in which the z position of the decay vertex found by the UTC does not agree with the kaon energy deposit (and thus path length) in the target. Both these signatures are characteristic of a decay pion that started in the beam direction in the kaon fiber, and then scattered into the detector. The difference in PV rejection between different classes with adequate statistics was used as an estimate for the systematic uncertainty.

Due to the loss of statistics in the rejection branch for the tight box [3], the rejection of the tight (30%) photon veto is measured on a rejection branch that uses the loose versions of the kinematic box, the TD cuts and DELCO. In doing this it is assumed that the rejection of the (30%) photon on these classes is the same for the loose and tight cuts. Table 20 shows that the rejection does not change within statistical error when applying the tight versions of these cuts. Since these statistical errors are so large, this comparison

[3] Here, the tight box refers to the application of the tight KIN, TD and DELCO cuts

Rejection Branch - Loose Box							
CLASS	PNN2BOX (PV60)				KP2BOX (PV60)		
	bef. PV	af. PV	rejection	bg (3/3)	bef. PV	af. PV	rejection
1	N/A	N/A	N/A	N/A	60670	35	1733.4±292.9
2	24672	9	2741.3±913.6	0.558±0.188	147607	121	1219.9±110.9
3	2692	3	897.3±517.8	1.707±0.989	59429	54	1100.5±149.7
4	4220	3	1406.7±811.9	1.088±0.631	61703	38	1623.8±263.3
5	30209	12	2517.4±726.6	0.608±0.178	183128	147	1245.8±102.7
6	4069	3	1356.3±782.8	1.129±0.654	86702	72	1204.2±141.9
7	24574	6	4095.7±1671.8	0.374±0.153	89458	57	1569.4±207.8
8	356	1	356.0±355.5	4.310±4.320	13635	11	1239.5±373.6
9	23976	10	2397.6±758.0	0.638±0.204	172316	141	1222.1±102.9
10	11037	4	2759.2±1379.4	0.555±0.278	29962	28	1070.1±202.1
11	48	1	48.0±47.5	32.553±32.931	3009	2	1504.5±1063.5
12	26613	10	2661.3±841.4	0.575±0.184	159607	129	1237.3±108.9
13	3215	3	1071.7±618.4	1.429±0.828	65626	58	1131.5±148.5

Table 18: The rejection branch for the $K_{\pi 2}$ TG scatter background in the loose box: PV rejection using the loose photon veto (PV60) for the $\pi\nu\overline{\nu}(2)$ and $K_{\pi 2}$ boxes, and respective background, for the 12 classes. The classes that are skipped do not have enough statistics for a meaningful measurement. The same setup cuts as in the normalization branch (Table 24) are applied.

of rejections using different tight cuts was repeated using the loose (60%) and super-loose (90%) photon vetos. Table 21 verify that within statistical error the photon veto rejection is the same for the loose and tight sets of cuts.

The purity of the rejection sample can be examined with respect to the setup cuts used. In class 12 of the rejection branch (see 18) there are 10 events surviving the loose (60%) PV. The fractions of total events remaining that are $K_{\pi 2}$ scatters for various combinations of loose and tight versions of the setup cuts were assessed by a visual scan and are found in Table 23. This table shows that the sample purity does not change significantly for the various combinations of loose and tight setup cuts.

9.1.2 Normalization Branch

In the normalization branch (see Table 24), all the cuts in TGCUT06 were applied, and the PV was inverted. Some contamination from $K_{\pi 2}$-RS scatters and $K_{\pi 2\gamma}$ is expected, but these backgrounds are small compared to $K_{\pi 2}$-TG scatters. The ptot distribution of the events remaining in the normalization branch after the inversion of PVCUTPNN2, after the application of all the TGCUT06 except CCDPUL, and after the application of CCDPUL is shown in Figure 25. In the same figure, the ptot distribution of the events in class 12 of the rejection branch is also shown before and after PVCUTPNN2. Both of those distributions look adequately $K_{\pi 2}$-scatter-like.

Rejection Branch - Tight Box							
CLASS	PNN2BOX loose (PV30)				KP2BOX loose (PV30)		
	bef. PV	af. PV	rejection	bg (3/3)	bef. PV	af. PV	rejection
1	N/A	N/A	N/A	N/A	60670	35	1733.4±292.9
2	24672	3	8224.0±4747.8	0.093±0.054	147607	121	1219.9±110.9
3	2692	1	2692.0±2691.5	0.285±0.286	59429	54	1100.5±149.7
4	4220	1	4220.0±4219.5	0.182±0.182	61703	38	1623.8±263.3
5	30209	4	7552.2±3775.9	0.102±0.051	183128	147	1245.8±102.7
6	4069	1	4069.0±4068.5	0.189±0.189	86702	72	1204.2±141.9
7	24574	1	24574.0±24573.5	0.031±0.031	89458	57	1569.4±207.8
8	356	1	356.0±355.5	2.163±2.171	13635	11	1239.5±373.6
9	23976	3	7992.0±4613.9	0.096±0.056	172316	141	1222.1±102.9
10	11037	1	11037.0±11036.5	0.070±0.070	29962	28	1070.1±202.1
11	48	1	48.0±47.5	16.340±16.546	3009	2	1504.5±1063.5
12	26613	4	6653.2±3326.4	0.115±0.058	159607	129	1237.3±108.9
13	3215	1	3215.0±3214.5	0.239±0.239	65626	58	1131.5±148.5

Table 19: The rejection branch for the $K_{\pi 2}$ TG scatter background in the tight (ke4-phobic) box: PV rejection using the tight photon veto (PV30) for the $\pi\nu\overline{\nu}(2)$ and $K_{\pi 2}$ boxes, and respective background, for the 12 classes. The rejection of the tight photon veto was measured on the loose versions of DELCO, TDCUTS and the kinematic box as there were not enough statistics when using the tight versions of these cuts. The classes that are skipped do not have enough statistics for a meaningful measurement. The same setup cuts as in the normalization branch (Table 24) are applied.

PV30 Rejection					
CLASS	All Loose	Ke4 Box	DELCO6	TDTIGHT	All Tight
2	24672/3 = 8224±4747.8	18528/3 = 6176±3565.4	21272/1 = 21272±21271.5	18419/1 = 18419±18418.5	11921/0 = 11921±11920.5
3	2692/1 = 2692±2691.5	2065/1 = 2065±2064.5	2163/1 = 2163±2162.5	2033/0 = 2033±2032.5	1250/0 = 1250±1249.5
4	4220/0 = 4220±4219.5	3262/0 = 3262±3261.5	3734/0 = 3734±3733.5	3135/0 = 3135±3134.5	2123/0 = 2123±2122.5
5	30209/4 = 7552.25±3775.9	22778/4 = 5694.5±2847	26345/2 = 13172.5±9314	22520/2 = 11260±7961.7	14795/1 = 14795±14794.5
6	4069/1 = 4069±4068.5	3164/1 = 3164±3163.5	3296/1 = 3296±3295.5	3066/0 = 3066±3065.5	1926/0 = 1926±1925.5
7	24574/1 = 24574±24573.5	18632/1 = 18632±18631.5	21929/1 = 21929±21928.5	18317/1 = 18317±18316.5	12376/1 = 12376±12375.5
8	356/0 = 356±355.5	297/0 = 297±296.5	305/0 = 305±304.5	253/0 = 253±252.5	186/0 = 186±185.5
9	23976/3 = 7992±4613.9	18018/3 = 6006±3467.3	20549/1 = 20549±20548.5	17838/1 = 17838±17837.5	11486/0 = 11486±11485.5
10	11037/1 = 11037±11036.5	7981/1 = 7981±7980.5	9876/1 = 9876±9875.5	8211/1 = 8211±8210.5	5292/1 = 5292±5291.5
11	48/0 = 48±47.5	43/0 = 43±42.5	39/0 = 39±38.5	33/0 = 33±32.5	24/0 = 24±23.5
12	26613/4 = 6653.25±3326.4	19957/4 = 4989.25±2494.4	23061/2 = 11530.5±8152.9	19847/2 = 9923.5±7016.6	12881/1 = 12881±12880.5
13	3215/1 = 3215±3214.5	2430/1 = 2430±2429.5	2572/1 = 2572±2571.5	2410/0 = 2410±2409.5	1451/0 = 1451±1450.5

Table 20: Rejection of the tight (30%) photon veto for the various classes with different combinations of loose and tight versions of the setup cuts: kinematic box cut, TD cuts and DELCO. The 'All Loose' and 'All Tight' columns mean that those three sets of cuts were all loose or all tight. For the other three columns, all the cuts are loose except the one listed, which is tight. The numbers shown are the number of events before the photon veto is applied divided by the number of events remaining after the photon veto is applied and the resulting rejection with statistical error. If there are zero events remaining after the photon veto is applies, the rejection is determined assuming 1 event remained.

PV60 Rejection					
CLASS	All Loose	Ke4 Box	DELCO6	TDTIGHT	All Tight
2	24672/9 = 2741.33±913.6	18528/7 = 2646.86±1000.2	21272/3 = 7090.67±4093.5	18419/4 = 4604.75±2302.1	11921/1 = 11921±11920.5
3	2692/3 = 897.333±517.8	2065/3 = 688.333±397.1	2163/2 = 1081.5±764.4	2033/1 = 2033±2032.5	1250/1 = 1250±1249.5
4	4220/3 = 1406.67±811.9	3262/1 = 3262±3261.5	3734/3 = 1244.67±718.3	3135/3 = 1045±603	2123/1 = 2123±2122.5
5	30209/12 = 2517.42±726.6	22778/8 = 2847.25±1006.5	26345/6 = 4390.83±1792.3	22520/7 = 3217.14±1215.8	14795/2 = 7397.5±5230.5
6	4069/3 = 1356.33±782.8	3164/3 = 1054.67±608.6	3296/2 = 1648±1165	3066/1 = 3066±3065.5	1926/1 = 1926±1925.5
7	24574/6 = 4095.67±1671.8	18632/2 = 9316±6587.1	21929/4 = 5482.25±2740.9	18317/5 = 3663.4±1638.1	12376/2 = 6188±4375.2
8	356/0 = 356±355.5	297/0 = 297±296.5	305/0 = 305±304.5	253/0 = 253±252.5	186/0 = 186±185.5
9	23976/10 = 2397.6±758	18018/7 = 2574±972.7	20549/4 = 5137.25±2568.4	17838/5 = 3567.6±1595.3	11486/1 = 11486±11485.5
10	11037/4 = 2759.25±1379.4	7981/3 = 2660.33±1535.7	9876/2 = 4938±3491.3	8211/3 = 2737±1579.9	5292/2 = 2646±1870.7
11	48/0 = 48±47.5	43/0 = 43±42.5	39/0 = 39±38.5	33/0 = 33±32.5	24/0 = 24±23.5
12	26613/10 = 2661.3±841.4	19957/8 = 2494.63±881.8	23061/4 = 5765.25±2882.4	19847/5 = 3969.4±1774.9	12881/2 = 6440.5±4553.8
13	3215/3 = 1071.67±618.4	2430/3 = 810±467.4	2572/2 = 1286±909	2410/1 = 2410±2409.5	1451/1 = 1451±1450.5

Table 21: Rejection of the loose (60%) photon veto for the various classes with different combinations of loose and tight versions of the setup cuts: kinematic box cut, TD cuts and DELCO. The 'All Loose' and 'All Tight' columns mean that those three sets of cuts were all loose or all tight. For the other three columns, all the cuts are loose except the one listed, which is tight. The numbers shown are the number of events before the photon veto is applied divided by the number of events remaining after the photon veto is applied and the resulting rejection with statistical error. If there are zero events remaining after the photon veto is applies, the rejection is determined assuming 1 event remained.

PV90 Rejection					
CLASS	All Loose	Ke4 Box	DELCO6	TDTIGHT	All Tight
2	24672/141 = 174.979±14.7	18528/102 = 181.647±17.9	21272/106 = 200.679±19.4	18419/111 = 165.937±15.7	11921/63 = 189.222±23.8
3	2692/13 = 207.077±57.3	2065/13 = 158.846±43.9	2163/9 = 240.333±79.9	2033/9 = 225.889±75.1	1250/7 = 178.571±67.3
4	4220/31 = 136.129±24.4	3262/23 = 141.826±29.5	3734/27 = 138.296±26.5	3135/23 = 136.304±28.3	2123/13 = 163.308±45.2
5	30209/178 = 169.713±12.7	22778/129 = 176.574±15.5	26345/138 = 190.906±16.2	22520/139 = 162.014±13.7	14795/80 = 184.938±20.6
6	4069/14 = 290.643±77.5	3164/14 = 226±60.3	3296/10 = 329.6±104.1	3066/10 = 306.6±96.8	1926/8 = 240.75±84.9
7	24574/130 = 189.031±16.5	18632/97 = 192.082±19.5	21929/103 = 212.903±20.9	18317/102 = 179.578±17.7	12376/62 = 199.613±25.3
8	356/0 = 356±355.5	297/0 = 297±296.5	305/0 = 305±304.5	253/0 = 253±252.5	186/0 = 186±185.5
9	23976/139 = 172.489±14.6	18018/103 = 174.932±17.2	20549/105 = 195.705±19.1	17838/105 = 169.886±16.5	11486/60 = 191.433±24.6
10	11037/88 = 125.42±13.3	7981/59 = 135.271±17.5	9876/68 = 145.235±17.6	8211/71 = 115.648±13.7	5292/40 = 132.3±20.8
11	48/0 = 48±47.5	43/0 = 43±42.5	39/0 = 39±38.5	33/0 = 33±32.5	24/0 = 24±23.5
12	26613/156 = 170.596±13.6	19957/114 = 175.061±16.3	23061/119 = 193.79±17.7	19847/121 = 164.025±14.9	12881/71 = 181.423±21.5
13	3215/17 = 189.118±45.7	2430/17 = 142.941±34.5	2572/12 = 214.333±61.7	2410/13 = 185.385±51.3	1451/10 = 145.1±45.7

Table 22: Rejection of the loose (90%) photon veto for the various classes with different combinations of loose and tight versions of the setup cuts: kinematic box cut, TD cuts and DELCO. The 'All Loose' and 'All Tight' columns mean that those three sets of cuts were all loose or all tight. For the other three columns, all the cuts are loose except the one listed, which is tight. The numbers shown are the number of events before the photon veto is applied divided by the number of events remaining after the photon veto is applied and the resulting rejection with statistical error. If there are zero events remaining after the photon veto is applies, the rejection is determined assuming 1 event remained.

Setup Cuts	Total Events	$K_{\pi 2}$ TG-Scatter Events	Fraction	Other Ke4	Possible Ke4	2-Beam
All Loose	10	7	0.70 ± 0.15	1	1	1
Ke4-phobic Kinematic Box	8	6	0.75 ± 0.15	1	0	1
DELCO6	4	3	0.75 ± 0.22	0	0	1
TDTIGHT	5	2	0.40 ± 0.22	1	1	1
All Tight	2	1	0.50 ± 0.35	0	0	1

Table 23: Categorization of events by visual scan for events surviving the loose photon veto in the $K_{\pi 2}$ scatter rejection branch Class 12. The combinations of loose and tight setup cuts are described in Table 21.

9.1.3 Background

Using the numbers from Tables 18 and 24, the $K_{\pi 2}$ target scatter background for the loose box is

$$\begin{aligned} n_{K_{\pi 2}-TGscat} &= 3 \times \frac{N}{R_{PV class12} - 1} \\ &= 3 \times \frac{510}{(2661.3 \pm 841.4) - 1} \\ &= 0.575 \pm 0.184(\text{stat.})^{+0.063}_{-0.201}(\text{sys.}) \end{aligned} \tag{2}$$

The systematic error comes from the difference in background predicted by the class with the highest (CLASS7) and lowest (CLASS9) PV rejection, with respect to the central value from CLASS12. Only classes with adequate statistics are considered.

Using the numbers from Tables 19 and 24, the $K_{\pi 2}$ target scatter background for the tight box is

$$\begin{aligned} n_{K_{\pi 2}-TGscat} &= 3 \times \frac{N}{R_{PV class12} - 1} \\ &= 3 \times \frac{256}{(6653.2 \pm 3326.4) - 1} \\ &= 0.115 \pm 0.058(\text{stat.})^{+0.039}_{-0.022}(\text{sys.}) \end{aligned} \tag{3}$$

The lower bound on the systematic error comes from the difference in background predicted by the class with the highest (CLASS2) PV rejection, with respect to CLASS12. Only classes with adequate statistics are considered. The upper bound on the systematic error comes from the difference in background for CLASS12 between the "All Loose" and "Ke4-phobic kinematic box" setups cuts as shown in Table 20.

9.2 $K^+ \to \pi^+ \pi^o$ Range Stack Scatters

Pions from the $K_{\pi 2}$ decay can also undergo inelastic scattering in the Range Stack and fall into the $\pi\nu\overline{\nu}(2)$ kinematic box by losing energy in the scattering process. However,

CUT	PNN2BOX loose	PNN2BOX tight	KP2BOX
ALL_EVENTS	92709440	92709440	92709440
BAD_RUN,KERROR	90192880	90192880	90192880
SKIM5,RECON	2635077	2635077	2635077
PSCUT06	952180	952180	952180
DELCO3*	945357	778661	945357
TDCUT02*	711847	428074	711847
KINCUT06	417199	257607	417199
BOX*	38835 (10.7429)	18911 (13.6221)	337622 (1.2357)
$\overline{PVCUT}$	38820 (1.00039)	18907 (1.00021)	337377 (1.00073)
B4EKZ(IC)	27787 (1.39706)	13617 (1.38848)	307443 (1.09736)
TGZFOOL	27396 (1.01427)	13437 (1.0134)	302502 (1.01633)
EPITG	17250 (1.58817)	8228 (1.63308)	265780 (1.13817)
EPIMAXK	17250 (1)	8228 (1)	265780 (1)
TARGF	14700 (1.17347)	6914 (1.19005)	256810 (1.03493)
DTGTTP	14700 (1)	6914 (1)	256803 (1.00003)
RTDIF	14590 (1.00754)	6870 (1.0064)	254618 (1.00858)
DRP	14388 (1.01404)	6791 (1.01163)	253746 (1.00344)
TGKTIM	14144 (1.01725)	6761 (1.00444)	251265 (1.00987)
EIC	13847 (1.02145)	6623 (1.02084)	247096 (1.01687)
TIC	13847 (1)	6623 (1)	247095 (1)
TGEDGE	13621 (1.01659)	6535 (1.01347)	244792 (1.00941)
TGDEDX	12809 (1.06339)	6120 (1.06781)	243294 (1.00616)
TGENR	12533 (1.02202)	5988 (1.02204)	236833 (1.02728)
PIGAP	12342 (1.01548)	5883 (1.01785)	235171 (1.00707)
TGB4	11082 (1.1137)	5251 (1.12036)	221207 (1.06313)
KIC	11076 (1.00054)	5248 (1.00057)	221103 (1.00047)
PHIVTX	8289 (1.33623)	3826 (1.37167)	213725 (1.03452)
OPSVETO	7238 (1.14521)	3374 (1.13397)	204252 (1.04638)
TGLIKE	6812 (1.06254)	3176 (1.06234)	197703 (1.03313)
TIMKF	5542 (1.22916)	2621 (1.21175)	175933 (1.12374)
NPITG	5542 (1)	2621 (1)	175933 (1)
ALLKFIT	5295 (1.04665)	2507 (1.04547)	169905 (1.03548)
TPICS	5291 (1.00076)	2504 (1.0012)	169877 (1.00016)
EPIONK	4970 (1.06459)	2321 (1.07885)	159031 (1.0682)
CHI567	4143 (1.19961)	1898 (1.22287)	138310 (1.14982)
VERRNG	3455 (1.19913)	1592 (1.19221)	129595 (1.06725)
CHI5MAX	3454 (1.00029)	1591 (1.00063)	129595 (1)
ANGLI	3445 (1.00261)	1588 (1.00189)	129524 (1.00055)
CCDBADFIT	3083 (1.11742)	1426 (1.1136)	114548 (1.13074)
CCDBADTIM	2999 (1.02801)	1386 (1.02886)	112173 (1.02117)
CCD31FIB	2999 (1)	1386 (1)	112171 (1.00002)
CCDPUL	510 (5.88039)	256 (5.41406)	60635 (1.84994)

Table 24: The normalization branch for the $K_{\pi2}$-TG scatter background: events after setup cuts and TGCUTS and their rejection (in brackets), for $\pi\nu\overline{\nu}(2)$ loose, $\pi\nu\overline{\nu}(2)$ ke4-phobic, and $K_{\pi2}$ boxes. For the tight box, tight versions of the cuts marked with '*' were applied. Note that the loose 60% photon veto is inverted for both the loose and tight normalization branches.

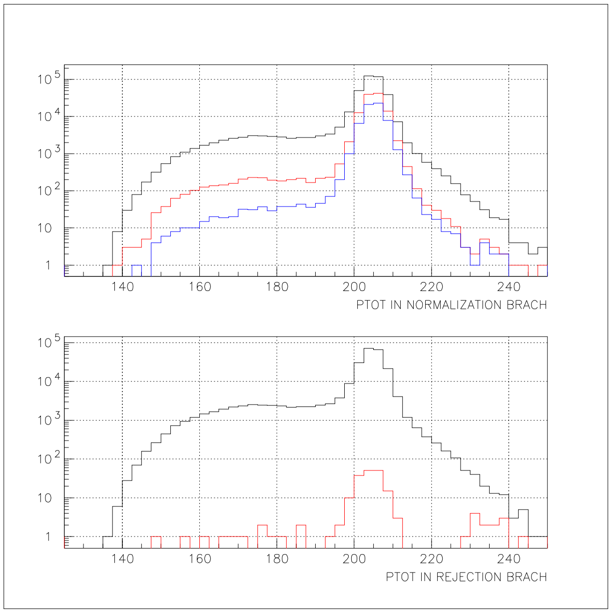

Figure 25: Top: ptot distribution of the events remaining in the normalization branch of the $K_{\pi2}$ TG scatter study after the inversion of PVCUT (black), after the application of all the TGCUT06 except CCDPUL (red), and after the application of CCDPUL (blue). Bottom: ptot distribution of the events in CLASS12 of the rejection branch of the $K_{\pi2}$ TG scatter study before (black) and after (red) PVCUT.

for these events to be a background for this analysis, the pion momentum also has to be mis-measured and the photons from the π^o decay have to be missed. Therefore, this background is expected to be smaller compared to the $K_{\pi2}$ target scattered background. It should be noted that these background events are already included in the normalization branch in Table 24[4], but they are not included in the rejection branch in Table 18 because the target cuts were reversed to measure this PV rejection. The $K_{\pi2}$ events which scattered in the RS should be assigned the same Photon Veto rejection as the $K_{\pi2}$ peak events, since the pion did not scatter in the target. The method used to determine this background was originally formulated by Milind et al. [1].

The most effective cuts against this background are the Range Stack track quality cuts RSDEDX and PRRF (collectively referred to as RSCT), the BOX cut on *ptot* and the Photon Veto cut. Tables 25 and 26 summarize this background study. The SETUP cuts are the same as the $K_{\pi2}$ target scatter normalization branch. Table 25 contain events in the $K_{\pi2}$ momentum peak. Events with the momentum of the $K_{\pi2}$ peak events, but lowered in range and energy are assumed to have scattered in the Range Stack.

The efficiency ϵ_{RSCT} and the rejection R_{RRSCT} of these cuts can be measured as

$$\begin{aligned} \epsilon_{RSCT}(\text{loose}) &= 60670/82060 &= 0.739 \pm 0.002 \\ R_{RSCT}(\text{loose}) &= 637/82 &= 7.768 \pm 0.801 \end{aligned} \tag{4}$$

[4]Correcting the normalization of $K_{\pi2}$-TG scatters for $K_{\pi2}$-RS scatters does not make a significant difference in the background, given the statistical uncertainty.

Rejection				
CUT	Loose Box		Tight Box	
	KP2BOX	PNN2 LOOSE RE BOX	KP2BOX	PNN2 TIGHT RE BOX
SETUP				
PBOX from KP2BOX	92680	720	61653	345
LAYER14	92627	720	61619	345
FIDUCIAL	85452	650	56897	308
UTCQUAL	82761	637	55098	303
RNGMOM	82060	637	54628	303
RSDEDX	71644	114	47810	63
PRRF	60670	82	40647	44
PVCUT	35	0	11	0

Table 25: Rejection branch for $K_{\pi 2}$-RS scatters. PBOX is the momentum cut and RE BOX the range and energy cut.

Normalization				
CUT	Loose Box		Tight Box	
	KP2BOX	PNN2BOX	KP2BOX	PNN2BOX
SETUP				
$\overline{\text{RSDEDX}}$.or.$\overline{\text{PRRF}}$	25001	218	16360	82
LAYER14	24981	218	16348	82
FIDUCIAL	22516	203	14744	76
UTCQUAL	21611	180	14135	69
RNGMOM	21390	154	13981	67
$\overline{\text{PVCUT60}}$	21381	154	13974	67

Table 26: Normalization branch for $K_{\pi 2}$-RS scatters.

$$
\begin{aligned}
\epsilon_{RSCT}(\text{tight}) &= 40647/54628 &= 0.744 \pm 0.002 \\
R_{RSCT}(\text{tight}) &= 303/44 &= 6.886 \pm 0.960
\end{aligned}
\tag{5}
$$

Table 26 shows the normalization branch. The RSCT cut is reversed and all other cuts are applied. The various contributions to the total 154 events left at the the end of the branch have to be considered in order to calculate the background of interest. The largest component of this sample comes from scattering in the target that contaminated the RSCT reversed sample because of the inefficiency of the RSCT cuts. On the other hand, the total 510 events in the loose box for the $K_{\pi 2}$ target scatter normalization branch (Table 24) have a target scattered (N_{tg}) and a RS scattered (N_{rs}) component. We can write

$$
\begin{aligned}
N_{tg} + N_{rs} &= 510 \\
\frac{1-\epsilon_{RSCT}}{\epsilon_{RSCT}} \times N_{tg} + (R_{RSCT} - 1) \times N_{rs} &= 154
\end{aligned}
\tag{6}
$$

Note that the form of the second equation has been corrected from that as used by Milind et al. [1]. Solving this system of equations gives a negative solution for the range stack scattered component N_{rs} for both the loose and tight boxes:

$$N_{rs}(\text{loose}) = -4.022 \pm 2.352$$

and using the tight box values

$$N_{rs}(\text{tight}) = -3.799 \pm 1.897$$

The final background from the RS scattered events can be measured by applying the $K_{\pi 2}$ peak Photon Veto rejection (CLASS1):

$$R_{PV-K_{\pi 2}peak}(\text{loose}) = 60670/35 = 1733.4 \pm 292.9 \tag{7}$$

$$R_{PV-K_{\pi 2}peak}(\text{tight}) = 40647/11 = 3695.2 \pm 1114.0 \tag{8}$$

to N_{rs} which gives

$$n_{K_{\pi 2}-RSscat}(\text{loose}) = 3 \times \frac{\mathrm{N_{rs}}}{\mathrm{R_{PV-K_{\pi 2}peak}} - 1} = -0.0070 \pm 0.0042 \tag{9}$$

$$n_{K_{\pi 2}-RSscat}(\text{tight}) = -0.0031 \pm 0.0018. \tag{10}$$

Since both of these values are negative, but consistent with zero, both the loose and tight backgrounds from the pion scattering (from the $K^+ \rightarrow \pi^+\pi^o$ decay) in the range stack are negligible for the 1/3 sample.

10 $K_{\pi 2\gamma}$ Background

The $K\pi 2\gamma$ ($K \rightarrow \pi^+\pi^0\gamma$) background is expected to be small as compared to the $K\pi 2$ scattering background in pnn2 analysis because of the presence of the extra photon and

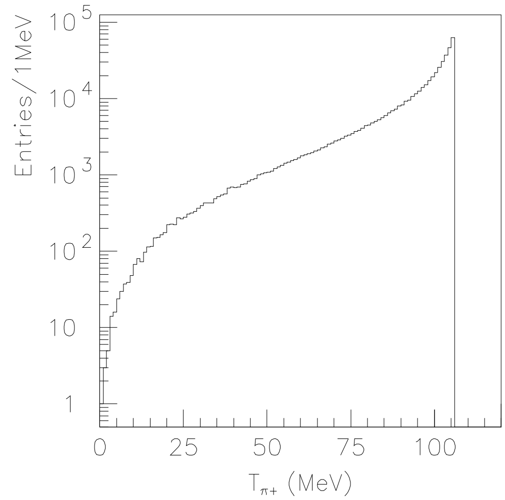

Figure 26: π^+ kinetic energy distribution in $K\pi 2\gamma$ events

the small branching ratio. For $K \to \pi^+\pi^0\gamma$ decay, the γ can be emitted by direct emission (DE) or inner bremsstrahlung (IB). The partial branching fraction for T_{π^+} in the range of 55-90 MeV is $(4.4 \pm 0.7) \times 10^{-6}$ for DE and $(2.75 \pm 0.15) \times 10^{-4}$ [15] for IB. Since it is difficult to isolate this background from the $K\pi 2$ scattering background, both Monte Carlo and data are used. The method can be summarized with the following formula [2]:

$$N_{Kp2\gamma} = \frac{N_{Kp2-peak}}{\kappa \cdot R_\gamma} .$$

$N_{Kp2-peak}$ is the number of $K\pi 2$ peak events which passed all pass2 cuts and $K\pi 2$ box cuts instead of pnn2 box cuts, and is estimated by data. The factor κ, estimated from UMC, is the relative acceptance of the charged track between $K\pi 2$ ($K\pi 2$ box) and $K\pi 2\gamma$ (pnn2 box) events. The extra PV rejection from the radiative γ is contained in R_γ.

$N_{Kp2-peak}$ is measured to be 11 and 35 for tight and loose cuts respectively. (Loose refers to loose PV, TD, KIN and DELCO3, while tight to tight PV, TD, KIN(ke4-phobic) and DELCO6.)

To study the relative acceptance κ for the charged track 2×10^5 $K\pi 2$ events and 5×10^5 $K\pi 2\gamma$ events are generated by UMC. The branching ratio of $K\pi 2$ is 0.2092 ± 0.0012 [15]. Fig. 26 shows the true kinematic energy distribution for $K\pi 2\gamma$ events. Note that the DE process is ignored due to its low branching ratio. With this information, the effective branching ratio for the range of 0-106 MeV can be calculated as:

$$Br(K\pi 2\gamma) = \frac{\displaystyle\int_0^{106} dN}{\displaystyle\int_{55}^{90} dN} \times (2.75 \pm 0.15) \times 10^{-4} = (1.11 \pm 0.06) \times 10^{-3} .$$

The generated UMC events are required to pass pnn1 or pnn2 trigger simulation without the online photon veto, L1.N or L0rr2 triggers. Then these events are required to pass all possible offline cuts for UMC. The photon veto cuts are not applied, and the

Table 27: Detailed information in κ estimation.

	$K\pi 2$	$K\pi 2\gamma$
N_{KT}	199986	499973
Passed pnn1 or pnn2 trigger	30625	64217
Passed Tight offline cuts	7608	7409
Passed Loose offline cuts	9776	11035

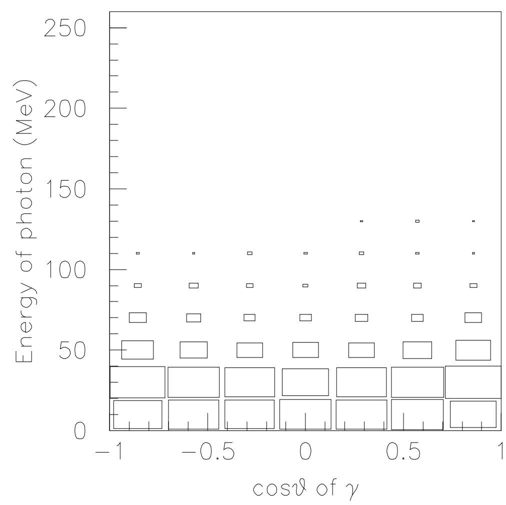

Figure 27: The UMC truth spatial and energy distribution of the third photon of $K\pi 2\gamma$ events after it passed all offline cuts. (Use loose offline cuts for example here.)

$K\pi 2$ and pnn2 box cuts are applied for the $K\pi 2$ and $K\pi 2\gamma$ events, respectively. κ is calculated as:

$$\kappa = \frac{Br(K\pi 2) \times \frac{N_{K\pi 2\ offline\ cuts}}{N_{K\pi 2\ KT}}}{Br(K\pi 2\gamma) \times \frac{N_{K\pi 2\gamma\ offline\ cuts}}{N_{K\pi 2\gamma\ KT}}}.$$

The result and detailed information in κ calculated are listed in Tab. 27. The value of κ is mainly determined by the relative branching ratio and kinematic box cuts, and is very insensitive to the other cuts.

The photon veto rejection due to the photons from π^0 decay for both $K\pi 2$ and $K\pi 2\gamma$ event is expected to be roughly equal. However the existence of the radiative γ in $K\pi 2\gamma$ background will give higher total rejection. The UMC truth spatial and energy distribution of the third photon, after the $K\pi 2\gamma$ events passed all offline cuts, is shown in Fig. 27 (Loose offline cuts). A single photon inefficiency A table [16] was built with conservative photon veto cuts with data [6] and is shown in Fig. 28. R_γ is calculated by convolving these two tables. All of the results and estimated backgrounds are summarized in Tab. 28. The tighter kinematic box also suppresses $K_{\pi 2\gamma}$.

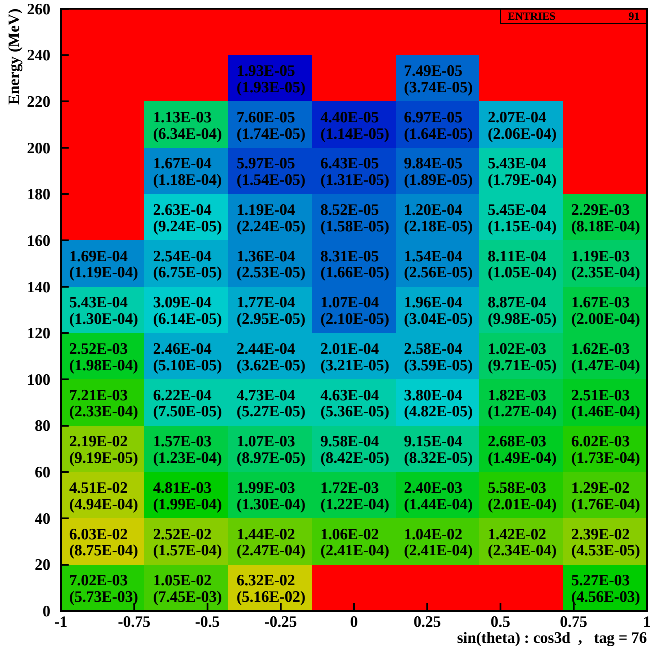

Figure 28: Inefficiency table for single photon. Missing entries are assumed to have 100% inefficiency.

Table 28: $K\pi2\gamma$ background number normalized to 3/3 data. The first error of $N_{Kp2\gamma}$ is statistical and the second error is from κ and R_γ.

	Tight cuts	Loose cuts
$N_{Kp2-peak}$	11	35
κ	483 ± 28	417 ± 24
R_γ	5.11 ± 0.11	5.04 ± 0.10
$N_{Kp2\gamma}$	$0.013 \pm 0.004 \pm 0.001$	$0.0500 \pm 0.0084 \pm 0.0030$

11 Beam Background

Further details of the beam background written in detail in Ref. [17]. The PV is applied at the same level as PNN1 for the beam backgrounds. Therefore, we must scale by $\frac{A_{PV_{pnn2}}}{A_{PV_{pnn1}}}$ where $A_{PV_{pnn1}} = 0.95$ and $A_{PV_{pnn2}} = 0.639$ for the loose signal region and $A_{PV_{pnn2}} = 0.356$ for the tight region. Scaling by the PV acceptance-loss is justified by these backgrounds not being dependent upon the PV cuts. Also, there is no expectation of additional rejection against these background for the PV cuts (except for the ADPV cut in the 2-beam background which is discussed in Section 11.2). Since the beam backgrounds involve very limited statistics, including the PV_{pnn2} cut will remove all events from the normalization branch well before all cuts are applied.

11.1 Single-Beam Background

Setup Branch (n)	beam loose	beam tight
Loose Setup	10327.5 ± 7302.3 (2)	17371.0 ± 17370.5 (1)
TD	17192.0 ± 17191.5 (1)	10480.0 ± 10479.5 (1)
$TD \cdot KIN$	6239.0 ± 6238.5 (1)	3755.0 ± 3754.5 (1)

Table 29: **1-Beam Rejection Summary**. Each row is a different branch to measure the DELCO rejection. First number is the rejection. The number is parenthesis is the number of events remaining that the rejection is based upon. The minimum rejection is used in calculation of the 1-BM background for a conservative estimate.

Norm. branches	beam loose	beam tight
$\overline{DELC3} \cdot PV_{pnn1}$	5.0 ± 2.2	2.0 ± 1.4

Table 30: **1-Beam Normalization Summary**

$$N_{1bm} = 3 \times \frac{A_{PV_{pnn2}}}{A_{PV_{pnn1}}} \times \frac{N_{1bm}}{R_{delco} - 1} \tag{11}$$

$$\begin{aligned} N_{1bm_{loose}} &= 3 \times \frac{0.639}{0.95} \times \frac{5.0 \pm 1.0}{(6239.0 \pm 6238.5) - 1} \\ &= (1.57 \pm 1.57) \times 10^{-3} \end{aligned} \tag{12}$$

$$\begin{aligned} N_{1bm_{tight}} &= 3 \times \frac{0.356}{0.95} \times \frac{2.0 \pm 1.0}{(3755 \pm 3754.5) - 1} \\ &= (0.55 \pm 0.55) \times 10^{-3} \end{aligned} \tag{13}$$

If we "measure" the tight value from scaling from 1-beam loose value, we obtain the following: Note that the factor of 3 is included in the value of $N_{1bm_{loose}}$.

$$N^{scaled}_{1bm_{tight}} = \frac{A_{PV_{tight}}}{A_{PV_{loose}}} \times \frac{A_{TD_{tight}}}{A_{TD_{loose}}} \times \frac{A_{BOX_{tight}}}{A_{BOX_{loose}}} \times \frac{A_{DELCO_{tight}}}{A_{DELCO_{loose}}} \times N_{1bm_{loose}} \quad (14)$$

$$\begin{aligned} N^{scaled}_{1bm_{tight}} &= \frac{0.356}{0.639} \times \frac{0.704}{0.942} \times (0.68) \times \frac{0.704}{0.857} \times 0.00157 \\ &= (0.35 \pm 0.35) \times 10^{-3} \quad (15) \end{aligned}$$

$N^{scaled}_{1bm_{tight}}$ is consistent with $N_{1bm_{tight}}$. If we use the $Rej_{delco} = 6239$ from the loose region (which has more statistics) for the tight region then $N_{1bm_{tight}} = 0.33 \times 10^{-3}$.

11.2 Double-Beam Background

The normalization of double-beam background measurement was modified since Ref. [17]. It was known, but no implemented here, that ADPV had additional rejection of double-beam events. Previously, the double-beam background was scaled with respect to the acceptance of the offline PV cuts. However, if ADPV has additional rejection above acceptance loss then there should be a some correction applied. Instead of a correction, bifurcation of each double beam (KK and Kpi) was changed, see bottom of Fig. 29(b). In addition, the ADPV should be less correlated with the B4 and TG compared to the bifurcation strategy employed in E949-PNN1 [4] which bifurcated B4 and TG cuts.

Table 31 corresponds to Fig. 29(a) and Table 32 corresponds to Fig. 29(b).

11.2.1 2-beam results

$rejection\ (n)$	beam loose	beam tight
$R_{KK}:\ BWTRS \cdot CkTRS \cdot CkTail$	61.9 ± 9.8 (39)	59.9 ± 12.7 (22)
$R_{Kpi}:\ BWTRS \cdot CpiTRS \cdot CpiTail$	352.5 ± 124.5 (8)	274.3 ± 111.8 (6)

Table 31: **2-Beam Rejection Summary**. First number is the rejection. The number in parenthesis is the number of events remaining that the rejection is based upon. K-K is the case where two Kaons are entering the beam. K-pi is the case where we have a Kaon and a Pion entering. $\overline{B4TRS \cdot B4CCD}$ is applied.

11.2.2 KK-beam background

- Scale by acceptance by $PV_{no\ AD}$ due to applying ADPV in the normalization branch.

$$N_{KK} = 3 \times \frac{A_{PV_{noAD}}}{A_{PV_{pnn1}}} \times \frac{(\frac{n_{KK}}{r_{KK}})}{R_{KK} - 1} \quad (16)$$

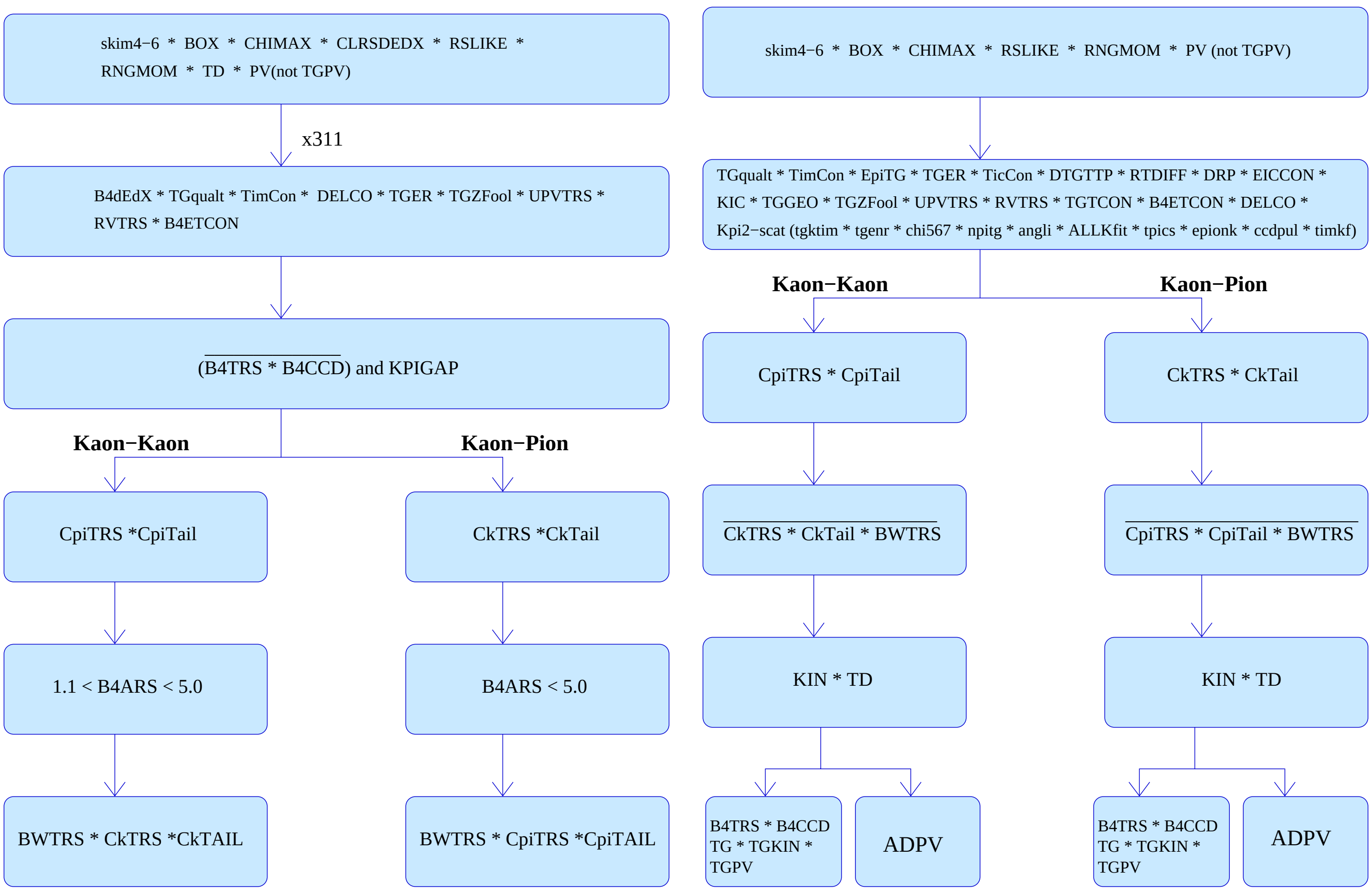

(a) Rejection (b) Normalization

Figure 29: **2-Beam Bifurcations (Kaon-Kaon and Kaon-Pion).** *DELCO* changes depending on the study. *DELCO*=DEL3 OR DELC6 depending on what signal region is being studied.

$Norm.\ branches$	beam loose	beam tight
$n_{KK}:\ TG \cdot TGKIN \cdot TGPV \cdot B4TRS \cdot B4CCD$	8.0 ± 2.8	1.0 ± 1.0
$r_{KK}:\ ADPV$	7.3 ± 2.6	7.3 ± 3.9
N_{KK}	1.1 ± 0.55	0.136 ± 0.136
$n_{Kpi}:\ TG \cdot TGKIN \cdot TGPV \cdot B4TRS \cdot B4CCD$	10.0 ± 3.2	3.0 ± 1.7
$r_{Kpi}:\ ADPV$	21.0 ± 10.2	45.0 ± 44.5
N_{Kpi}	0.5 ± 0.3	0.1 ± 0.1

Table 32: **2-Beam Normalization Summary**. The 2-BM Normalization has 2 branches that are further bifurcated. $K\text{-}K_{r,n}$, $K\text{-}pi_{r,n}$ are the results of the bifurcations, r=rejection, n=normalization, which we used to determine the last two rows. N_{K-K} *and* N_{K-pi} are the 2-BM normalization values which are employed in the calculation of the beam-background. For KK (Kpi), $\overline{CkTRS \cdot CkTAIL \cdot BWTRS}$ ($\overline{CpiTRS \cdot CpiTAIL \cdot BWTRS}$) is applied

$$
\begin{aligned}
N_{KK_{loose}} &= 3 \times \frac{0.0673}{0.95} \times \frac{(\frac{8}{51/7.})}{61.9 - 1} \\
&= (37.1 \pm 19.5) \times 10^{-3}
\end{aligned} \tag{17}
$$

$$
\begin{aligned}
N_{KK_{tight}} &= 3 \times \frac{0.3752}{0.95} \times \frac{(\frac{1}{22/3.})}{59.9 - 1} \\
&= (2.53 \pm 2.53) \times 10^{-3}
\end{aligned} \tag{18}
$$

11.2.3 $K\pi$-beam background

- Only measure the background in the data before the $\pi\nu\nu(2)$ C_π trigger change. This entails scaling by 2.54 to extrapolate to the full running period.
- Scale by the acceptance for the PV_{pnn1} cut.
- Do not apply ADPV due to lack of statistics (lower statistics compared to KK due to C_π trigger change.

$$
N_{K\pi} = 3 \times 2.54 \times \frac{A_{PV_{pnn2}}}{A_{PV_{pnn1}}} \times \frac{(\frac{n_{K\pi}}{r_{K\pi}})}{R_{K\pi} - 1} \tag{19}
$$

$$
\begin{aligned}
N_{K\pi_{loose}} &= 3 \times 2.54 \times \frac{0.639}{0.95} \times \frac{(\frac{10}{84/4.})}{352.5 - 1} \\
&= (6.73 \pm 6.73) \times 10^{-3}
\end{aligned} \tag{20}
$$

$$
\begin{aligned}
N_{K\pi_{tight}} &= 3 \times 2.54 \times \frac{0.356}{0.95} \times \frac{(\frac{3}{45/1.})}{274.3 - 1} \\
&= (0.646 \pm 0.646) \times 10^{-3} \qquad (21)
\end{aligned}
$$

The beam background was scaled by the ratio of PV_{pnn1} acceptance to PV_{pnn2} acceptance; PV_{pnn1} was applied to increase statistics. The acceptance values used are 0.95 for pnn1, 0.619 for loose pnn2, 0.330 for tight pnn2. For the K-K background, ADPV is used in the normalization branch. The acceptance of PV_{pnn2} without ADPV is 0.652 (0.3455) for loose (tight). The addition of ADPV was used in the K-K background due to ADPV having additional rejection against 2-beam background and the K-K branch has sufficient statistics to be applied. K-π does not have sufficient statistics due to only using the "1^{st} half of the data because of the C_π trigger change.

11.3 Beam Background Summary

$Bkgrnd$ ($\times 10^{-3}$)	k034	e787	beam loose	beam tight
1-BM	3.86 ± 2.36	1.66 ± 1.66	0.00157 ± 0.00157	0.00035 ± 0.00035
2-BM KK	0.983 ± 0.983	145.9 ± 145.9	37.1 ± 19.5	2.53 ± 2.53
2-BM Kpi	0.106 ± 0.106	19.7 ± 19.7	6.73 ± 4.57	0.646 ± 0.646
2-BM	1.14 ± 1.14	165.6 ± 165.6	0.0438 ± 0.0200	0.00317 ± 0.00317
$Total\ Beam$	5.00 ± 2.62	167.3 ± 167.3	45.37 ± 20.08	3.72 ± 3.22

Table 33: **Total Beam-Background.** Scaled to the 3/3 sample. k034 column is the result of e949-pnn1 analysis [4]. e787 is the result of the e787-PNN2 analysis [2]. The other columns are current results that are expanded upon throughout the rest of the tables. The errors are statistical. KB_{live} for k034 is 1.77×10^{12} and for e787 is 1.71×10^{12} . e787 background has been scaled up accordingly for comparison purposes.

12 Muon Background

The muon background is expected to come mainly from $K^+ \to \mu^+\nu\gamma$ and $K^+ \to \pi^0\mu^+\nu$ decays ($K_{\mu 2\gamma}$) in the PNN2 kinematic region. This background is expected to be small, because for these processes to be confused with signal, both the muon has to be misidentified as a π^+ and the photon(s) have to be missed. The cuts used to suppress the muon background are the $\pi^+ \to \mu^+ \to e^+$ decay sequence cuts (TDCUT02) and the pion-muon kinematic separation cut, RNGMOM.

Cut	Loose	Tight
badrun	12892493 (0.00)	12892493 (0.00)
Trigger	12823737 (1.01)	12823737 (1.01)
DUPEV	12823737 (1.00)	12823737 (1.00)
rdtrk	12823737 (1.00)	12823737 (1.00)
trktim	12823737 (1.00)	12823737 (1.00)
target	12823737 (1.00)	12823737 (1.00)
stlay	12823737 (1.00)	12823737 (1.00)
utc	12823737 (1.00)	12823737 (1.00)
rdutm	12823737 (1.00)	12823737 (1.00)
badstc	12823737 (1.00)	12823737 (1.00)
pdc	12823737 (1.00)	12823737 (1.00)
bfdedx	11409696 (1.12)	11409696 (1.12)
bwtrs	8868972 (1.29)	8868972 (1.29)
bftrs	8220794 (1.08)	8220794 (1.08)
bfetcon	8135020 (1.01)	8135020 (1.01)
bfccd	8036604 (1.01)	8036604 (1.01)
cpitrs	7688327 (1.05)	7688327 (1.05)
cpitail	7684992 (1.00)	7684992 (1.00)
cktrs	5335463 (1.44)	5335463 (1.44)
cktail	5062839 (1.05)	5062839 (1.05)
tgqualt	4815371 (1.05)	4815371 (1.05)
timcon	4789227 (1.01)	4789227 (1.01)
tgtcon	4683555 (1.02)	4683555 (1.02)
rvtrs	4666832 (1.00)	4666832 (1.00)
upvtrs	4585317 (1.02)	4585317 (1.02)
delco	3976305 (1.15)	3311966 (1.38)
tggeo	2926088 (1.36)	2429497 (1.36)
combops	2926088 (1.00)	2429497 (1.00)
TDcutloose	1281533 (2.28)	1063862 (2.28)
box	38855 (32.98)	17540 (60.65)
bfekz	30992 (1.25)	13555 (1.29)
epitg	25723 (1.20)	10884 (1.25)
epimaxk	25723 (1.00)	10884 (1.00)
targf	24081 (1.07)	10043 (1.08)
tger	24046 (1.00)	10035 (1.00)
dtgttp	24045 (1.00)	10035 (1.00)
rtdif	23839 (1.01)	9953 (1.01)
drp	23652 (1.01)	9894 (1.01)
tgktim	23396 (1.01)	9869 (1.00)
eiccon	22901 (1.02)	9638 (1.02)
ticcon	22901 (1.00)	9638 (1.00)
tgedge	22639 (1.01)	9557 (1.01)
tgenr	22213 (1.02)	9365 (1.02)
pigap	21995 (1.01)	9254 (1.01)
combotglik	20470 (1.07)	8582 (1.08)
tgdbf	19954 (1.03)	8378 (1.02)
tgdbftip	19698 (1.01)	8237 (1.02)
tgdvxtip	19582 (1.01)	8171 (1.01)
tgdvxpi	19296 (1.01)	8016 (1.02)
combotgbf	19296 (1.00)	8016 (1.00)
phivtx	18042 (1.07)	7319 (1.10)
opsveto	16980 (1.06)	6906 (1.06)
timkf	14996 (1.13)	6091 (1.13)
npitg	14996 (1.00)	6091 (1.00)
kic	14992 (1.00)	6088 (1.00)
tgzfool	14732 (1.02)	5996 (1.02)
layv	14732 (1.00)	5996 (1.00)
tgpvcut	14291 (1.03)	5798 (1.03)
rngmom	1014 (14.09)	628 (9.23)
costd	978 (1.04)	604 (1.04)
zfrf	977 (1.00)	603 (1.00)
zutout	970 (1.01)	598 (1.01)
rsdedxmax	856 (1.13)	533 (1.12)
rsdedxcl	752 (1.14)	476 (1.12)
rslike	752 (1.00)	476 (1.00)

continued on next page

Cut	Loose	Tight
$rsdedx$	752 (1.00)	476 (1.00)
$utcqual$	684 (1.10)	437 (1.09)
$prrf$	678 (1.01)	433 (1.01)
$prrfz$	620 (1.09)	394 (1.10)
$comboprrf$	620 (1.00)	394 (1.00)
$tggeo$	620 (1.00)	394 (1.00)
$piflg$	595 (1.04)	381 (1.03)
$tgdedx$	579 (1.03)	370 (1.03)
$ccdpul$	110 (5.26)	75 (4.93)
$epionk$	109 (1.01)	74 (1.01)
$ccdbadtim$	107 (1.02)	73 (1.01)
$ccdfib$	107 (1.00)	73 (1.00)
$verrng$	81 (1.32)	53 (1.38)
$angli$	81 (1.00)	53 (1.00)
$allkfit$	79 (1.03)	52 (1.02)
$tpics$	79 (1.00)	52 (1.00)
$tgdedx$	79 (1.00)	52 (1.00)
$chifss$	64 (1.23)	45 (1.16)
$chifmax$	64 (1.00)	45 (1.00)
$pvpnn$	**0** (64.00)	**0** (45.00)
Norm	1 ± 1.00	1 ± 1.00

Table 34: Normalization Branch for Muon Background. Tight has the tight version of PV, DELCO, TD, BOX applied. The numbers represent the number of events remaining after application of the cut designated on a given row. Number in parenthesis is the rejection of the cut.

After some setup cuts that remove $K_{\pi 2}$ decays and beam backgrounds, in the normalization branch (Table 34) the loose TDCUT02 is inverted for both the loose and tight regions; this is done to prevent us from looking in the box. When the remaining cuts are applied (KCUTS and PVPNN2), zero events remains in the normalization branch, as shown in Table 34, therefore N=1 will be used for the background estimation. In the rejection branch, RNGMOM is inverted and the rejection of the TDCUT02 is measured on this sample. Using these values, the muon background is

$$
\begin{aligned}
N_{muon_{loose}} &= 3 \times \frac{N_{loose}}{R_{TD_{loose}} - 1} && (22) \\
&= 3 \times \frac{1 \pm 1}{(107.82 \pm 32.36) - 1} \\
&= 0.0281 \pm 0.0281 && (23)
\end{aligned}
$$

$$
\begin{aligned}
N^{meas}_{muon_{tight}} &= 3 \times \frac{N_{loose}}{R_{TD_{tight}} - 1} && (24) \\
&= 3 \times \frac{1 \pm 1}{(517.0 \pm 516.5) - 1} \\
&= 0.00581 \pm 0.00581 && (25)
\end{aligned}
$$

$$
\begin{aligned}
N^{scale}_{muon_{tight}} &= \frac{A_{PV_{tight}}}{A_{PV_{loose}}} \times \frac{A_{BOX_{tight}}}{A_{BOX_{loose}}} \times \frac{A_{BOX_{tight}}}{A_{BOX_{loose}}} \times N_{muon_{loose}} && (26) \\
&= \frac{0.356}{0.639} \times \frac{0.704}{0.942} \times (0.68) \times \frac{0.704}{0.857} \times 0.0281 \pm 0.0281 \\
&= 0.00374 \pm 0.00374 && (27)
\end{aligned}
$$

Equation 25 is the value for the muon background in the tight region when measured directly. Equation 25 is the value for the muon background in the tight region when we scale $N_{muon_{loose}}$ by the acceptance loss (i.e. scaling method). PNN2 analyzers have chosen to use acceptance scaling to measure the backgrounds in other signal regions such as the tight box.

Muon background was scaled to the 3/3 and scaled by the acceptance loss from the PV_{pnn2}. The acceptance values used are 0.95 for pnn1, 0.619 for loose pnn2, 0.330 for tight pnn2. The "All PV" and "PV ERbox" already has PV_{pnn2} applied, so PV acceptance scaling is not applied. As shown, the applying the pnn2 level PV is consistent with scaling by acceptance loss. However, in the ERbox there is not sufficient statistics when applying PV_{pnn2}.

Branches	Loose	Tight
All	$\mathbf{65.10 \pm 6.97}$	$\mathbf{279.72 \pm 65.81}$
ERbox	63.58 ± 18.21	348.00 ± 245.72
All PV	107.82 ± 32.36	517.00 ± 516.50
PV ERbox	49.00 ± 48.50	21.00 ± 20.49
Norm	1 ± 1.00	1 ± 1.00

Table 35: Rejection and Normalization Summary Table.

Branches	Loose	Tight
Band All	$\mathbf{30.50 \pm 30.50}$	$\mathbf{3.74 \pm 3.74}$
Band ERbox	31.23 ± 31.23	3.00 ± 3.00
Band All PV	28.08 ± 28.08	5.81 ± 5.81
Band PV ERbox	62.5 ± 62.5	$150. \pm 150.$

Table 36: Muon background summary table. Scaled to the 3/3 ($\times 10^{-3}$).

13 Charge exchange background

The Charge EXchange (CEX) background is expected to come mainly from $K^+n \to K^0p$ followed by $K^0_L \to \pi^+e^-\nu_e$ and $K^0_L \to \pi^+\mu^-\nu_\mu$. The main K^0_S decay products ($\pi^+\pi^-$ or $\pi^0\pi^0$) cannot constitute a background. In E787 this background is primarily determined by UMC. A more data-driven approach is tried for CEX background in E949 with a normalization sample is found in data containing clear CEX events. The number in normalization branch might be overestimated, but it can be well understood. Due the low statistic and difficulty to isolate this background, a reliable simulation is used to get the rejection of reversed cuts in normalization. Thus the systematic error can be easily controlled, since only a few cuts are involved in UMC.

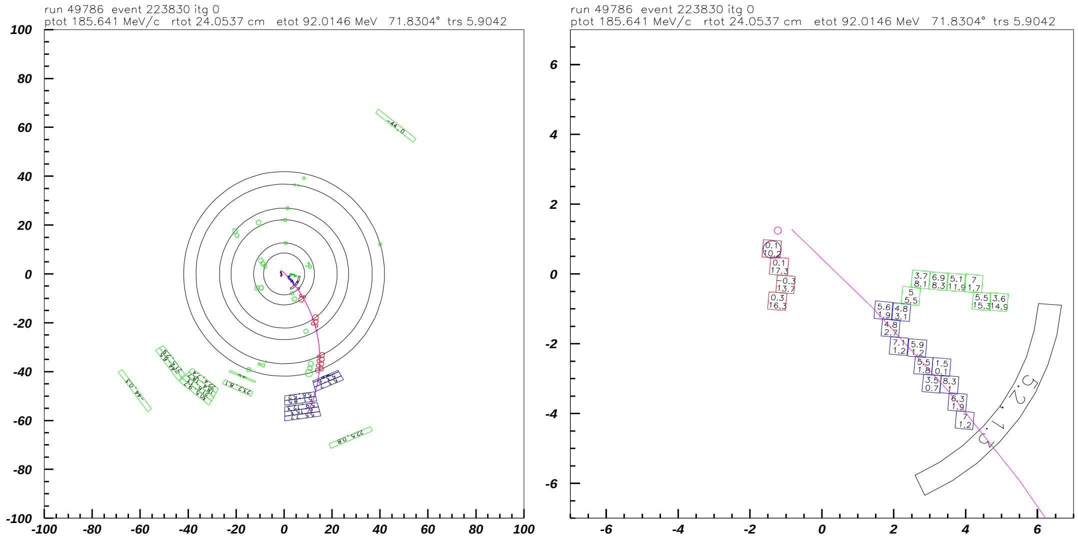

Figure 30: A CEX candidate. The x-y view and target view.

Three steps are taken to analyze CEX background. The first step is to find a normalization sample to be used for a visual scan. The probability for CEX process to happen is quite low, and many cuts are effective to this background. The observation of a clear CEX-like events will give strong confidence to this method.

The setup cuts is set to be very loose. TGPV, OPSVETO, DELCO, B4EKZ, EPITG, EPIMAX, EPIONK, DRP, TGB4, PHIVTX, CHI567, VERRNG, ANGLI, TGFITALLK and CCDPUL are turned off. KPIGAP is used to select events with the expected 'gap' between the kaon and pion fibers. (KPIGAP is a modified version of an inverted TARGF cut that takes into account target fibers identified as 'photon' fibers.) 27 candidates are left after all the criteria. All these events are scanned by eye. One CEX-like event is found there, while the others are not so easy to classify. The candidate is shown in Fig. 30

The second sample is built based on the first sample. The setup cuts are tightened with respect to previous set. The cuts which should be turned off are delicately selected. KPIGAP ($\approx \overline{\text{TARGF}}$) is used and DELCO is turned off as TARGF and DELCO have a large rejection for CEX background. These cuts basically exploit the lifetime of K_L^0 which is well-simulated, so their rejection can be measured with UMC. TGPV, OPSVETO and CCDPUL also can remove CEX background. The method used in $Ke4$ study is used here again to get their rejection and to estimate the uncertainty. For CEX events, the consistency between B4 , the kaon target fiber energy and the z of the outgoing pion should be poor so B4EKZ will suppress CEX background. CHI567, CHI5MAX, VERRNG, ANGLI, TGFITALLK and CCDPUL are turned off. They do not have large rejection for background and it is almost impossible to get a appropriate simulation for them. Their rejection is taken to be the acceptance loss of signal. After these modifications, 1 events survives the tight cuts and 3 events for loose cuts in the normalization branch (Table 37).

For the simulation of CEX background the $K_S^0 \to \pi^+\pi^-$ triggered events are studied. Information concerning the K_L^0 production points and momentum vector is thus obtained

Table 37: The pass2 cuts history of the normalization branch of the 1/3 data for the CEX study.

	Tight cuts	Loose cuts
skim567	12621399	12621399
delco2	7716700	7716700
KCUTS	206709	289592
CKTRS	182952(0.885)	256241(0.884)
CKTAIL	178646(0.976)	250182(0.976)
CPITRS	126363(0.707)	186280(0.744)
CPITAIL	126224(0.998)	186108(0.999)
BWTRS	119382(0.945)	176467(0.948)
B4DEDX	118158(0.989)	174641(0.989)
B4TRS	108812(0.920)	161046(0.922)
B4CCD	107089(0.984)	158536(0.984)
TIMCON	106186(0.991)	156924(0.989)
IPIFLG	105642(0.994)	156112(0.994)
ELVETO	98219(0.929)	145296(0.930)
TDFOOL	98051(0.998)	145025(0.998)
TDVARNN	67226(0.685)	133473(0.920)
PVCUT	188(0.002)	1395(0.010)
KPIGAP	12(0.063)	62(0.044)
TGZFOOL	8(0.666)	50(0.806)
EPITG	3(0.375)	29(0.580)
EPIMAXK	3(1.000)	29(1.000)
EPIONK	3(1.000)	29(1.000)
TIMKF	2(0.666)	18(0.620)
KIC	2(1.000)	14(0.777)
TGQUALT	2(1.000)	14(1.000)
NPITG	2(1.000)	14(1.000)
TGER	2(1.000)	14(1.000)
DTGTTP	2(1.000)	14(1.000)
RTDIF	2(1.000)	14(1.000)
DRP	2(1.000)	14(1.000)
TGKTIM	2(1.000)	14(1.000)
TGEDGE	2(1.000)	13(0.928)
TGDEDX	2(1.000)	13(1.000)
TGENR	2(1.000)	13(1.000)
PIGAP	2(1.000)	13(1.000)
TGLIKE	2(1.000)	9(0.692)
TGB4	2(1.000)	5(0.555)
PHIVTX	1(0.500)	5(1.000)
TPICS	1(1.000)	5(1.000)
TGTCON	1(1.000)	5(1.000)
B4ETCON	1(1.000)	5(1.000)
TGGEO	1(1.000)	3(0.600)

Table 38: CEX background number normalized to 3/3 data. The first error of N_{CEX} is statistical and the second error is the estimated systematic uncertainty due to TGPV, OPSVETO and CCDPUL.

	Tight cuts	Loose cuts
N_{norm}	1	3
$N_{targf,\ UMC}$	6^{+6}_{-2}	50^{+33}_{-10}
$N_{kpigap,\ UMC}$	3332	4136
N_{CEX}	$0.0046 \pm 0.0046^{+0.0046}_{-0.0015}$	$0.092 \pm 0.053^{+0.070}_{-0.018}$

from data. The corresponding B4 and K fiber information are also recorded from this $K^0_S \to \pi^+\pi^-$ study. The rejection of TARGF, DELCO, TGPV, OPSVETO and CCDPUL are estimated by UMC. For TGPV and OPSVETO T_{xtg} (energy deposit in all photon veto fibers) is used. E_{hide}, the energy from the K^0_L decay products in the kaon fibers, is extracted from UMC truth and used to estimate the CCDPUL rejection.

The CEX background is estimated as

$$N_{CEX} = N_{norm,\ data} \times \frac{N_{targf,\ UMC}}{N_{kpigap,\ UMC}} \times ACC_{unapplied}\ ,$$

where $N_{targf,\ UMC}$ is the number of events passing TARGF, DELCO, TGPV, OPSVETO and CCDPUL, $N_{kpigap,\ UMC}$ is the number of events passed KPIGAP which is equivalent to normalization branch in data, $ACC_{unapplied}$ is taken as 85% for CHI567 etc. Comparing with the uncertainty of the simulation of TARGF and DELCO, the systematic error associated with the mismatch of the energy scale in the target fibers between UMC and data is larger. The result of $T_{xtg} < 1.2MeV$ and $E_{hide} < 2.5MeV$ are taken as mean rejection and variations in the range of T_{xtg} $0.6 - 1.8MeV$ and E_{hide} $1.5 - 5MeV$ are considered as determining the systematic error of this background as summarized in Table 38

14 K_{e4} background

The K_{e4} decay ($K^+ \to \pi^+\pi^-e^+\nu_e$) with a branching ratio of $(4.09 \pm 0.09) \times 10^{-5}$ [15] and with the π^+ maximum momentum at 203 MeV could be a serious background in the pnn2 region because this decay contains no photon in the final state to veto on and the π^- and e^+ could be undetectable. Fig. 31 shows the total kinetic energy (T_2) of the π^- and e^+ versus the momentum of π^+ ($ptot$) for Monte Carlo events that passed the pnn2 trigger. When T_2 is very low, the π^- and the e^+ can not fly out of the target and they might escape detection if they deposit all their energy in some insensitive material or if their path overlaps with kaon fibers. For these low T_2 events the distribution of $ptot$ concentrates around 160 MeV which is in the range of the pnn2 signal box.

The low statistics of this background makes it hard to use bifurcated analysis here. Both data and UMC have to be used to evaluate the background. When T_2 is very low, the only effective cuts for this background are TGPV, OPSVETO and CCDPUL cut. A normalization sample is selected using data with $\overline{TGPV \cdot OPSVETO}$ and a Monte Carlo sample is used to estimated the rejection of TGPV·OPSVETO.

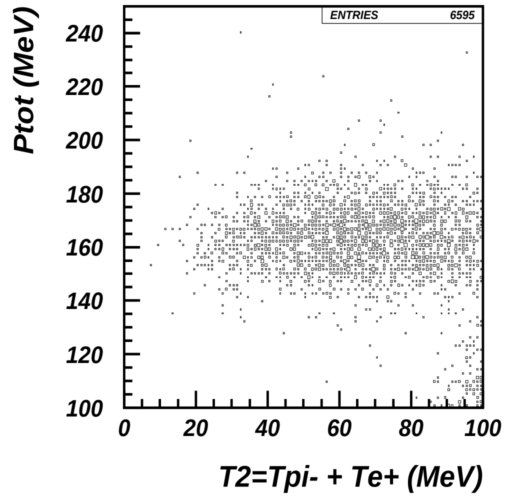

Figure 31: Total kinetic energy (T_2) of the π^- and the e^+ versus the momentum of the π^+ (P_{tot}) for Monte Carlo events that passed the trigger.

The pass2 cuts history of the normalization branch of the 1/3 data is tabulated in Table 39. For the loose box, 66 events remain at the end, before the final cut CCDPUL and EPIONK. To get further understanding of this sample, these events are scanned by eye. Obvious signatures of K_{e4} are found in most of them with some contamination by $K\pi2$ events followed by Dalitz decay. Fig. 32 and Fig. 33 give two example events from this sample. This sample could be used as the normalization branch for a bifurcated analysis. However, it is not possible to get a clean data sample to estimate the rejection of TGPV·OPSVETO, so a Monte Carlo approach is used.

In order to understand the rejection of TGPV·OPSVETO and CCDPUL, Monte Carlo is used to simulate the energy deposit of charged tracks in the target. The main source of uncertainty in simulation comes from the absorption of π^- in the target. The π^- absorption is modeled with an experimental measurement of stopped π^- in the Range Stack [18]. Fig. 34 shows the distribution of the difference between the measured and expected energy of stopped π^- from experiment. In simulation the absorption energy is sampled according to this distribution. If the simulated absorption energy is negative, then it is assigned 0. In this model all the absorption energy is deposited in a single fiber promptly. Possible energy deposition in neighboring fibers is not simulated.

About 2×10^8 K_{e4} events are generated with this model with an additional cut at $T_2 < 50MeV$ in order to enhance the phase space region most responsible for the background. To study the correlation between TGPV·OPSVETO and CCDPUL, two variables are used: the total energy deposit, T_{xtg}, in any fibers not identified as pion or kaon by the reconstruction, corresponding to the energy deposits available to TGPV·OPSVETO, and the total energy deposit, E_{hide}, of the negative pion and positron in kaon fibers, corresponding to the energy deposit that would be found by the CCDPUL. Because there is no simulation for CDD pulse, E_{hide} is taken directly from UMC truth.

UMC events are required to pass all possible cuts. Fig. 35 shows the correlation between T_{xtg} and E_{hide} of the remaining sample. In Tab. 40 and Tab. 41 for loose and tight

	Loose cuts	Tight cuts
skim567	12892189	12129662
KCUTS	764547	534649
PCUTS	179878	113377
TDCUTS	152873	71493
PVCUT	3011	489
DELC	1648 (0.547)	254 (0.519)
DELC3	1644 (0.997)	224 (0.881)
TGZFOOL	1579 (0.960)	213 (0.950)
R-cut	1554 (0.984)	211 (0.990)
PVICVC	1118 (0.719)	130 (0.616)
B4EKZ	933 (0.834)	113 (0.869)
EPITG	569 (0.609)	76 (0.672)
EPIMAXK	569 (1.000)	76 (1.000)
TIMKF	422 (0.741)	57 (0.750)
KIC	410 (0.971)	56 (0.982)
TGQUALT	374 (0.912)	54 (0.964)
NPITG	374 (1.000)	54 (1.000)
TGER	374 (1.000)	54 (1.000)
TARGF	359 (0.959)	51 (0.944)
DTGTTP	359 (1.000)	51 (1.000)
RTDIF	356 (0.991)	51 (1.000)
DRP	327 (0.918)	46 (0.901)
TGKTIM	327 (1.000)	46 (1.000)
TGEDGE	312 (0.954)	44 (0.956)
TGDEDX	287 (0.919)	40 (0.909)
TGENR	282 (0.982)	39 (0.975)
PIGAP	277 (0.982)	37 (0.948)
TGLIKE	257 (0.927)	33 (0.891)
TGB4	250 (0.972)	33 (1.000)
PHIVTX	105 (0.420)	14 (0.424)
CHI567	93 (0.885)	13 (0.928)
CHI5MAX	93 (1.000)	13 (1.000)
VERRNG	81 (0.870)	10 (0.769)
ANGLI	81 (1.000)	10 (1.000)
TGFITALLK	80 (0.987)	10 (1.000)
TPICS	80 (1.000)	10 (1.000)
TGTCON	80 (1.000)	10 (1.000)
B4ETCON	80 (1.000)	10 (1.000)
CCDBADTIM	76 (0.950)	9 (0.900)
CCDBADFIT	66 (0.868)	6 (0.666)
CCD31FIB	66 (1.000)	6 (1.000)
CCDPUL	3 (0.045)	1 (0.166)
EPIONK	3 (1.000)	1 (1.000)

Table 39: The pass2 cuts history of the normalization branch of the 1/3 data for K_{e4} study. R-cut is $\overline{TGPV \cdot OPSVETO}$.

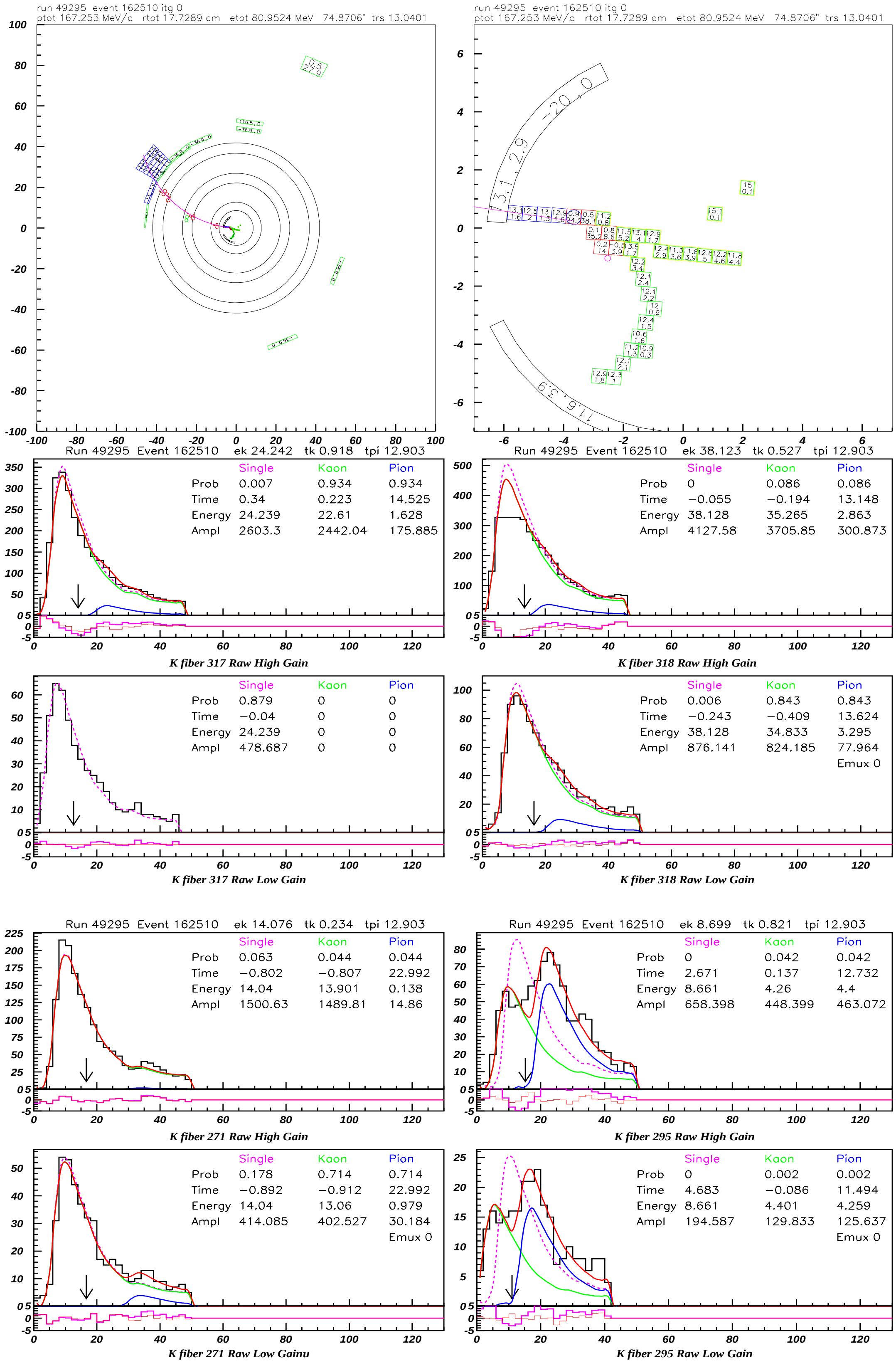

Figure 32: A possible K_{e4} candidate. The X-Y view, target and all double pulse hits in kaon fibers are plotted.

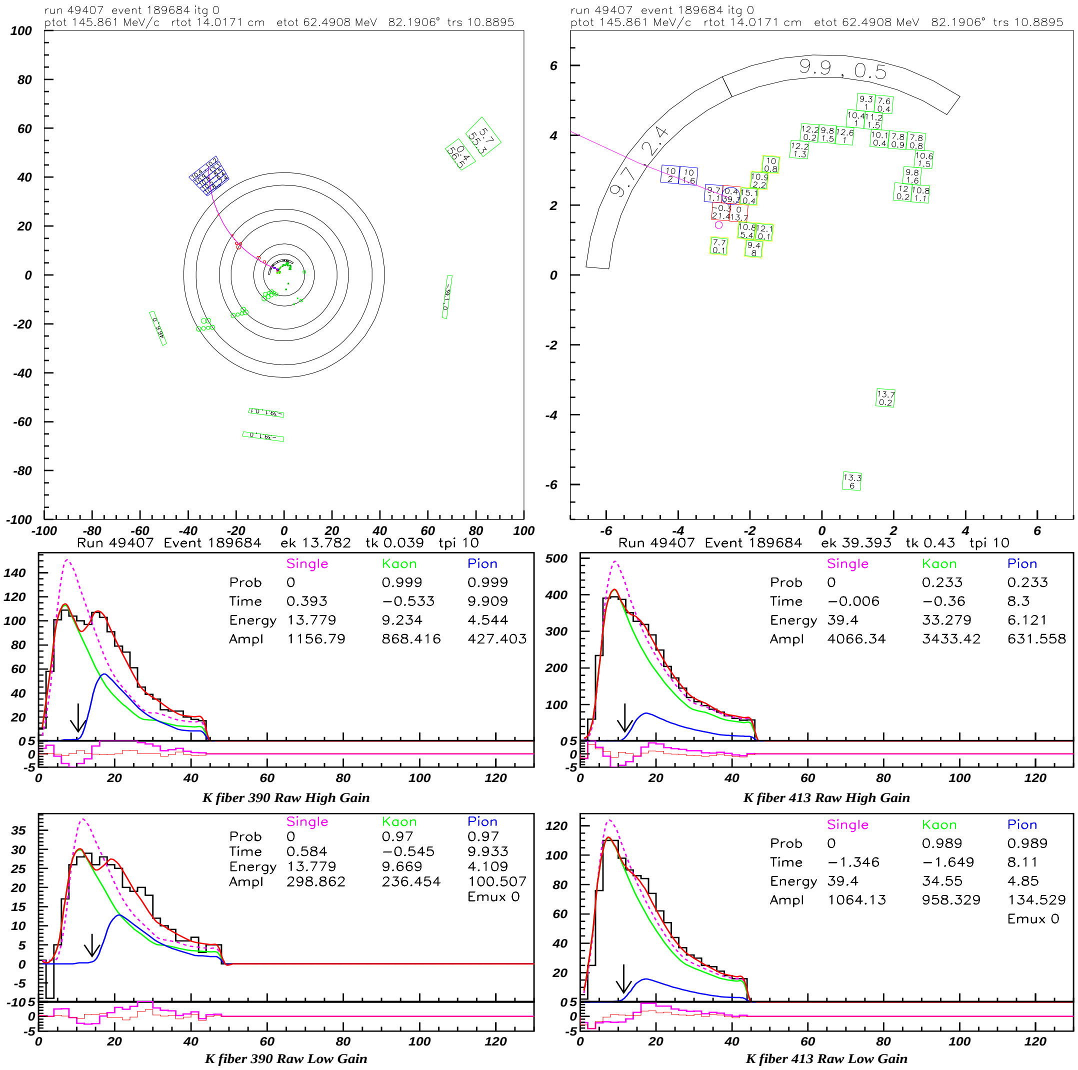

Figure 33: Another possible K_{e4} candidate. The X-Y view, target and all double pulse hits in kaon fibers are plotted.

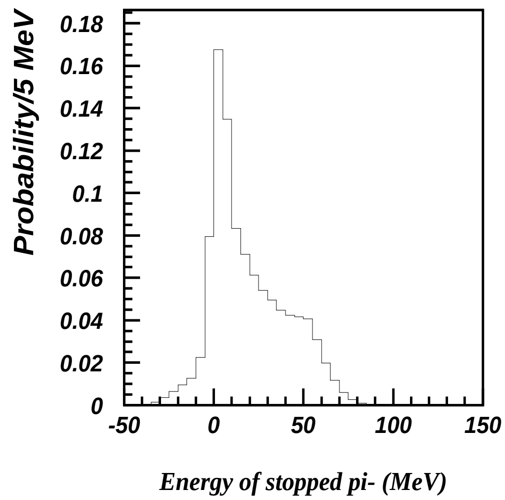

Figure 34: Observable absorption energy of π^- stopped in the RS.

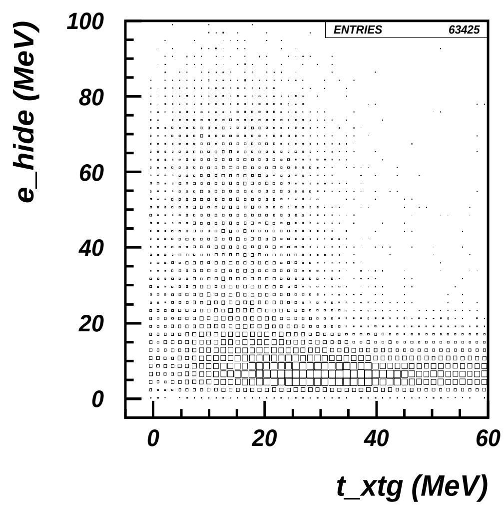

Figure 35: E_{hide} versus T_{xtg}.

Table 40: Rejection of $R_{TGPV \cdot OPSVETO}$ as a function of E_{hide} for loose cuts.

	$T_{xtg} < 0.6$	$T_{xtg} < 1.2$	$T_{xtg} < 1.8$
$E_{hide} < 1.6$	$2250/66 = 34$	$2250/86 = 26$	$2250/98 = 23$
$E_{hide} < 2.5$	$6769/100 = 68$	$6769/129 = 52$	$6769/149 = 45$
$E_{hide} < 4.0$	$34992/202 = 173$	$34992/288 = 122$	$34992/335 = 104$
$E_{hide} < 10.0$	$97100/627 = 155$	$97100/888 = 109$	$97100/1105 = 88$

Table 41: Rejection of $R_{TGPV \cdot OPSVETO}$ as a function of E_{hide} for tight cuts.

	$T_{xtg} < 0.6$	$T_{xtg} < 1.2$	$T_{xtg} < 1.8$
$E_{hide} < 1.6$	$389/18 = 22$	$389/20 = 19$	$389/22 = 18$
$E_{hide} < 2.5$	$2282/23 = 99$	$2282/26 = 88$	$2282/31 = 74$
$E_{hide} < 4.0$	$15105/43 = 351$	$15105/53 = 285$	$15105/65 = 232$
$E_{hide} < 10.0$	$37174/160 = 232$	$37174/206 = 180$	$37174/269 = 138$

cuts respectively the rejection of a T_{xtg} cut (corresponding to the TGPV·OPSVETO cuts) is calculated as a function of the cut on E_{hide}, which simulates the effect of CCDPUL cut. Since the matching of the energy between UMC and data is uncertain, the cut on E_{hide} is varied from 1.6 to 10 MeV, and the cut on T_{xtg} between 0.6 and 1.8 MeV. The central value for the rejection $R_{TGPV \cdot OPSVETO}$, 52 and 88, are used for background calculation for loose and tight cuts, and the variation with E_{hide} are introduced as the systematic error. The background numbers are summarized in Tab. 42.

15 Acceptance

15.1 Acceptance Factors from $K_{\mu 2}$ Events

$K_{\mu 2}$ events which have an incoming K$^+$, one charged track entering the fiducial region, and no photons products are ideal in emulating signal event criteria for beam conditions, target reconstruction, tracking, and photons. To obtain appropriate samples for these aspects of the $K^+ \to \pi^+ \nu \bar{\nu}$ decay, setup cuts listed in Table 43 were employed.

To measure event reconstruction in the RS, see Table 44, the setup cuts chosen, $Setup_{Recon}$, created a sample with good tracks by requiring that the TG and UTC, which

Table 42: K_{e4} background number normalized to 3/3 data. The first error of $N_{K_{e4}}$ is statistical and the second error is from $R_{TGPV \cdot OPSVETO}$.

	Loose cuts	Tight cuts
N_{norm}	3	1
$R_{TGPV \cdot OPSVETO}$	52^{+121}_{-29}	88^{+263}_{-70}
$N_{K_{e4}}$	$0.176 \pm 0.102^{+0.233}_{-0.124}$	$0.034 \pm 0.034^{+0.142}_{-0.026}$

$K_{\mu 2}$ **Setups**	**Component cuts**
$Setup_{RS\ track}$	TRIGGER, ICBIT, $t_{IC} - t_{Ck} > 5$ ns, B4DEDX, UTC, UTC_QUAL
$Setup_{recon}$	TRIGGER, ICBIT, $t_{IC} - t_{Ck} > 5$ ns, B4DEDX, CPITRS, CPITAIL, CKTRS, CKTAIL, BWTRS, RDTRK, TRKTIM, $\|t_{IC} - t_{RS}\| < 5$ ns, PVCUTPNN2(noBV+BVL)
$Setup_{beam}$	TRIGGER, ICBIT, RDTRK, TRKTIM, RDUTM, KM2PBOX, COS3D
$Setup_{PV}$	$Setup_{beam}$, A_{beam} cuts, stopping layer< 19

Table 43: Setup cuts used for the $K_{\mu 2}$-based acceptance measurements. "A_{beam} cuts" are the cuts whose acceptance is measured in "beam" category. ICBIT is the online-IC-trigger bit, KM2PBOX selects events with 226 MeV/c $< ptot <$ 246 MeV/c.

Cut	Loose Box		Tight Box	
	Events	**Acceptance**	**Events**	**Acceptance**
$Setup_{RS\ track}$	2925784		2925784	
RD_TRK	2925784	1.0000	2925784	1.0000
TRKTIM	2925591	0.9999	2925591	0.9999
A_{RS}	0.99993 ± 0.000005		0.99993 ± 0.000005	

Table 44: RS reconstruction acceptance using $K_{\mu 2}(1)$ monitor events.

are independent of the RS, have a valid reconstruction, a delayed-coincidence style cut using $\check{C}_K$ and IC, K^+ entering the TG (B4DEDX). Measuring the reconstruction efficiency of the TG and UTC, see Table 45, requires a sample with a single K^+ (B4DEDX) and no beam π^+'s entering the detector (CPITRS, CPITAIL, CKTRS, CKTAIL, BWTRS). A requirement that insures a delayed coincidence using $\check{C}_K$ and IC[5] ($t_{IC} - t_{Ck} > 5$ ns), a good charged track traversing the UTC detector ($|t_{IC} - t_{RS}| < 5$ ns, RD_TRK, TRKTIM), and no photons (PVCUTPNN2(noBV+BVL)). BV and BVL photon-vetoing criteria is not used for the A_{RS} sample, so that the sample will not remove events with μ^+'s traversing the entire RS and entering the BVL and BV.

The acceptances associated with the beam and target-region cuts require a sample which is definitely a single K^+ decay with no photons. So the $K_{\mu 2}$ decay was chosen with requirements on the track momentum (KM2PBOX), on the quality of the track (RD_TRK, TRKTIM, RDUTM), and on the fiducial region (COS3D). The cuts in Table 46 were ordered in a way that would allow for a more meaningful acceptance value for each cut (e.g. TGQUALT was placed at the beginning because many of the following cuts require a successful TG reconstruction before they work properly.)

[5]DELCO could not be used in here because DELCO requires a TG reconstruction which in turn requires a reconstructed track from the UTC and RS.

Cut	Loose Box		Tight Box	
	Events	**Acceptance**	**Events**	**Acceptance**
$Setup_{recon}$	1520985		748449	
RDUTM	1520125	0.9994 ± 0.00002	748183	0.9996 ± 0.00002
TARGET	1520125	1.0000	748183	1.0000
A_{recon}	0.99943 ± 0.000019		0.99965 ± 0.000022	

Table 45: TG and UTC reconstruction acceptance using $K_{\mu 2}(1)$ monitor events.

Cut	Loose Box		Tight Box	
	Events	**Acceptance**	**Events**	**Acceptance**
$Setup_{beam}$	3771613		3771613	
TGCUT	3689137	0.9781 ± 0.00008	3689137	0.9781 ± 0.00008
TGQUALT	3560525	0.9651 ± 0.00010	3560525	0.9651 ± 0.00010
NPITG	3560525	1.0000	3560525	1.0000
TIMCON	3555328	0.9985 ± 0.00002	3555328	0.9985 ± 0.00002
TGTCON	3516829	0.9892 ± 0.00005	3516829	0.9892 ± 0.00005
B4ETCON	3481951	0.9901 ± 0.00005	3481951	0.9901 ± 0.00005
DCBIT	3067147	0.8809 ± 0.00017	3067147	0.8809 ± 0.00017
DELCO	2628388	0.8569 ± 0.00020	2160585	0.7044 ± 0.00026
PSCUT	2493148	0.9485 ± 0.00014	2045546	0.9468 ± 0.00015
B4DEDX	2479504	0.9945 ± 0.00005	2034267	0.9945 ± 0.00005
BWTRS	2275862	0.9179 ± 0.00017	1865809	0.9172 ± 0.00019
CPITRS	2272021	0.9983 ± 0.00003	1862726	0.9983 ± 0.00003
CPITAIL	2270965	0.9995 ± 0.00001	1861874	0.9995 ± 0.00002
CKTRS	2256478	0.9936 ± 0.00005	1852681	0.9951 ± 0.00005
CKTAIL	2220172	0.9839 ± 0.00008	1841678	0.9941 ± 0.00006
B4TRS	2163250	0.9744 ± 0.00011	1792894	0.9735 ± 0.00012
B4CCD	2134064	0.9865 ± 0.00008	1773887	0.9894 ± 0.00008
UPVTRS	2099003	0.9836 ± 0.00009	1745815	0.9842 ± 0.00009
RVTRS	2097001	0.9990 ± 0.00002	1744246	0.9991 ± 0.00002
TGGEO	2012822	0.9599 ± 0.00014	1672775	0.9590 ± 0.00015
B4EKZ	1834958	0.9116 ± 0.00020	1522582	0.9102 ± 0.00022
TGZFOOL	1812291	0.9876 ± 0.00008	1503775	0.9876 ± 0.00009
TARGF	1754010	0.9678 ± 0.00013	1455287	0.9678 ± 0.00014
DTGTTP	1754003	1.0000	1455280	1.0000
RTDIF	1737206	0.9904 ± 0.00007	1441269	0.9904 ± 0.00008
TGKTIM	1720074	0.9901 ± 0.00007	1436006	0.9963 ± 0.00005
EICCON	1673926	0.9732 ± 0.00012	1397533	0.9732 ± 0.00013
TICCON	1673922	1.0000	1397530	1.0000
PIGAP	1659315	0.9913 ± 0.00007	1385358	0.9913 ± 0.00008
TBDB4	1614464	0.9730 ± 0.00013	1347219	0.9725 ± 0.00014
TGDB4TIP	1606252	0.9949 ± 0.00006	1340136	0.9947 ± 0.00006
TGDVXTIP	1602025	0.9974 ± 0.00004	1336547	0.9973 ± 0.00004
TGDVXPI	1566607	0.9779 ± 0.00012	1309007	0.9794 ± 0.00012
Table 46 continued on next page				

Table 46 continued from previous page				
Cut	Loose Box		Tight Box	
	Events	**Acceptance**	**Events**	**Acceptance**
PHIVTX	1519604	0.9700 ± 0.00014	1265387	0.9667 ± 0.00016
CCDPUL	687795	0.4526 ± 0.00040	627481	0.4959 ± 0.00044
EPIONK	684627	0.9954 ± 0.00008	624313	0.9950 ± 0.00009
CCDBADTIM	679562	0.9926 ± 0.00010	619649	0.9925 ± 0.00011
CCD31FIB	679553	1.0000	619640	1.0000
TIMKF	613292	0.9025 ± 0.00036	558769	0.9018 ± 0.00038
VERRNG	571441	0.9318 ± 0.00032	520584	0.9317 ± 0.00034
ANGLI	571092	0.9994 ± 0.00003	520260	0.9994 ± 0.00003
ALLKFIT	563903	0.9874 ± 0.00015	513528	0.9871 ± 0.00016
TPICS	563178	0.9987 ± 0.00005	512822	0.9986 ± 0.00005
KIC	563015	0.9997 ± 0.00002	512669	0.9997 ± 0.00002
A_{beam}	0.14928 ± 0.000183		0.13593 ± 0.000176	

Table 46: Target and Beam acceptance based on $K_{\mu 2}(1)$ events

Cut	Loose Box		Tight Box	
	Events	**Acceptance**	**Events**	**Acceptance**
$Setup_{PV}$	61031		54888	
LHEX	56983	0.9337 ± 0.00101	51233	0.9334 ± 0.00106
HEXAFTER	54888	0.9632 ± 0.00079	49374	0.9637 ± 0.00083
PVONLINE	52544	0.9573 ± 0.00086	47265	0.9573 ± 0.00091
LAY20or21	52129	0.9921 ± 0.00039	46891	0.9921 ± 0.00041
STLAY	51643	0.9907 ± 0.00042	46450	0.9906 ± 0.00045
RSHEX	49767	0.9637 ± 0.00082	44737	0.9631 ± 0.00087
PVCUT	47888	0.9622 ± 0.00085	43045	0.9622 ± 0.00090
TGPVCUT	47425	0.9903 ± 0.00045	42630	0.9904 ± 0.00047
TGPVTR	47425	1.0000	42630	1.0000
TGPV	45969	0.9693 ± 0.00079	39225	0.9201 ± 0.00131
ICPV	45923	0.9990 ± 0.00015	39108	0.9970 ± 0.00028
VCPV	45894	0.9994 ± 0.00012	39033	0.9981 ± 0.00022
COPV	45639	0.9944 ± 0.00035	38884	0.9962 ± 0.00031
MCPV	45634	0.9999 ± 0.00005	38873	0.9997 ± 0.00009
ECinner	42180	0.9243 ± 0.00124	30927	0.7956 ± 0.00205
ECouter	36778	0.8719 ± 0.00163	24669	0.7977 ± 0.00228
EC 2nd	36522	0.9930 ± 0.00043	22849	0.9262 ± 0.00166
RSPV	33844	0.9267 ± 0.00136	16253	0.7113 ± 0.00300
BVPV	31413	0.9282 ± 0.00140	14921	0.9180 ± 0.00215
BVLPV	30914	0.9841 ± 0.00071	14719	0.9865 ± 0.00095
ADPV	29410	0.9513 ± 0.00122	14069	0.9558 ± 0.00169
EARLY_{BV}	29385	0.9991 ± 0.00017	14063	0.9996 ± 0.00017
DSPV	29381	0.9999 ± 0.00007	14061	0.9999 ± 0.00010
EARLY_{BVL}	29381	1.0000	14061	1.0000
PV_{PNN2}	0.6391 ± 0.0022		0.3585 ± 0.0024	
A_{PV}	0.48141 ± 0.002023		0.25618 ± 0.001863	

Table 47: Online and offline photon-veto acceptance using $K_{\mu2}(1)$ monitor events. PV_{PNN2} is the total acceptance of all offline PV cuts; it is composed of TGPV through EARLY_{BVL}. PV_{PNN2} is not an additional cut, but simply the offline acceptance of the PV cuts from TGPV to $\mathrm{EARLY}_{\mathrm{BVL}}$ inclusive. A_{PV} is the acceptance of all the cuts listed in the table.

Measuring the photon-veto criteria required a valid decay and successfully reconstructed $K_{\mu2}$ event without any additional secondary beam particles at decay time ($Setup_{beam}$, A_{beam}). Since a μ^+ from a $K_{\mu2}$ decay could penetrate the whole RS and reach the BVL or BV photon detector, a requirement of *stopping layer* < 19 was imposed. Both the online and offline PV cuts are measured with $K_{\mu2}(1)$ since there was no online PV requirement in the trigger.

The total acceptance measured using $K_{\mu2}$-monitor events is calculated via Eq. (28) and is summarized in Table 48.

$$A_{K_{\mu2}} = A_{RS} \times A_{recon} \times A_{beam} \times A_{PV} \tag{28}$$

	Loose Box	Tight Box
A_{RS}	0.99993 ± 0.000005	0.99993 ± 0.000005
A_{recon}	0.99943 ± 0.000019	0.99965 ± 0.000022
A_{beam}	0.14928 ± 0.000183	0.13593 ± 0.000176
A_{PV}	0.48141 ± 0.002023	0.25618 ± 0.001863
$A_{K_{\mu 2}}$	0.07183 ± 0.001981	0.0348 ± 0.0074

Table 48: $K_{\mu 2}$ acceptance summary.

15.2 Acceptance Factors from $\pi_{scatter}$ Events

Since the π^+ from $K^+ \to \pi^+ \nu \bar{\nu}$ events has a spectrum of energy and range values, unlike π^+'s from $K_{\pi 2}$, π_{scat}'s are ideal to measure acceptances dealing with RS kinematics. The π^+ from π_{scat} events have a continuous stopping-layer distribution, as is expected with $K^+ \to \pi^+ \nu \bar{\nu}$ events, which is advantageous in considering possible layer dependences within the RS (such as the TD cuts). The setup cuts used to create these samples are listed in Table 49.

$\pi_{scatter}$ **Setups**	**Component cuts**
$Setup_{bad\_stc}$	RD_TRK, TRKTIM, STLAY, UTC, RDUTM, PDC, ICBIT, $b4abm2 < 1.3MeV$, $\lvert t_\pi - t_{RS} \rvert < 5$ ns, $\lvert t_{IC} - t_{RS} \rvert < 5$ ns, TARGF, DTGTTP, RTDIF, TGQUALT, TGZFOOL, CKTRS, CKTAIL, PVCUTPNN2(only RS), COS3D, LAYV4, PNN2BOX
$Setup_{RSkin}$	$Setup_{bad\_stc}$, BAD_STC, TDCUT02
$Setup_{\pi \to \mu \to e}$	$Setup_{bad\_stc}$, BAD_STC, RNGMOM, ZFRF, ZUTOUT, LAYER14, UTC_QUAL, EIC

Table 49: Setup cuts used for the $\pi_{scatter}$ based acceptance measurements. $b4abm2$ is the energy of the B4 hit near beam time.

Creating a sample of single-beam π^+'s which scatter in the TG required removing events with K^+ particles in the beam ($b4abm2 < 1.3MeV$, CKTRS, CKTAIL); the requirement $|t_\pi - t_{RS}| < 5$ ns requires a scattering of the incoming particle and $|t_{IC} - t_{RS}| < 5$ ns requires that the track in the RS and TG are from the same particle. The RS photon-vetoing requirements are applied so as to remove coincident activity within the RS that would otherwise artificially lower the acceptance. PVPNN2 was not applied due to the photon cuts removing events with additional activity at decay time; since a decay does not occur, timing used by the photon cuts are not as meaningful. The remaining cuts which make up $Setup_{bad\_stc}$ require a nicely reconstructed track.

BADSTC, as discussed in Section 8, removes events when the TD in the determined stopping counter was not working properly.

Cut	Loose Box		Tight Box	
	Events	**Acceptance**	**Events**	**Acceptance**
$Setup_{bad\_stc}$	153716		73145	
BADSTC	153474	0.9984 ± 0.00010	73089	0.9992 ± 0.00010
A_{badstc}	0.99843 ± 0.000101		0.99923 ± 0.000102	

Table 50: BADSTC acceptance using $\pi_{scatter}$ monitor events.

15.3 Range-Stack-Kinematic Acceptance

Measuring the kinematic acceptance in the RS (A_{RSkin}) required further refinements to the sample employed by the A_{badstc} measurement. The particle-identification cuts TDCUT02 were utilized, requiring a stopped π^+ in the RS. Without the TDCUT02 requirement a π^+, after entering the RS, could decay in flight yielding kinematics similar to a μ^+ or e^+. A sample with decay-in-flight π^+'s included would artificially lower A_{RSkin}.

Cut	Loose Box		Tight Box	
	Events	**Acceptance**	**Events**	**Acceptance**
$Setup_{RSkin}$	88719		31525	
UTCQUAL	84373	0.9510 ± 0.00072	30038	0.9528 ± 0.00119
RNGMOM	82845	0.9819 ± 0.00046	29506	0.9823 ± 0.00076
RSDEDXMAX	80449	0.9711 ± 0.00058	28764	0.9749 ± 0.00091
RSDEDXCL	76828	0.9550 ± 0.00073	27586	0.9590 ± 0.00117
RSLIKE	76828	1.0000	27586	1.0000
PRRF1	76196	0.9918 ± 0.00033	27433	0.9945 ± 0.00045
PRRFZ	73596	0.9659 ± 0.00066	26577	0.9688 ± 0.00105
A_{RSkin}	0.82954 ± 0.001262		0.84305 ± 0.002049	

Table 51: RS-kinematic acceptance using $\pi_{scatter}$ monitor events.

In order to account for the systematics associated with poor target reconstruction of the π_{scat} events, which is a function of the kinematics, the kinematic box cut was varied. The PNN2BOX was the nominal box cut. The size of the smaller and larger box cut was a shrunken or expanded PNN2BOX.

The difference in reconstruction quality for $\pi_{scatter}$ events and $K_{\pi 2}$ events was evaluated from the resolution of the reconstructed π^+ mass, $m_\pi = \frac{ptot^2 - etot^2}{2 \cdot etot}$, of the two samples. The distributions from π_{scat} and $K_{\pi 2}$ samples, shown in Fig. 36, have resolutions of 13.8 and 8.4 respectively. The fractional uncertainty in $\pi_{scatter}$-target-track reconstruction is therefore $\sqrt{13.8^2 - 8.4^2}/140.0 \simeq 7.8\%$.

Since *ptot* and *etot* contribute roughly equally to the resolution, their uncertainties are $7.8\%/\sqrt{2} = 5.5\%$. *rtot* scales approximately linearly with *etot*, so its uncertainty is also 5.5%. The boundaries of the nominal PNN2 kinematic box were varied by 5.5% yielding

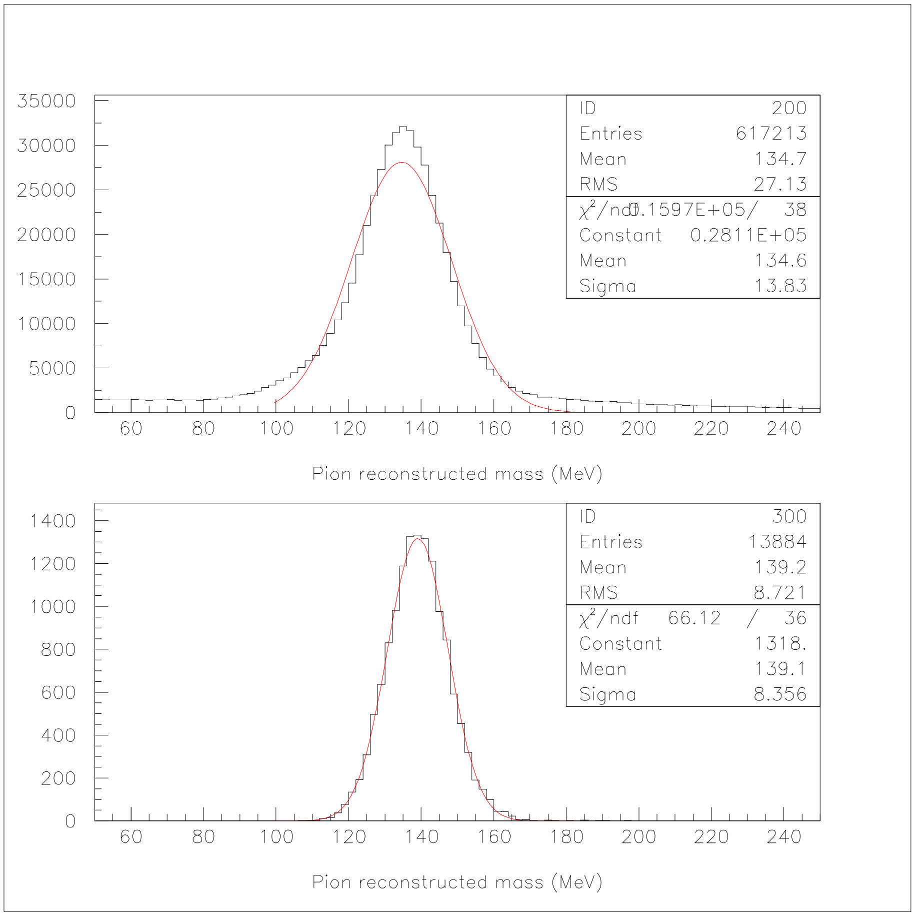

Figure 36: Distributions of the reconstructed π^+ mass from $\pi_{scatter}$ (top) and $K_{\pi 2}$ events (bottom).

the following small and large boxes:

$$\begin{aligned}
&\text{Small box :} && \\
147.7\ \text{MeV/c} &< ptot < && 188.1\ \text{MeV/c} \\
12.7\ \text{cm} &< rtot < && 26.5\ \text{cm} \\
63.3\text{Me}V &< etot < && 95.0\text{Me}V \\
&\text{Large box :} && \\
132.3\ \text{MeV/c} &< ptot < && 209.9\ \text{MeV/c} \\
11.3\ \text{cm} &< rtot < && 29.5\ \text{cm} \\
56.7\text{Me}V &< etot < && 106.0\text{Me}V
\end{aligned}$$

The variation in the kinematic box determines the systematic error associated with the RS-kinematic cuts, as determined in Eq. (29).

$$\Delta A^{sys}_{RSkin} = \frac{|A^{large\ box}_{RSkin} - A^{small\ box}_{RSkin}|}{2} \tag{29}$$

Cut	Loose Box		Tight Box	
	Events	**Acceptance**	**Events**	**Acceptance**
$Setup_{RSkin}^{small}$	63400		29195	
UTCQUAL	60350	0.9519 ± 0.00085	27906	0.9558 ± 0.00120
RNGMOM	59251	0.9818 ± 0.00054	27396	0.9817 ± 0.00080
RSDEDXMAX	57778	0.9751 ± 0.00064	26746	0.9763 ± 0.00092
RSDEDXCL	55375	0.9584 ± 0.00083	25685	0.9603 ± 0.00119
RSLIKE	55375	1.0000	25685	1.0000
PRRF1	55017	0.9935 ± 0.00034	25548	0.9947 ± 0.00045
PRRFZ	53324	0.9692 ± 0.00074	24778	0.9699 ± 0.00107
LAYER14	53324	1.0000	24778	1.0000
$A_{RSkin}^{small\ box}$	0.84107 ± 0.001452		0.84871 ± 0.002097	

Table 52: RS kinematic acceptance in the small box using $\pi_{scatter}$ monitor events. The "Tight box" of the rightmost two columns refers to tight PV, TD and DELCO cuts.

Cut	Loose Box		Tight Box	
	Events	**Acceptance**	**Events**	**Acceptance**
$Setup_{RSkin}^{large}$	110317		51078	
UTCQUAL	104830	0.9503 ± 0.00065	48730	0.9540 ± 0.00093
RNGMOM	102909	0.9817 ± 0.00041	47846	0.9819 ± 0.00060
RSDEDXMAX	99517	0.9670 ± 0.00056	46347	0.9687 ± 0.00080
RSDEDXCL	94726	0.9519 ± 0.00068	44201	0.9537 ± 0.00098
RSLIKE	94726	1.0000	44201	1.0000
PRRF1	93737	0.9896 ± 0.00033	43806	0.9911 ± 0.00045
PRRFZ	90176	0.9620 ± 0.00062	42205	0.9635 ± 0.00090
LAYER14	90176	1.0000	42205	1.0000
$A_{RSkin}^{large\ box}$	0.81743 ± 0.001163		0.82629 ± 0.001676	

Table 53: RS kinematic acceptance in the large box using $\pi_{scatter}$ monitor events. The "Tight box" of the rightmost two columns refers to tight PV, TD and DELCO cuts.

Hence, the RS-kinematic acceptance is

$$A^{loose}_{RSkin} = 0.82954 \pm 0.001262 \pm 0.012 \tag{30}$$

$$A^{tight}_{RSkin} = 0.84305 \pm 0.002049^{+0.006}_{-0.017} \tag{31}$$

15.4 $\pi^+ \to \mu^+ \to e^+$ Identification Acceptance

In an analogous way as the RS-kinematic-acceptance sample was created, the $\pi^+ \to \mu^+ \to e^+$ acceptance ($A_{\pi\to\mu\to e}$) requires the sample to be purified via cuts which are uncorrelated to the $\pi \to \mu \to e$ criteria (or simply TD cuts) being measured. RS-kinematic requirements were used to insure that the track was from a π^+. Since the $\pi_{scatter}$ did not include the online LEV1.1 and LEV1.2, the acceptances of these online requirements on the $\pi\nu\bar{\nu}(1)$ and $\pi\nu\bar{\nu}(2)$ could also be measured.

RSDEDX is correlated with EV5 due to μ^+ accidentals along the track causing EV5 to reject the event along with RSDEDX rejecting the event due to incorrect dE/dX value. PRRF1's dependence on the stopping-counter energy correlates it to the TD-pulse fitting utilized by TDNN. Tables 54 and 55 show the measured acceptances without and with RSDEDX and PRRF1,PRRFZ included in the setup cuts (A_{TD1}, A_{TD2}), respectively.

$A_{\pi\to\mu\to e}$ will be determined by the average of A_{TD1} and A_{TD2} and the systematic error is calculated from the difference. A 1.014% correction for π^+ decay-in-flight and π^+ absorption in the stopping counter, estimated from Monte Carlo, was applied to A_{TD2}.

Cut	Loose Box		Tight Box	
	Events	**Acceptance**	**Events**	**Acceptance**
$Setup_{\pi\to\mu\to e}$	126239		60258	
PIFLG	104055	0.8243 ± 0.00107	49850	0.8273 ± 0.00154
RSHEX2	102123	0.9814 ± 0.00042	48999	0.9829 ± 0.00058
LEV1.1	82659	0.8094 ± 0.00123	39953	0.8154 ± 0.00175
LEV1.2	69374	0.8393 ± 0.00128	35850	0.8973 ± 0.00152
TDCUT	65186	0.9396 ± 0.00090	33754	0.9415 ± 0.00124
ELVETO	62425	0.9576 ± 0.00079	32471	0.9620 ± 0.00104
TDFOOL	62208	0.9965 ± 0.00024	32365	0.9967 ± 0.00032
TDNN	58607	0.9421 ± 0.00094	27401	0.8466 ± 0.00200
EV5	58607	1.0000	22794	0.8319 ± 0.00226
A_{TD1}	0.46425 ± 0.001404		0.37827 ± 0.001976	

Table 54: $\pi^+ \to \mu^+ \to e^+$ acceptance using $\pi_{scatter}$ monitor events.

The $\pi^+ \to \mu^+ \to e^+$ and total acceptance measured using $\pi_{scatter}$-monitor events is calculated via Eq. (32) and is summarized in Table 56

$$A_{\pi_{scat}} = A_{badstc} \times A_{RSkin} \times A_{\pi\to\mu\to e} \tag{32}$$

Cut	Loose Box		Tight Box	
	Events	**Acceptance**	**Events**	**Acceptance**
$Setup_{\pi\to\mu\to e}$	126239		60258	
RSDEDXMAX				
RSDEDXCL				
RSLIKE				
PRRF1				
PRRFZ	107124		51828	
PIFLG	90161	0.8417 ± 0.00112	43749	0.8441 ± 0.00159
RSHEX2	88616	0.9829 ± 0.00043	43045	0.9839 ± 0.00060
LEV1.1	72545	0.8186 ± 0.00129	35471	0.8240 ± 0.00184
LEV1.2	61913	0.8534 ± 0.00131	32333	0.9115 ± 0.00151
TDCUT	58288	0.9415 ± 0.00094	30492	0.9431 ± 0.00129
ELVETO	55833	0.9579 ± 0.00083	29339	0.9622 ± 0.00109
TDFOOL	55655	0.9968 ± 0.00024	29255	0.9971 ± 0.00031
TDNN	52472	0.9428 ± 0.00098	24807	0.8480 ± 0.00210
EV5	52472	1.0000	20673	0.8334 ± 0.00237
$A_{uncorr\ TD2}$	0.48983 ± 0.001527		0.39888 ± 0.002151	
π^+ DIF/abs	$\times 1.014$			
A_{TD2}	0.4967 ± 0.0015		0.4045 ± 0.0022	

Table 55: $\pi^+ \to \mu^+ \to e^+$ acceptance using $\pi_{scatter}$ monitor events. $A_{uncorr\ TD2}$ is the acceptance before the correction factor for decay-in-flight (DIF) and π^+ absorption (abs) in the stopping counter (π^+ DIF/abs).

	Loose	Tight Box
A_{badstc}	0.99843 ± 0.000101	0.99923 ± 0.000102
A_{RSkin}	$0.82954 \pm 0.001262 \pm 0.012$	$0.84305 \pm 0.002049^{+0.006}_{-0.017}$
$A_{\pi\to\mu\to e}$	$0.4805 \pm 0.0015 \pm 0.016$	$0.3914 \pm 0.0022 \pm 0.013$
$A_{\pi_{scat}}$	$0.3980 \pm 0.0014 \pm 0.014$	$0.3297 \pm 0.0020^{+0.011}_{-0.013}$

Table 56: $\pi_{scatter}$ acceptance summary for loose and tight regions.

15.5 Acceptance Factors from $K_{\pi 2}$ Events

Within the E949 analysis, events from $K_{\pi 2}(1)$ monitors are similar to $K^+ \to \pi^+\nu\bar{\nu}$ events in a few aspects: (1) They both have a single π^+ track emerging from a single incoming K^+. (2) The π^+ within the TG is minimum ionizing. Condition (1) allows for a valid target reconstruction with a good decay-vertex determination. These properties allow acceptances to be measured for target kinematics.

$K_{\pi 2}$ **Setups**	**Component cuts**
$Setup_{utc}$	TRIGGER, RD_TRK, TRKTIM, STLAY, BAD_STC
$Setup_{ops}$	$Setup_{utc}$, UTC, RDUTM, PDC, PSCUT06, KCUTS, TGCUT06 without the ones measured, TDCUT02, KP2BOX
$Setup_{TGkin}$	$Setup_{ops}$, OPSVETO, TGPVCUT

Table 57: Setup cuts used for the $K_{\pi 2}$-based acceptance measurements.

To obtain a sample of PNN2 signal-like events, setup cut in Table 57 were utilized on $K_{\pi 2}(1)$ triggers. Measuring the acceptance of the PASS1 UTC cuts required reconstructing the TG and RS.

Cut	**Events**	**Acceptance**
$Setup_{utc}$	1502895	
UTC	1417906	0.9435 ± 0.00019
A_{utc}	0.94345 ± 0.000188	

Table 58: UTC acceptance using $K_{\pi 2}(1)$ monitor events.

The acceptance measurement of OPSVETO, Table 59, requires a sample with valid reconstruction within the TG and RS along with the requirement that there are no secondary beam particles (PSCUT06). Applying KP2BOX and TDCUT02 further purifies the sample to be valid $K_{\pi 2}$ decays.

Cut	**Events**	**Acceptance**
$Setup_{ops}$	62989	
OPSVETO	61365	0.9742 ± 0.00063
A_{tgkin}	0.97422 ± 0.000631	

Table 59: OPSVETO acceptance using $K_{\pi 2}(1)$ monitor events.

Obtaining the best sample to measure acceptance of target kinematics is a combination of (1) good TG reconstruction, which is not available in a $\pi_{scatter}$ sample due to poor reconstruction of the TG at very small delayed-coincidence, and (2) π^+'s with kinetic energies spread throughout the PNN2 signal region ($60.0MeV \leq E_{\pi^+} \leq 100.5MeV$), which is not available in a $K_{\pi2}(1)$ sample. That is, E949 montior samples do not satisfy both (1) and (2). In the $\pi_{scatter}$ sample, TG fiber hits may be identified as a π^+-fiber near the scattering point (ideally reconstructed as the decay vertex) could have energy much greater than a normal π^+ from a $K^+ \to \pi^+\nu\bar{\nu}$ decay. Thus, using a $\pi_{scatter}$ sample would yield a TG kinematic acceptance systematically lower than the true value.

Measuring the acceptance of TGDEDX with the sample used for calibration, $\pi_{scatter}$, would bias the acceptance measurement (see Section 7.3). Therefore, the clean $K_{\pi2}$ sample obtained by applying $Setup_{TGkin}$ is employed. The rest of the cuts in Table 60 employed the $K_{\pi2}$ sample due to their dependence on good determination of the decay vertex and assuming no π^+ energy dependence.

Cut	Loose Box		Tight Box	
	Events	**Acceptance**	**Events**	**Acceptance**
$Setup_{TGkin}$	60696		36719	
TGDEDX	60044	0.9893 ± 0.00042	36319	0.9891 ± 0.00054
TGER	60029	0.9998 ± 0.00006	36310	0.9998 ± 0.00008
TGENR	58065	0.9673 ± 0.00073	35058	0.9655 ± 0.00096
TGLIKE1	57014	0.9819 ± 0.00055	34413	0.9816 ± 0.00072
TGLIKE2	56103	0.9840 ± 0.00053	33858	0.9839 ± 0.00068
EPITG	50297	0.8965 ± 0.00129	30427	0.8987 ± 0.00164
EPIMAXK	50297	1.0000	30427	1.0000
TGEDGE	50018	0.9945 ± 0.00033	30271	0.9949 ± 0.00041
DRP	49932	0.9983 ± 0.00019	30214	0.9981 ± 0.00025
CHI567	43649	0.8742 ± 0.00148	26432	0.8748 ± 0.00190
CHI5MAX	43648	1.0000 ± 0.00002	26431	1.0000 ± 0.00004
A_{tgkin}	0.71913 ± 0.001824		0.71982 ± 0.002344	

Table 60: TG kinematic acceptance using $K_{\pi2}(1)$ monitor events.

The total acceptance of cuts measured using $K_{\pi2}$-monitor events, as shown in Eq. (33), is summarized in Table 61.

$$A_{K_{\pi2}} = A_{utc} \times A_{opsveto} \times A_{TGkin} \tag{33}$$

15.6 UMC based acceptance

The acceptance of the online trigger and the phase space and solid angle cuts and the acceptance loss due to pion decay-in-flight and pion nuclear interactions ("NIDIF") are calculated with $K^+ \to \pi^+\nu\bar{\nu}$ Monte Carlo simulated events. About 10^5 signal events were generated with NIDIF on and another 10^5 with NIDIF off. The trigger A_{tr} and phase space A_{ps} acceptance are measured with NIDIF-off sample, and then are corrected

	Loose Box	Tight Box
A_{utc}	0.94345 ± 0.000188	0.94345 ± 0.000188
$A_{opsveto}$	0.97422 ± 0.000631	0.97357 ± 0.000821
A_{TGkin}	0.71913 ± 0.001824	0.71982 ± 0.002344
$A_{K_{\pi 2}}$	0.6610 ± 0.0017	0.6612 ± 0.0022

Table 61: $K_{\pi 2}$ acceptance summary.

for NIDIF by comparing with the NIDIF-on sample (A_{NIDIF}). The results are shown in Tab. 62. UFATE, USTMED and USTOP_HEX cuts are based on UMC truth variables. UFATE requires that the pion stopped without decay or interaction. USTMED requires that the pion stopped in the RS scintillator, and USTOP_HEX requires that the offline reconstructed stopping counter agrees with the real one. The SETUP cut is $ptot < 300\ MeV$.

	NIDIF on	NIDIF off
	99999	100000
T•2	39227	41036
$3_{ct} \cdot 4_{ct} \cdot 5_{ct} \cdot 6_{ct}$	27575	33742
pnn1 or pnn2	26288	32914
A_{tr}	0.2629 ± 0.0014	0.3291 ± 0.0015
SETUP	25793	32887
UFATE	22688	32887
USTMED	22517	32620
USTOP_HEX	21743	32500
COS3D	20870	31294
LAYER14	20838	31282
ZFRF	20175	30083
ZUTOUT	20148	30063
Ke4 BOX	7758	10812
A_{Ke4}	0.3008 ± 0.0029	0.3288 ± 0.0026
Loose BOX	9552	13334
A_{loose}	0.3703 ± 0.0030	0.4054 ± 0.0027

Table 62: UMC based acceptance.

15.7 Acceptance Summary

The total acceptance is summarized in Table 63.

	Loose Box	Tight Box	From Table
$A_{K_{\mu2}}$	0.07183 ± 0.001981	0.0348 ± 0.0074	48
$A_{\pi_{scat}}$	$0.3980 \pm 0.0014 \pm 0.014$	$0.3297 \pm 0.0020^{+0.011}_{-0.013}$	56
$A_{K_{\pi2}}$	0.6610 ± 0.0017	0.6612 ± 0.0022	61
A_{UMC}	$0.0974 \pm 0.0021 \pm 0.0097$	$0.0791 \pm 0.016 \pm 0.0079$	62
A_{tot}	$\mathbf{(1.841 \pm 0.065^{+0.194}_{-0.194}) \times 10^{-3}}$	$\mathbf{(0.600 \pm 0.176^{+0.063}_{-0.064}) \times 10^{-3}}$	-

Table 63: Total acceptance for PNN2.

16 Kaon exposure

The total KB_{Live} was measured to be 1.7096×10^{12}. This took into account runs which were removed after E949-PNN1 analysis, see [22]. This also included all runs listed in `$PASS2_ANAL/func/ bad_run_02.function` which include runs removed by Joss due to bad cktbm data and bad target ccd data.

17 Single Cut Failure Study

A single-cut failure study helps to determine if there are any backgrounds which were not included *a priori* or if there are loop-holes for background processes to pass E949 cuts and become a candidate event. A single-cut failure study was performed by grouping correlated cuts together. By construction, each background process is suppressed by two independent methods; grouping correlated cuts would be the only method to determine if the two independent methods were working properly. Thirteen groups were created and are listed as follows:

- Seven non-grouped cuts include the following:

  BOX, Photon-Veto not including ADPV or TGPV, ADPV, DELC3, B4EKZ, TGZFOOL.

- *Extra Target Energy* Cuts:

  TGPV, OPSVETO.

- π^+ *Energy in* K^+ *Fibers* Cuts:

  CCDPUL, CCDBADFIT, CCDBADTIM, CCD31FIB, EPIONK, TIMKF.

- *Target/IC geometry* Cuts:

  TGGEO, KIC.

- *TD* Cuts:

  PIFLG, ELVETO, TDFOOL, TDNN, RSHEX, RSHEX2.

- *Kinematics* Cuts:

  COS3D, ZFRF, ZUTOUT, UTCQUAL, TICCON, EICCON, RNGMOM, PRRF1, PRRFZ, RSDEDXMAX, RSDEDXCL, RSLIKE, LAYER14.

- *Beam* Cuts:

  BWTRS, CKTRS, CKTAIL, CPITRS, CPITAIL, B4DEDX, B4TRS, B4CCD, TIMCON, UPVTRS, RVTRS.

- *Other* Cuts:

  TGQUALT, NPITG, EPITG, EPIMAXK, TGER, TARGF, DTGTTP, RTDIF, DRP, TGKTIM, TGEDGE, TGDEDX, TGENR, PIGAP, TGLIKE1, TGLIKE2, TBDB4, TGDB4TIP, TGDVXTIP, TGDVXPI, PHIVTX, CHI567, CHI5MAX, ALLKFIT, TPICS, TGTCON, B4ETCON.

Group	number of events	"true" single-cut failures
BOX	36 (37)	0
PV(no AD, no TG)	190 (192)	20
ADPV	0 (1)	0 (1)
DELC3	0	0
B4EKZ	0	0
TGZFOOL	0	0
Extra TG Energy	1	0
π^+ energy in K^+ fiber	3	2
TG/IC	1	1
TD	0	0
Kinematics	2 (3)	1
Beam	0	0
Other	3	1
Total	236 (240)	25 (26)

Table 64: Number of single-cut failures listed by grouped-cuts. "true" single-cut failures refer to events which only fail one individual cut within the cut group. The numbers in parenthesis are the number of single-cut failures (only when a difference occurs) before application of the safety cuts (i.e. initial study).

For an event to become a single-cut failure, it must fail cuts only in one group. The event can fail multiple cuts in the group and still be considered a single-cut failure. Events are of additional interest if they only fail one cut within a cut group category ("true" single-cut failures). The results of the single-cut failure study are shown in Table 64.

Events of interest were visually inspected; these included all single-cut events except for the events which failed multiple PV cuts (66 events in total). The 20 events which failed only one cut within the PV category were very far away from the cut threshold; 16 of the 20 failed ECouter. The reconstruction of these events leads to the conclusion that one or two very energetic photons ($> 60\mathrm{M}eV$) from a $K_{\pi 2}$ decay were converted and contained solely within one photon detector. All other events are consistent with expectation due to cut efficiencies.

17.1 Safety Cuts

An initial single-cut failure study yielded 240 events. The four additional events (compared to Table 64) included one ADPV event, one BOX event, and two PV events.

Analysis of the ADPV lead to the creation of CCDBADTIM. The reconstruction of the event showed a $K_{\pi 2}$ TG-scatter event where a photon was detected within the AD. The scatter in the TG was reconstructed in the TG-CCD-pulse fitting. However, the fit was erroneous due to the extremely large second pulse ($\sim 8\mathrm{M}eV$). CCDBADTIM requires that the times of the single and double pulse are consistent with the times of the TG reconstruction. This cut removed three events from the initial single-cut failure study (the ADPV event and two from the PV group).

Analysis of the "true" single-cut PV failure events yielded a possible loop-hole process. This occurred when the two photons from a π^0 converts in the same BVL element. This pathological process causes the timing to be mismeasured, possibly allowing the π^0 to go undetected. The cut which was devised against this process was named EARLY$_{BVL}$. EARLY$_{BVL}$ removes events when the mean time of the hit in a BVL element is between -5.0 ns and -2.0 ns, the time difference between the hits on each end is less than 4.0 ns, and the energy of the hit is greater than $10.0\mathrm{M}eV$. This additional cut removed one event from the BOX group in the initial single-cut failure study. EARLY$_{BVL}$ also effected at least two other PV single-cut failure events.

17.2 Comparing before and after implementation of safety cuts

All events from the 'skim' (June 2007) and the 'new' (Oct 2007) studies have been verified that they are the same events (barring the events that are now 2-cut failures). The numbers are consistent. We have changed a few cuts and included some safety cuts. The change of 2 PV was expected from the $EARLY_{BVL}$ safety cut. The change of 1 in the ADPV was due to a change in the CCDPUL-cuts (CCDBADTIM was created to remove events such as this). However, further investigation was performed to determine if there is a one-to-one correspondence of the single-cut failures in each group and determine the fate of the events that no longer in the single-cut sample.

17.3 early BVL PV cut

Three events which were visually scanned, including run 48206 event 29700, had the property of an early hit in the BVL which had large energy. This was observed by Kentaro [6] a safety cut was devised based upon his plots. The early timing is due to both γ's from the π^0 hitting the same BVL counter. The cut will remove events if the following conditions exist:

- $|\Delta t| < 4$ ns and $-5 < \bar{t} < -2$ ns, such that $|\Delta t| = t_1 - t_2$ and $\bar{t} = \frac{t_1+t_2}{2}$, t_1 and t_2 are the time of hit at each BVL end.
- $E_{intime} > 10 MeV$

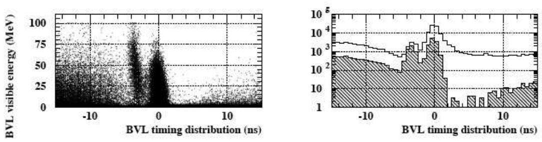

Figure 54: Observed photon hits in the BVL. The BVL had a micro structure of two peaks in the timing distribution (left figure). The earlier peak had higher energy. The peak distribution with the energy cut of $E^{BVL}_{visible} > 30$ MeV was plotted in the right plot. The open histogram is the timing distribution before the cut, and the hatched histogram is that with the energy cut. Smaller suppression was seen in the earlier peak compared with the later peak.

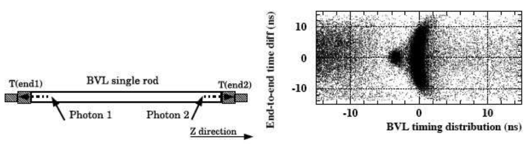

Figure 55: Illustration of the possible mechanism of the earlier peak in the BVL. The earlier peak was generated with events with whose two photons of $\pi^0 \to \gamma\gamma$ hit the same BVL rod (left figure). The right figure is a scatter plot of the BVL hit timing vs end-to-end time difference of the hit; T(upstream) - T(downstream). The localized spot gave the supporting evidence of the BVL double-hit mechanism.

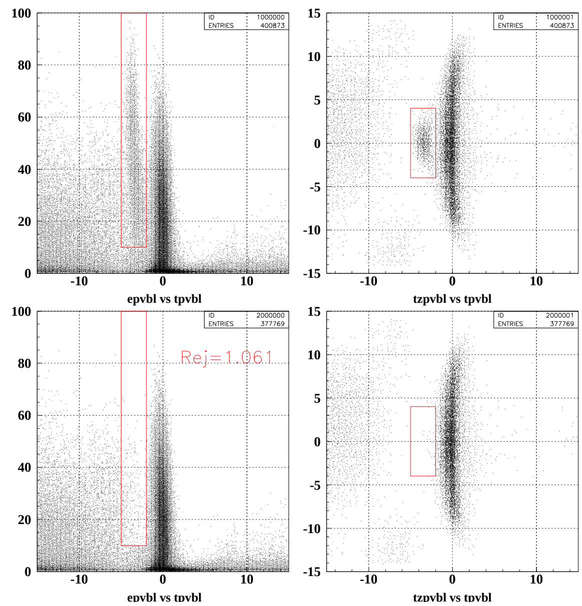

Figure 37: Left: Plots from Kentaro's thesis pg.83 [6]. Right: Reproduction of Kentaro's plots using PNN2 1/3 ntuples tagged by inverting $K_{\pi 2}$ box.

The acceptance of *early BVL* is 1.00, using Km2_07 monitors. As seen in Fig. 37, the safety cuts works as advertised. The safety cut removes the following 3 events:

- (49069,255066): fails Box group (pbox,rbox,ebox). π^0 completely contained within one BVL element.
- (48366,51102): fails PV group (RD,BV,BVL cuts)
- (48206,29700): fails PV group (BV cut)

17.4 Events Removed by Safety Cuts

17.4.1 Change in Box Group

Event 255066 Run 49069 is no longer in the single-cut failures. The event is now a 2-cut failure by also failing the Photon-Veto Group. This was expected as π^0 photons were completely contained in this event leading to EARLY_BVL cut failing.

17.4.2 Change in PV Group

- Event 87966 Run 50179 is no longer in the single-cut failure list. It now fails the EKaon group as well as the PV. CCDBADTIM was created to remove this event.
- Event 24636 Run 50086 now also fails Ekaon. CCDBADTIM was created to remove this event.

17.4.3 Change in ADPV Group

Event 19149 Run 49905 now also fails the Ekaon group. CCDBADTIM was created to remove this event.

18 Sensitivity

18.1 Single event sensitivity

Single event sensitivity ($S.E.S.$) is defined as

$$S.E.S. = A_{tot} \times \epsilon_{T\bullet 2} \times f_s \times KB_{live}.$$

In the absence of background, the $S.E.S.^{-1}$ is the lowest branching ratio that could be meansured by this analysis.

	value	Location
A_{tot}	$(1.841 \pm 0.065^{+0.194}_{-0.194}) \times 10^{-3}$	Table 63
$\epsilon_{T\bullet 2}$	$0.9505 \pm 0.0012 \pm 0.0143$	[4, 5]
f_s	0.7740 ± 0.0011	[4, 5]
KB_{live}	1.7096×10^{12}	Section 16

Table 65: Values used in SES determination. The column labeled 'Location' is where the number was extracted.

The $S.E.S.^{-1}$ is $(0.432 \pm 0.015^{+0.046}_{-0.046}) \times 10^{-9}$ for loose box and $(1.325 \pm 0.389^{+0.141}_{-0.143}) \times 10^{-9}$ for the tight region.

18.2 E949 pnn2 Cell definition

Nine cells are defined for E949 pnn2 analysis. They are based on the combinations of the following four cuts.

- KIN: Ke4 phobic box,
- PV: Tight PV, at 30% offline acceptance,
- DELCO: DELCO6,

- TD: The tight cut corresponds to the E949 PNN1-level TDCUTS. For the loose cut, EV5 is removed and the TDVARNN cut is loosened.

We present the following description of the calculation of each background component to each cell.

The Ke4 phobic box can effectively suppress K_{e4} and $K_{\pi 2}$ background. The rejection of Ke4 phobic box on K_{e4} background is estimated with UMC sample like in Sec. 5.2, while the rejection on $K_{\pi 2}$ background is estimated with its normalization branch. The rejection of TGPV·OPSVETO for K_{e4} background and the rejection of PVCUT for $K_{\pi 2}$ are not sensitive for this change of kinematic range. When tightening the upper bound of kinematic cut, the possible momentum of π^+ from $K_{\pi 2\gamma}$ decay will decrease. Correspondingly the minimum energy of the inner bremsstrahlung increases. The higher the energy of the gamma is, the higher rejection of PVCUT. So besides shrinking the effect phase space of $K_{\pi 2\gamma}$ background, tightening kinematic cut also contributes more rejection. However its rejection is almost the same with acceptance loss. Muon, beam and CEX background are thought to be not dramatically affected by this cut. Acceptance loss are taken into account for the decrease of these background.

Only muon background situation is significantly improved by tightening TDCUTS. Acceptance loss is used to explain the decrease of the other backgrounds.

DELCO will suppress single beam and CEX backgrond. However single beam background is only several percents of total beam background. Attention is only put onto CEX background.

Tight PV cut also suppress $K_{\pi 2}$ and $K_{\pi 2\gamma}$ background. Acceptance loss are calculated for the other background.

The rejections of these cuts and the acceptance losses of them are summarized in Table 66.

	KIN	TD	DELCO	PV
Acc loss	81.2%	81.5%	91.1%	54.7%
Rej for specific bkg	2.0 (Kp2) 2.7 (Ke4) 1.2 (Kp2g)	4.2 (Muon)	6.7 (CEX) 4.3 (beam)	2.5 (kp2,kp2g)

Table 66: Assumed acceptance loss and rejection for each background for each of the 4 cuts.

The low statistics in pnn2 background study does not allow a more intensive analysis for these four cuts and does not allow to have too more cells. And from the material shown in the following sections one can find that more cells also does not provide more useful information for signal search and final BR measurement. Tab. 67 gives a summary for the acceptance and background. Tab. 68 is a breakdown of each kind of backgrounds in each cells. Loose is for entire E949 pnn2 search region. Shorthand KIN means KIN is applied in addition to the loose cuts. And KIN* means the counterpart of KIN is applied inaddtion to the loose cuts. (KIN* = Loose kinematic box - tight kinematic box) The same definitions is also used to TD, TD*, DC, DC*, PV and PV*. The 9th cell is defined to the cell with KIN* since it has low acceptance and poor Acc/Bkg. No separation is done for that cell. $Kp2$ RS background is assumed zero here.

Cell No.	Cuts	Acc	Total bkg	Acc/Bkg
	Loose	1.000	$0.969 \pm 0.220^{+0.309}_{-0.246}$	1.032
9	KIN*	0.188	$0.438 \pm 0.113^{+0.163}_{-0.129}$	0.429
	KIN	0.812	$0.531 \pm 0.113^{+0.147}_{-0.117}$	1.530
1	KIN +TD +DC +PV	0.330	$0.141 \pm 0.032^{+0.040}_{-0.036}$	2.347
2	KIN +TD +DC +PV*	0.273	$0.174 \pm 0.043^{+0.035}_{-0.048}$	1.572
3	KIN +TD +DC*+PV	0.032	$0.054 \pm 0.018^{+0.025}_{-0.008}$	0.599
4	KIN +TD +DC*+PV*	0.027	$0.050 \pm 0.015^{+0.021}_{-0.008}$	0.532
5	KIN +TD*+DC +PV	0.075	$0.041 \pm 0.012^{+0.009}_{-0.008}$	1.842
6	KIN +TD*+DC +PV*	0.062	$0.047 \pm 0.012^{+0.008}_{-0.011}$	1.328
7	KIN +TD*+DC*+PV	0.007	$0.013 \pm 0.004^{+0.006}_{-0.002}$	0.560
8	KIN +TD*+DC*+PV*	0.006	$0.012 \pm 0.003^{+0.005}_{-0.002}$	0.501

Table 67: Acceptance and background summary of each cell. All the acceptance is normalized to that in loose cuts. Note that KIN* ≡ Loose kinematic box - tight kinematic box, etc. See text for additional details.

18.3 Junk method

Junk method is used for computing approximate confidence levels for searches for new particles where the expected signal and background levels are small enough to require the use of Poisson statistics. The results of many independent searches for the same particle may be combined easily, regardless of the discriminating variables which may be measured for the candidate events. The effects of systematic uncertainty in the signal and background models are incorporated in the confidence levels. The original paper is presented by Thomas Junk ([3]). Some effective tools can also be found in this website [19]. And more recent effort on this subject can be found in another web [20]. An intensive study on this method and its tools have been done since pnn1 analysis, like [5]. Here only the sketch of this method is explained.

For the case of n independent counting search analyses, one may define a test statistic X which discriminates signal-like outcomes from background-like ones. A choice for the test statistic is the likelihood ratio. If the estimated signal in the ith channel is s_i, the estimated background is b_i, and the number of observed candidates is d_i, then the likelihood ratio is:

$$X = \prod_{i=1}^{n} X_i$$

with

$$X_i = \frac{e^{-(s_i+b_i)}(s_i+b_i)^{d_i}}{d_i!} / \frac{e^{-b_i} b_i^{d_i}}{d_i!}$$

cuts	kp2 TG	kp2 RS	Beam	Muon	Ke4	Kp2g	CEX
Loose	$0.575 \pm 0.184^{+0.063}_{-0.201}$	0.000 ± 0.000	0.045 ± 0.020	0.030 ± 0.030	$0.176 \pm 0.102^{+0.233}_{-0.124}$	$0.050 \pm 0.008 \pm 0.003$	$0.092 \pm 0.053^{+0.070}_{-0.018}$
KIN*	$0.287 \pm 0.092^{+0.032}_{-0.101}$	0.000 ± 0.000	0.009 ± 0.004	0.006 ± 0.006	$0.111 \pm 0.064^{+0.147}_{-0.078}$	$0.008 \pm 0.001 \pm 0.000$	$0.017 \pm 0.010^{+0.013}_{-0.003}$
KIN	$0.287 \pm 0.092^{+0.032}_{-0.101}$	0.000 ± 0.000	0.037 ± 0.016	0.025 ± 0.025	$0.065 \pm 0.038^{+0.086}_{-0.046}$	$0.042 \pm 0.007 \pm 0.003$	$0.075 \pm 0.043^{+0.057}_{-0.015}$
KIN +TD +DC +PV	$0.085 \pm 0.027^{+0.009}_{-0.030}$	0.000 ± 0.000	0.004 ± 0.002	0.003 ± 0.003	$0.026 \pm 0.015^{+0.035}_{-0.019}$	$0.017 \pm 0.003 \pm 0.001$	$0.005 \pm 0.003^{+0.004}_{-0.001}$
KIN +TD +DC +PV*	$0.128 \pm 0.041^{+0.014}_{-0.045}$	0.000 ± 0.000	0.003 ± 0.001	0.002 ± 0.002	$0.022 \pm 0.013^{+0.029}_{-0.015}$	$0.014 \pm 0.002 \pm 0.001$	$0.004 \pm 0.002^{+0.003}_{-0.001}$
KIN +TD +DC*+PV	$0.008 \pm 0.003^{+0.001}_{-0.003}$	0.000 ± 0.000	0.013 ± 0.006	0.000 ± 0.000	$0.003 \pm 0.001^{+0.003}_{-0.002}$	$0.002 \pm 0.000 \pm 0.000$	$0.028 \pm 0.016^{+0.022}_{-0.006}$
KIN +TD +DC*+PV*	$0.013 \pm 0.004^{+0.001}_{-0.004}$	0.000 ± 0.000	0.010 ± 0.005	0.000 ± 0.000	$0.002 \pm 0.001^{+0.003}_{-0.002}$	$0.001 \pm 0.000 \pm 0.000$	$0.023 \pm 0.014^{+0.018}_{-0.005}$
KIN +TD*+DC +PV	$0.019 \pm 0.006^{+0.002}_{-0.007}$	0.000 ± 0.000	0.001 ± 0.000	0.009 ± 0.009	$0.006 \pm 0.003^{+0.008}_{-0.004}$	$0.004 \pm 0.001 \pm 0.000$	$0.001 \pm 0.001^{+0.001}_{-0.000}$
KIN +TD*+DC +PV*	$0.029 \pm 0.009^{+0.003}_{-0.010}$	0.000 ± 0.000	0.001 ± 0.000	0.008 ± 0.008	$0.005 \pm 0.003^{+0.007}_{-0.004}$	$0.003 \pm 0.001 \pm 0.000$	$0.001 \pm 0.001^{+0.001}_{-0.000}$
KIN +TD*+DC*+PV	$0.002 \pm 0.001^{+0.000}_{-0.001}$	0.000 ± 0.000	0.003 ± 0.001	0.001 ± 0.001	$0.001 \pm 0.000^{+0.001}_{-0.000}$	$0.000 \pm 0.000 \pm 0.000$	$0.006 \pm 0.004^{+0.005}_{-0.001}$
KIN +TD*+DC*+PV*	$0.003 \pm 0.001^{+0.000}_{-0.001}$	0.000 ± 0.000	0.002 ± 0.001	0.001 ± 0.001	$0.000 \pm 0.000^{+0.001}_{-0.000}$	$0.000 \pm 0.000 \pm 0.000$	$0.005 \pm 0.003^{+0.004}_{-0.001}$

Table 68: Detailed background information of each cell.

The confidence level for excluding the possibility of simultaneous presence of new particle production and background (the $s+b$ hypothesis) is

$$CL_{s+b} = P_{s+b}(X \leq X_{obs})$$

i.e., the probability, assuming the presence of both signal and background at their hapothesized levels, that the test statistic woulbe be less than or equal to that observed in the data. This probability is the sum of Poisson probabilities

$$P_{s+b}(X \leq X_{obs}) = \sum_{X(d_i') \leq X(d_i)} \prod_{i=1}^{n} \frac{e^{-(s_i+b_i)}(s_i+b_i)^{d_i'}}{d_i'!}$$

where $X(d_i)$ is the test statistic computed for the observed set of candidates in each channel d_i, and the sum runs over all possible configurations d_i' which have test statistics less than or equal to the observed one.

Another confidence level is for background alone,

$$CL_b = P_b(X \leq Xobs)$$

where the probability sum assumes the presence only of the background. i.e.

$$P_b(X \leq X_{obs}) = \sum_{X(d_i') \leq X(d_i)} \prod_{i=1}^{n} \frac{e^{-(b_i)}(b_i)^{d_i'}}{d_i'!}$$

The modified confidence level CL_s is defined as:

$$CL_s = CL_{s+b}/CL_b$$

And CL is introduced:

$$CL = 1 - CL_s$$

This CL is an extension of the common single channel confidence level calculation [21]. It doesn't have the traditional probability explaination of confidence level. (Classic Bayesian descripsion: given s_i and d_i, the probability of finding more than or equal to d_i events is CL.) However the CL of Junk method shows the same trend with Bayesian's result. And they are totally the same for singel channel case.

18.4 BR measurement

18.4.1 Reproducton of the result of the E949 pnn1 publication

Using the parameters from previous publications [23], [24], [25] and [26] and the cells' information from [5] as input, the E949 pnn1 CL curves are reproduced as a check of the implemenation of the Junk method and the acceptance and background of the cells of the previous analyses. See Fig. 38 for comparison.

- The published result in the E949 pnn1 paper [23] is $BR = (1.47^{+1.30}_{-0.89}) \times 10^{-10}$.
- The reproduced result is $BR = (1.47^{+1.34}_{-0.89}) \times 10^{-10}$. The slight difference in the confidence interval is due to systematic uncertainties not being taken into consideration here.

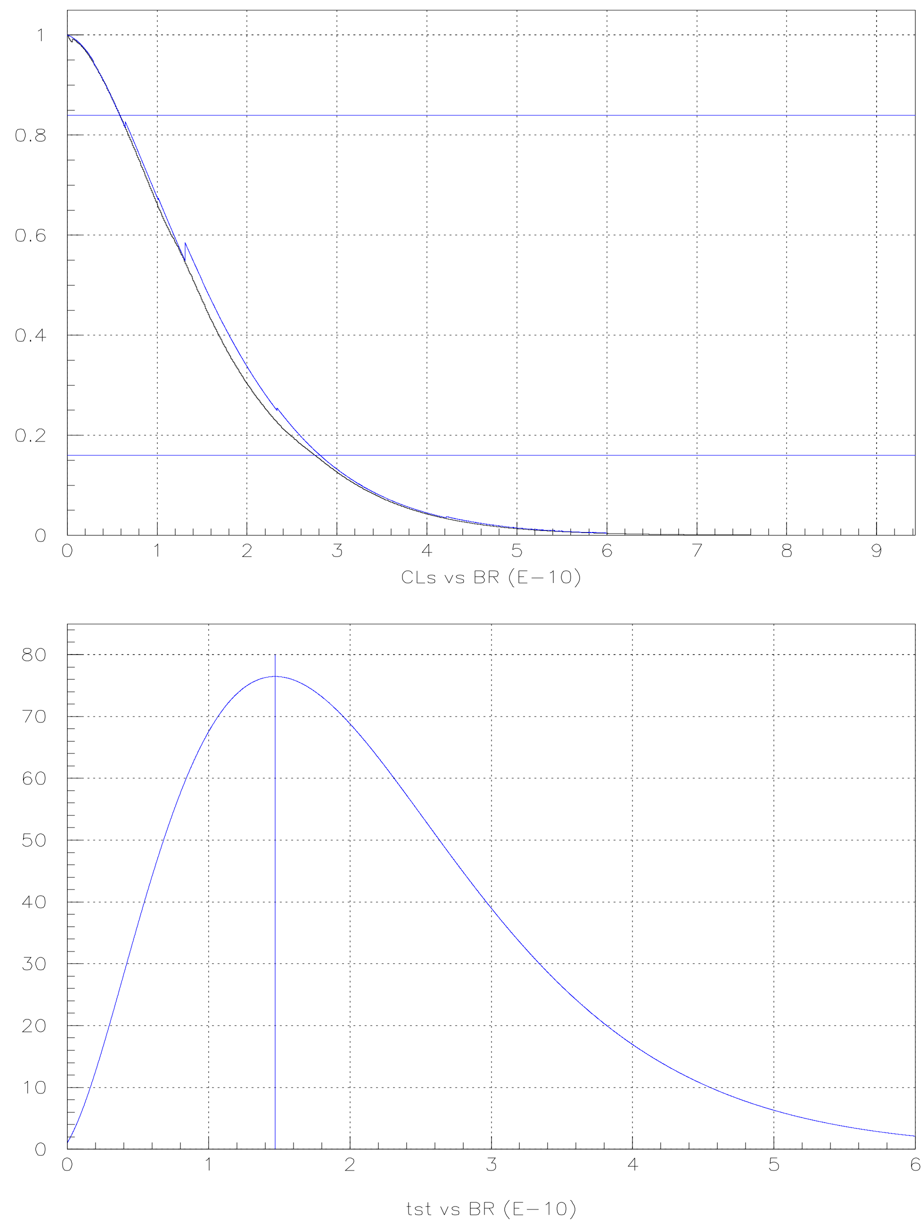

Figure 38: Reproduction of the E949 pnn1 CLs curve. The upper plot is for CLs curves. The blue and black curves are the published E949 pnn1 result and the one reproduced here respectively. Two horizontal lines denotes 68% coverage. The lower plot in the lower plot is the reproduced test statistic. The vertical line denotes 1.47×10^{-10}.

18.4.2 E949 pnn2 only

CLs curves and test statistic curves are computed for E949 pnn2 date set only. This shows the ability of making a discovery with E949 pnn2 alone. Fig. 39 presents the CLs and test statistic curves with 0 candidate or with 1 candidate in each of the 9 cells. Fig. 40 presents the CLs and test statistic curves with 2 candidate found in 9 cells. They might be in the same cell or in different cells. Systematic uncertainties are temporarily not taken into consideration here.

18.4.3 E787 and E949 pnn2 only

E787 [27] [28] and E949 pnn2 results are combined together here. Fig. 41 and Fig. 42 shows the combined CLs and test statistic curves for 0/1 and 2 candidates respectively. (Uncertainties are temporarily not taken into consideration here.)

18.4.4 All E787 and E949 result

Originally E787 pnn2 result are not combined into E949 pnn1 publication. Now it is a proper time to see how it will impact the whole $\pi\nu\bar{\nu}$ analysis. All the data of E787 and E949 analysis are inputed into Junk code. Fig. 43 and Fig. 44 shows the combined CLs and test statistic curves for 0/1 and 2 candidates respectively. (Uncertainties are temporarily not taken into consideration here.) Combining all $\pi\nu\bar{\nu}$ analysis result might change the central value of the BR in E949 pnn1 publication by about 20%. And that depends on whether some candidates were found or where they are found. It also might affect the 68% interval by less than 10%.

18.4.5 Correlated and uncorrelated uncertainties

From the study in [5] one can find that the uncertainties in background and sensitivity do not affect the final result dramatically. To facilitate the analysis and save lot of cpu time the study in previous sections ignored the systematic uncertainties. And it is believed it will not change the basic conclusion here. Certainly some quantities' changing of the BR might be possible.

Some helpful tools dealing with uncorrelated uncerntainties are already exploited by Junk [3] [19]. Here an exercise is done to find a way to solve the problem with correlated uncertainties. For example, like the acceptance measurement in all $\pi\nu\bar{\nu}$ analysis, the same approach is used for all these years. The systematic errors of these measurement could be 100% correlated. Sensitivities of each year are required to vary simultaneously. The variance is decribed as $\sigma_{SES} \times g$ where σ_{SES} is the error of the sensitivity and g is a varying parameter that obeys a normal distribution. Then a weighted sum of the resulting confidence level is calculated.

Here an example (Fig. 45) is shown for the E949 pnn1 result. The correlated errors of $S.E.S$ is involve in this calculation.

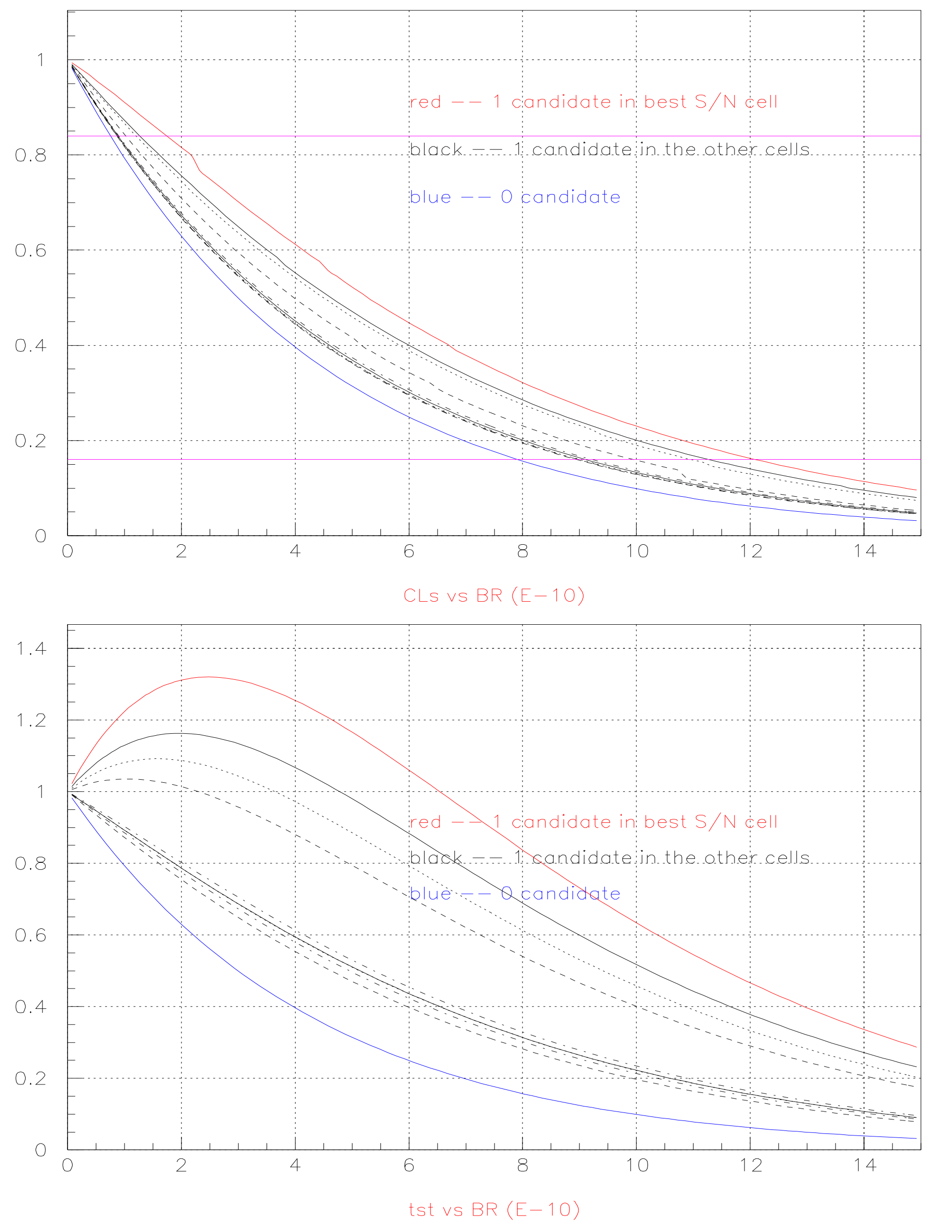

Figure 39: CLs (upper) and test statistic (lower) curves for E949 pnn2 data alone under the assumption of 0 or 1 candidate found. Two horizontal lines in the upper plot denotes 68% coverage.

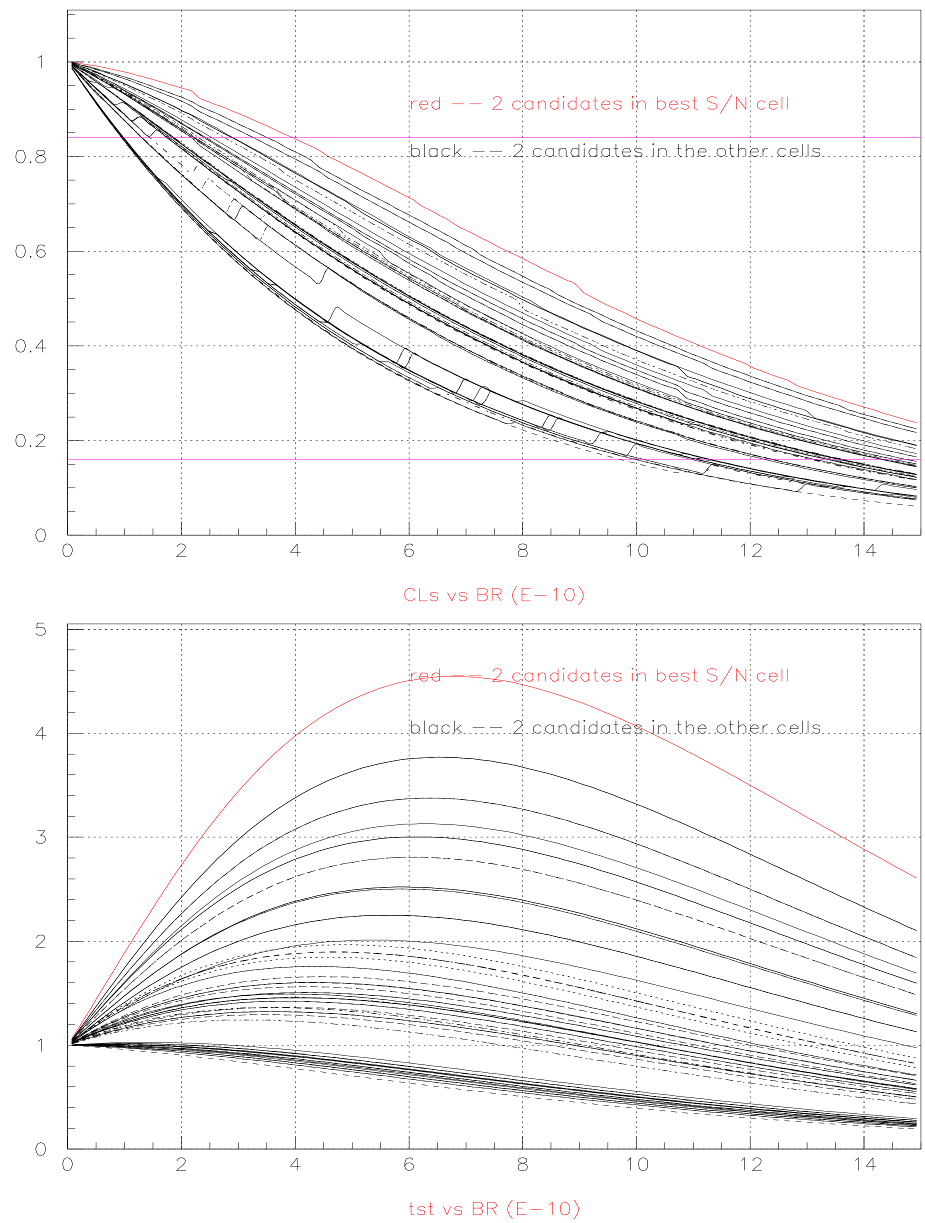

Figure 40: CLs (upper) and test statistic (lower) curves for E949 pnn2 data alone. Assume 2 candidates are found. Two horizontal lines in the upper plot denotes 68% coverage.

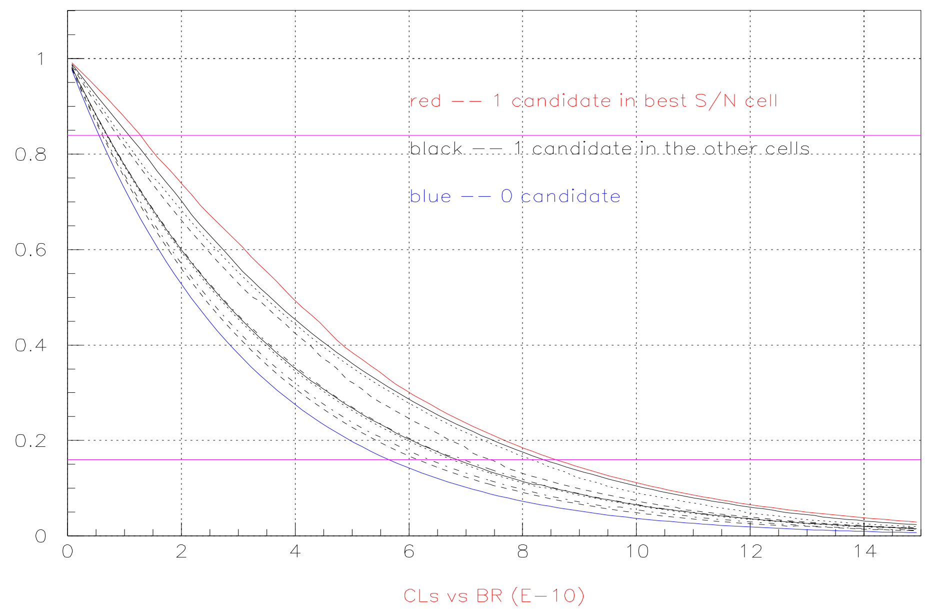

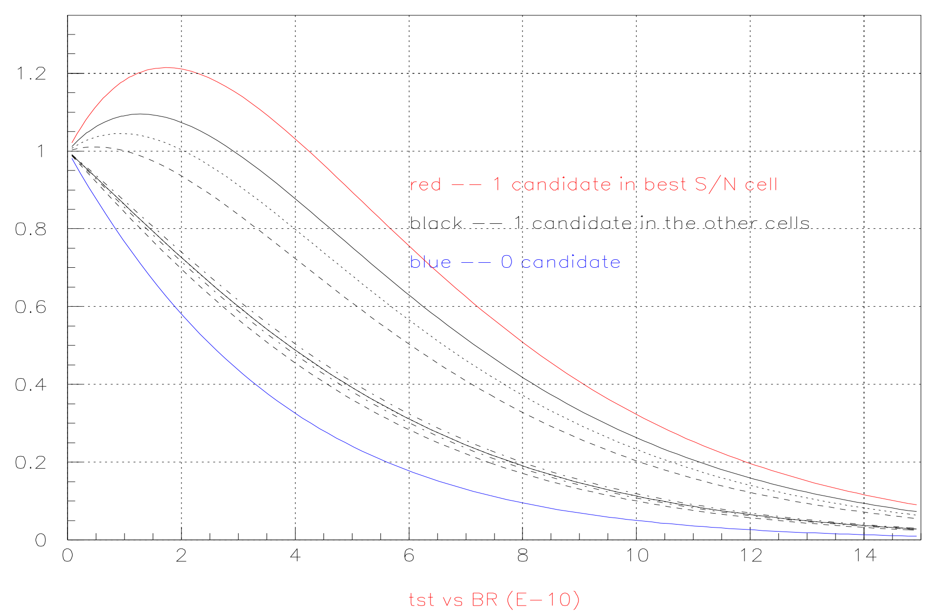

Figure 41: CLs (upper) and test statistic (lower) curves for E787 and E949 pnn2 data. Assume 0 or 1 candidate is found in E949 pnn2 study. Two horizontal lines in the upper plot denotes 68% coverage.

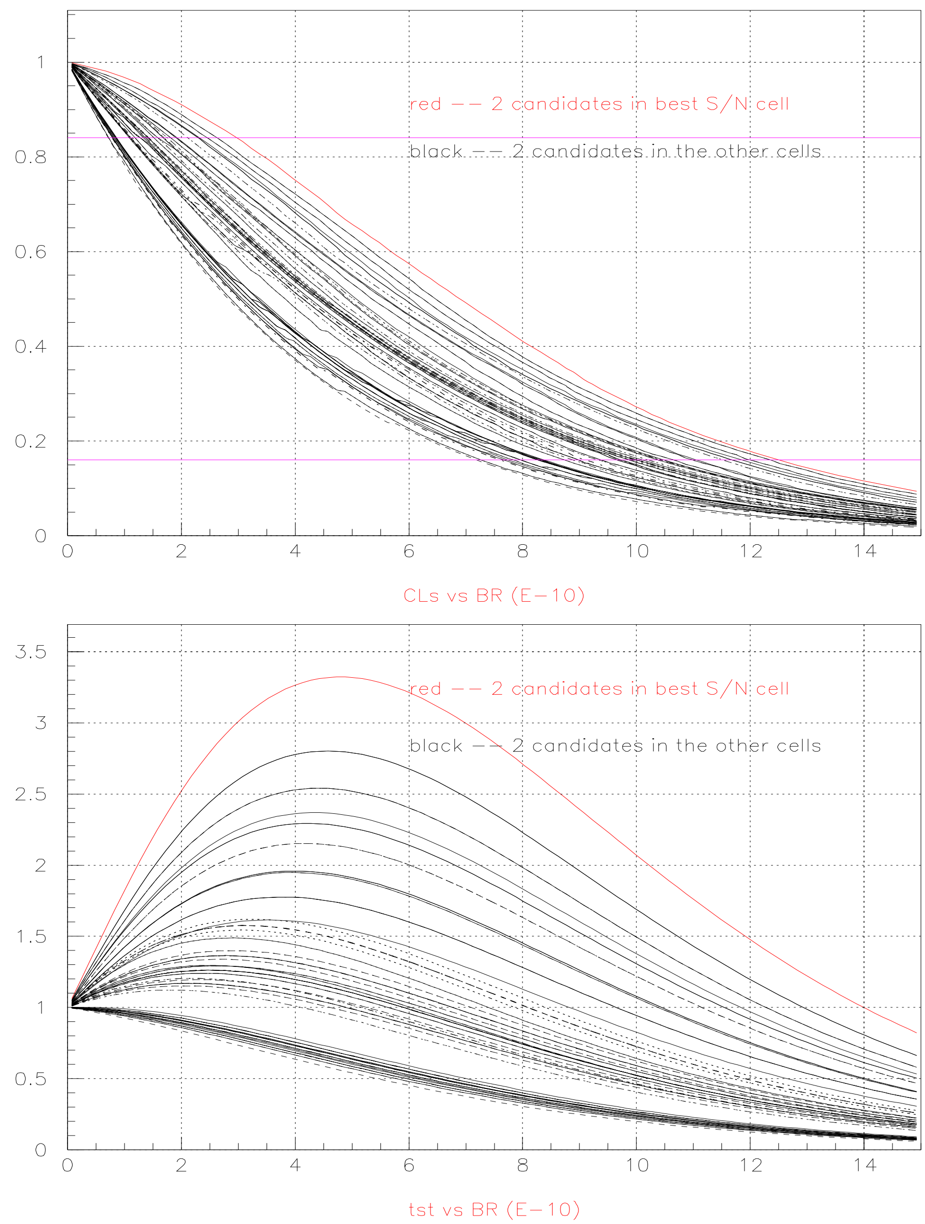

Figure 42: CLs (upper) and test statistic (lower) curves for E787 and E949 pnn2 data. Assume 2 candidates are found in E949 pnn2 study. Two horizontal lines in the upper plot denotes 68% coverage.

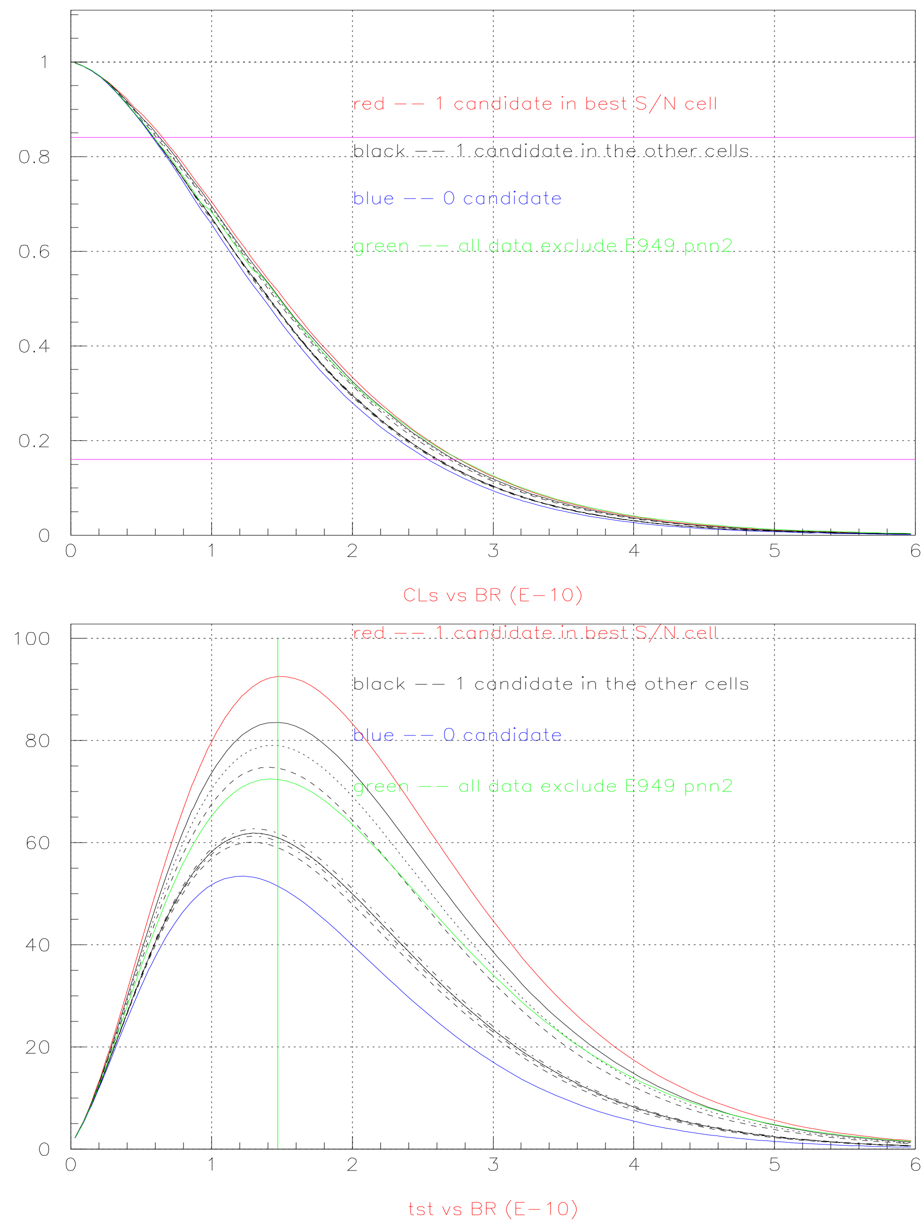

Figure 43: CLs (upper) and test statistic (lower) curves for all E787 and E949 data. Assume 0 or 1 candidate is found in E949 pnn2 study. Two horizontal lines in the upper plot denotes 68% coverage. The vertical line in the lower plot denotes 1.47×10^{-10}, E949 pnn1 publication.

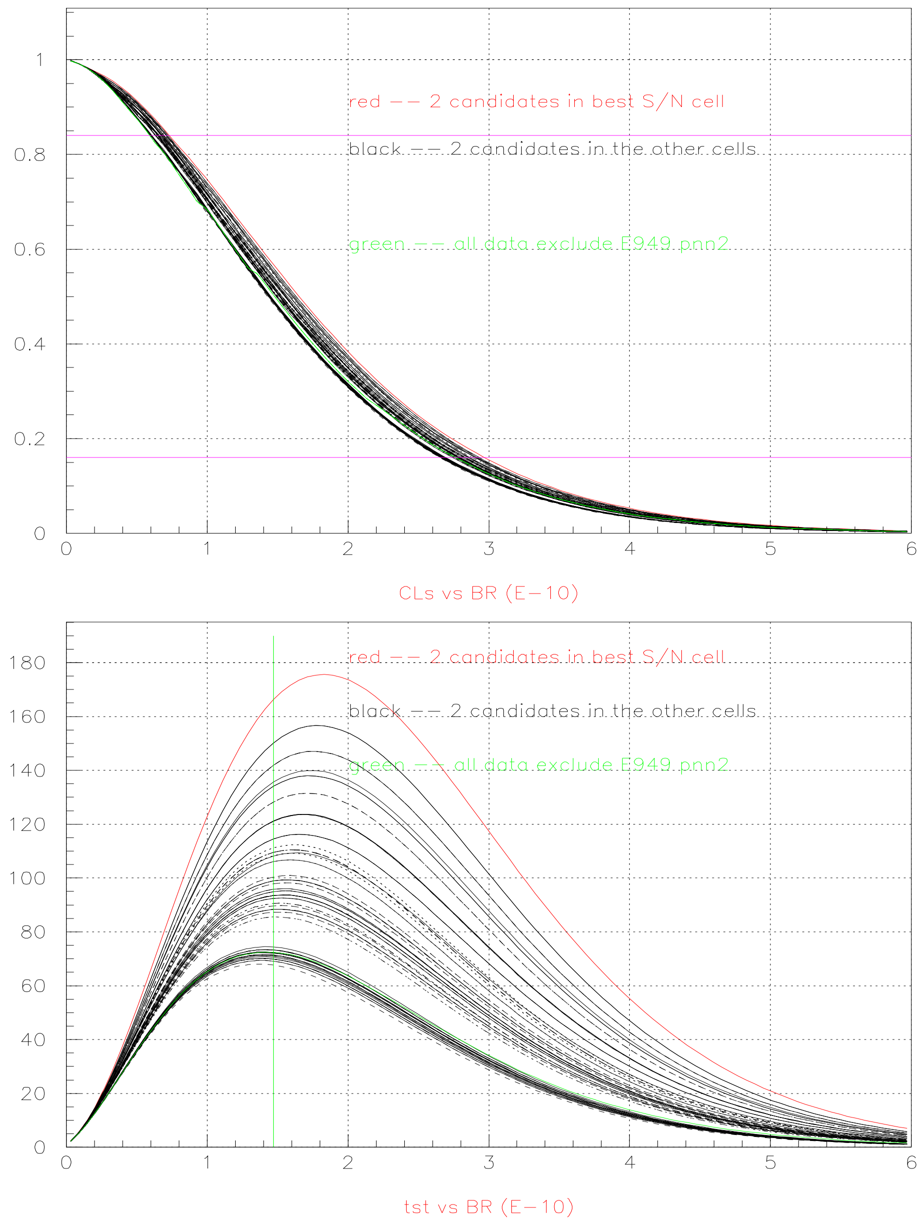

Figure 44: CLs (upper) and test statistic (lower) curves for all E787 and E949 data. Assume 2 candidates are found in E949 pnn2 study. Two horizontal lines in the upper plot denotes 68% coverage. The vertical line in the lower plot denotes 1.47×10^{-10}, E949 pnn1 publication.

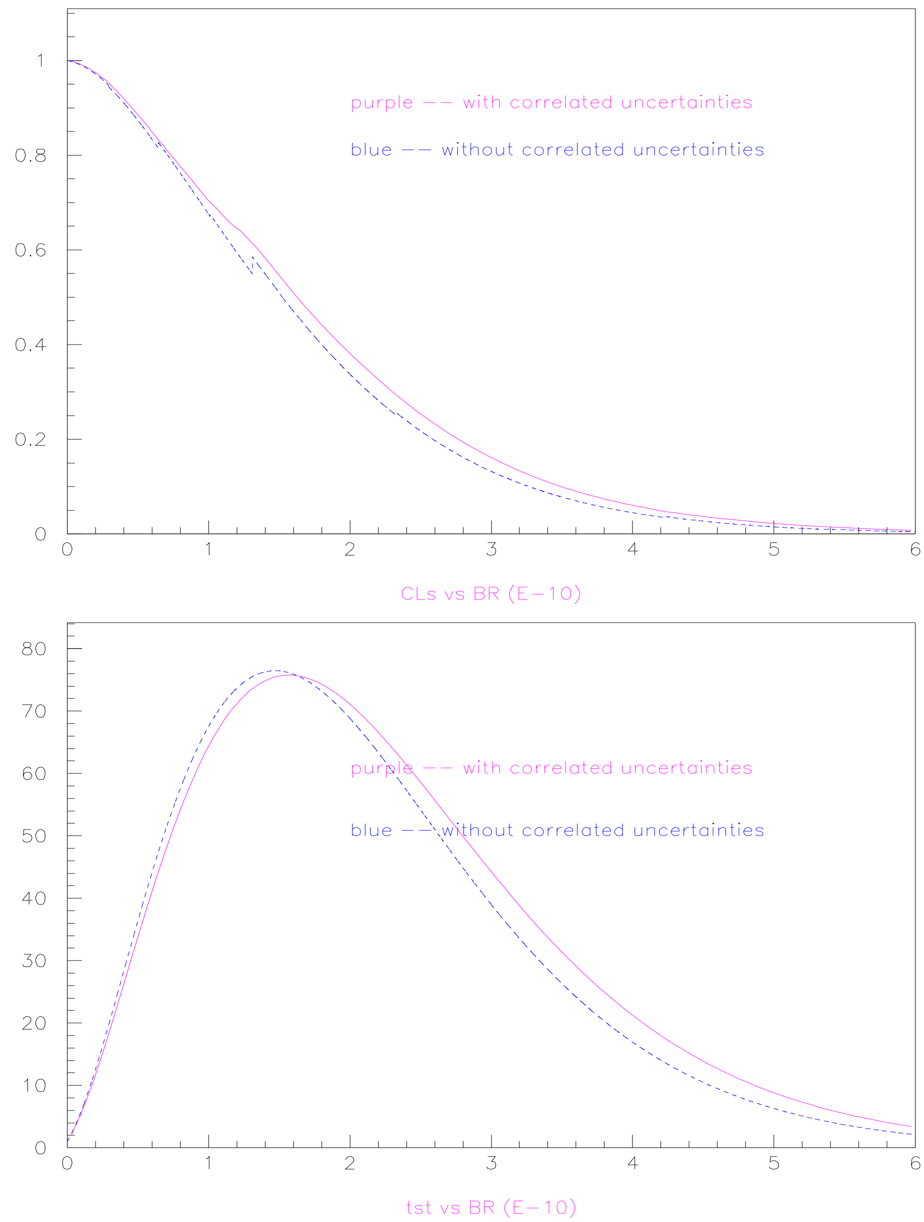

Figure 45: CLs (upper) and test statistic (lower) curves for all pnn1 result. The correlated uncertainties of $S.E.S$ is taken into account.

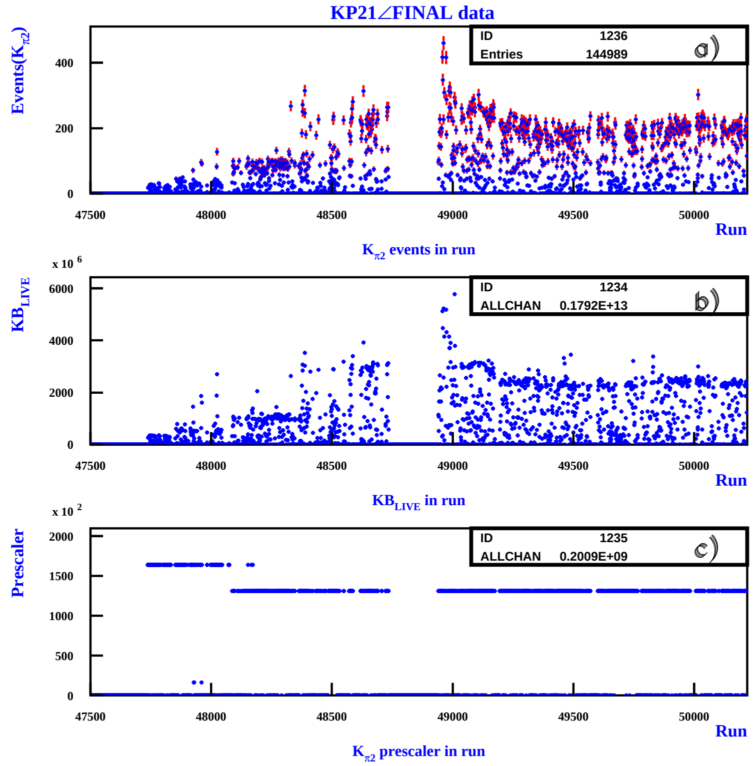

Figure 46: The $K_{\pi2}$ a) events, b) beam K^+-mesons and c) prescale factor versus run number.

19 Measurement of the $K_{\pi2}$ branching fraction

19.1 Introduction and experimental data

The purpose of $K_{\pi2}$ branching fraction measurement using the $K_{\pi2}(1)$ monitor sample is to check the validity of the f_s calculation and provide a consistency check of the pnn2 acceptance.

The $K_{\pi2}(1)$ monitor data set of the 2002 data taking run has been used in this analysis. Data have been taking by following trigger conditions:

$$(ONLINE\ \ TRIGGER)_{K_{\pi2}} = KB \times T \cdot 2 \times (6_{ct} + 7_{ct}) \times \overline{19_{ct}} \tag{34}$$

and with prescale factors of 163840 (runs 47737-48045) and 131072 after run 48045. The number of $K_{\pi2}$ events, number of beam K^+-mesons, and prescale factor versus run are shown on Fig. 46. It should be noted that a small fraction of $K_{\pi2}(1)$ monitor data was not used in analysis because of the absence end-of-spill information. Also note that no offline prescaling was applied to the $K_{\pi2}(1)$ monitor data for this analysis. For some runs (about 50) the prescaler factor in the prescaler file was not defined and have been taken equal to prescaler of previous run.

The $K_{\pi2}$ branching fraction is calculated according to following equation:

$$BR(K_{\pi2}) = \frac{N_{K_{\pi2}}}{\epsilon_{T\cdot2\cdot IC}\cdot(KB_{live})_{K_{\pi2}}\cdot A_{K_{\pi2,Br}}\cdot A^{UMC}_{K_{\pi2,kin}}\cdot f_S\cdot A^{UMC}_{K_{\pi2,trig}}} \quad (35)$$

where:

$$A_{K_{\pi2},Br} = A_{RD,Br}\times A_{RECO,Br}\times A_{REST,Br}\times A_{IPIFLG}\times A^{acc}_{\mu} \quad (36)$$

The values of f_s, $\epsilon_{T\cdot2\cdot IC}$, A^{acc}_{μ}(acceptance loss due to the $\overline{19_{ct}}$ requirement), and A_{IPIFLG} are taken from the 2002 PNN1 analyses [4]. The values of $A_{RD,Br}$, $A_{RECO,Br}$ and $A_{REST,Br}$ are given in Table 71. The values of $A^{UMC}_{K_{\pi2,kin}}$ and $A^{UMC}_{K_{\pi2,trig}}$ are given in Table 69. The value of $N_{K_{\pi2}}$ is given in Table 70.

19.2 Monte Carlo kinematic and trigger acceptances

The kinematic and trigger acceptances for $K_{\pi2}$ events have been defined by Monte Carlo simulation and are presented in Table 69 along with the result of 2002 PNN1 analyses [5] for comparison. The following additional cuts to remove muons, duplicate events and poorly reconstructed tracks are applied as setup or at the TRIGGER level in Tables 69, 70 and 71:

1. Remove $K_{\mu2}$ and duplicate events $(rngmom\_new3(0.)\leq 3)\cdot\overline{cut(6)}$
2. $tlay \leq 21$
3. PTOT $\neq 0\cdot$ PTOT $\neq 300$

It should be noted that these cuts do not affect the UMC data sample. Also note that the KP2BOX cut in the PNN1 analysis,

$$\texttt{KP2BOX} = |\mathrm{RDEV}|<3\cdot|\mathrm{EDEV}|<3\cdot|\mathrm{PDEV}|<3 \quad (37)$$

differs from the KP2BOX cut in this analysis. The description of the KP2BOX cut and the UMC cuts are in Sec. 19.6. Note that $A^{UMC}_{K_{\pi2},trig}$ is consistent with the 2002 measurement and that $A^{UMC}_{K_{\pi2},recon}$ and $A^{UMC}_{K_{\pi2},kin}$ differ due to changes in the UTCQUAL and TARGET cuts, and the KP2BOX cuts, respectively.

19.3 $K_{\pi2}$ event selection

The cuts applied to $K_{\pi2}(1)$ monitor data to select the $K_{\pi2}$ events are shown in table 70 and compared to the results of the 2002 PNN1 analysis in K-038 [5]. There are differences in the relative acceptance of some cuts due to changes to the cut definition for the PNN2 analysis (UTCQUAL, TGQUALT, B4EKZ, and KP2BOX) and the application of cuts at the TRIGGER level as described in Sec. 19.2.

19.4 Acceptance factors for the $K_{\pi2}$ branching fraction

The values of the acceptance factors $A_{RD,Br}$, $A_{RECO,Br}$ and $A_{REST,Br}$ are given in Table 71 along with a comparison to that for the PNN1 analysis taken from Table 23 of Ref. [5].

Cut	2002 (acc.)	2007 (acc.)
KT	49997	99993
T•A	22697(0.45397)	44891(0.44894)
Reach Layer B	19090(0.84108)	37605(0.83769)
$\overline{19}_{ct}$	18797(0.98465)	36986(0.98354)
UFATE	15910(0.84641)	31222(0.84416)
USTMED	15568(0.97850)	30518(0.97745)
USTOP_HEX	13909(0.89344)	27426(0.89868)
$A^{UMC}_{K_{\pi2},trig}$	0.27820 ± 0.00200	0.27428 ± 0.00141
UTC/RANGE	13909(1.00000)	———————–
RDUTM	———————-	27426(1.00000)
UTCQUAL	12660 (0.91020)	26910(0.98119)
TARGET	12532 (0.98989)	———————–
TARGET+TGQUALT	———————-	25659(0.95351)
$A^{UMC}_{K_{\pi2},recon}$	0.90100 ± 0.00253	0.93557 ± 0.00148
KPI2STOP	12072 (0.96329)	24639(0.96025)
COS3D	11878 (0.98393)	23671(0.96071)
KP2BOX(PNN1)	10840 (0.91261)	———————–
KP2BOX(PNN2)	———————-	20213(0.85391)
$A^{UMC}_{K_{\pi2},kin}$	0.86499 ± 0.00305	0.78775 ± 0.00255
$A^{UMC}_{K_{\pi2}}$	0.2168 ± 0.0018	0.20214 ± 0.00127

Table 69: UMC $K_{\pi2}$ acceptance of cuts applied in the $K_{\pi2}$ branching fraction analysis. NIDIF is on.

Cut & discrepancy	$N_{K_{\pi 21}}$ 2002	$N_{K_{\pi 21}}$ 2007	$N_{K_{\pi 21}} \times PS \times 10^{-10}$
ALL 0.000%	84844(0.000)	1938973(0.000)	25.4999(0.000)
BAD_RUN 1.254%	84803(0.99952)	1913712(0.98697)	25.3029(0.99227)
TRIGGER 54.108%	84803(1.00000)	878246(0.45892)	11.6109(0.45888)
BAD_STR 0.009%	84388(0.99511)	873864(0.99501)	11.5521(0.99494)
RD_TRK 0.000%	84388(1.00000)	873864(1.00000)	11.5521(1.00000)
TRKTIM 0.000%	84388(1.00000)	873864(1.00000)	11.5521(1.00000)
RDUTM 0.000%	84388(1.00000)	873864(1.00000)	11.5521(1.00000)
UTCQUAL -7.029%	67194(0.79625)	757238(0.86654)	10.0093(0.86645)
TARGET+TGQUALT 5.639%	65495(0.97471)	695393(0.91833)	9.19259(0.91841)
COS3D 3.695%	64425(0.98366)	658341(0.94672)	8.70245(0.94668)
B4DEDX 0.538%	62832(0.97527)	638520(0.96989)	8.43952(0.96979)
CPITRS 0.407%	61933(0.98569)	626788(0.98163)	8.28465(0.98165)
CPITAIL 0.007%	61882(0.99918)	626228(0.99911)	8.27728(0.99911)
ICBIT 0.001%	61857(0.99960)	625970(0.99959)	8.27389(0.99959)
TIC -0.429%	61352(0.99184)	623545(0.99613)	8.24150(0.99608)
TIMCON 0.193%	60882(0.99234)	617564(0.99041)	8.16218(0.99038)
TGTCON 0.332%	60212(0.98899)	608715(0.98567)	8.04531(0.98568)
DCBIT -0.542%	51016(0.84727)	519045(0.85269)	6.86302(0.85305)
DELC -0.236%	44193(0.86626)	450851(0.86862)	5.96163(0.86866)
CKTRS 0.082%	42835(0.96927)	436628(0.96845)	5.77414(0.96855)
CKTAIL -0.042%	41570(0.97047)	423918(0.97089)	5.60547(0.97079)
BWTRS 0.088%	39270(0.94467)	400092(0.94380)	5.28988(0.94370)
RVUPV -0.090%	38354(0.97667)	391120(0.97757)	5.17075(0.97748)
TARGF 0.324%	36430(0.94984)	370232(0.94659)	4.89491(0.94665)
DTGTTP -0.018%	36422(0.99978)	370219(0.99996)	4.89474(0.99996)
RTDIF -0.031%	36039(0.98948)	366439(0.98979)	4.84457(0.98975)
TGQUALT 0.000%	36039(1.00000)	366439(1.00000)	4.84457(1.00000)
PIGAP 0.175%	35657(0.98940)	361912(0.98765)	4.78419(0.98754)
TGB4 1.362%	33611(0.94262)	336217(0.92900)	4.44510(0.92912)
KIC -0.084%	33118(0.98533)	331568(0.98617)	4.38364(0.98617)
TGGEO 0.528%	27505(0.83052)	273622(0.82524)	3.61775(0.82528)
B4EKZ 4.915%	26657(0.96917)	251738(0.92002)	3.32839(0.92002)
B4ETCON -0.064%	26523(0.99497)	250633(0.99561)	3.31343(0.99550)
TGZFOOL 1.266%	26523(1.00000)	247461(0.98734)	3.27153(0.98735)
PV_noBV 0.000%	26523(1.00000)	247461(1.00000)	3.27153(1.00000)
IPIFLG 0.181%	18688(0.70460)	173913(0.70279)	2.29944(0.70286)
KPI2BOXM 4.515%	16469(0.88126)	145410(0.83611)	1.92215(0.83592)
KP2STOP -0.099%	16405(0.99611)	144989(0.99711)	1.91660(0.99711)
RTOT40 0.000%	16405(1.00000)	144989(1.00000)	1.91660(1.00000)
$N_{K_{\pi 2}}$ 2.836%	16405(0.193)	144989(0.165)	1.91660(0.165)

Table 70: The number of selected $K_{\pi 2}$ candidate events with a comparison to the 2002 PNN1 results.

Cut Acc2002-Acc2007%	$N_{K_{\pi 21}}$ (Acc) 2002	$N_{K_{\pi 21}}$ (Acc) 2007
$\boldsymbol{SETUP_{RD}}$	51416	490579
RD_TRK 0.000%	51416(1.00000)	490579(1.00000)
TRKTIM 0.000%	51416(1.00000)	490579(1.00000)
A_RD,Br 0.000%	1.00000 ± 0.00000	1.00000 ± 0.00000
$\boldsymbol{SETUP_{RECON}}$	32980	449621
RDUTM 0.000%	32980(1.00000)	449621(1.00000)
UTCQUAL -5.355%	28117(0.85255)	407402(0.90610)
TARGET+TGQUALT 4.116%	27831(0.98983)	386491(0.94867)
A_RECO,Br -1.572%	0.84388 ± 0.00200	0.85959 ± 0.00052
$\boldsymbol{SETUP_{REST}}$	32055	336407
TIC 0.070%	32055(1.00000)	336173(0.99930)
TIMCON 0.124%	31970(0.99735)	334866(0.99611)
TGTCON 0.757%	31847(0.99615)	331041(0.98858)
DCBIT 10.327%	31542(0.99042)	293685(0.88716)
DELC 0.883%	27898(0.88447)	257163(0.87564)
CKTRS -9.986%	24368(0.87347)	250305(0.97333)
CKTAIL 0.125%	23710(0.97300)	243233(0.97175)
B4DEDX -1.279%	23032(0.97140)	239389(0.98420)
CPITRS -0.636%	22657(0.98372)	237015(0.99008)
CPITAIL -0.872%	22442(0.99051)	236833(0.99923)
TARGF 4.115%	22431(0.99951)	226972(0.95836)
DTGTTP -4.295%	21467(0.95702)	226965(0.99997)
RTDIF 0.935%	21462(0.99977)	224789(0.99041)
TGQUALT -0.862%	21277(0.99138)	224789(1.00000)
PIGAP 1.024%	21277(1.00000)	222488(0.98976)
TGB4 5.875%	21098(0.99159)	207545(0.93284)
KIC -3.865%	20002(0.94805)	204785(0.98670)
TGGEO 16.326%	19855(0.99265)	169847(0.82939)
B4EKZ -10.248%	16358(0.82387)	157338(0.92635)
B4ETCON -2.463%	15886(0.97115)	156673(0.99577)
TGZFOOL 0.754%	15806(0.99496)	154703(0.98743)
BWTRS 4.324%	15806(1.00000)	148013(0.95676)
RVUPV -2.685%	14817(0.93743)	145339(0.98193)
A_REST,Br 3.891%	0.46224 ± 0.00278	0.43203 ± 0.00085
A_IPIFLG 1.100%	0.8350 ± 0.0054	0.8350 ± 0.0054
loss due to $\overline{19_{ct}}$ A_{μ}^{acc} 0.000%	0.9931 ± 0.0002	0.9931 ± 0.0002
$A_{K_{\pi 2},Br}$ 4.140%	0.3235 ± 0.0030	0.3080 ± 0.0021

Table 71: $K_{\pi 2}$-based acceptances of cuts applied in the $K_{\pi 2}$ BR analysis. A_IPIFLG and A_{μ}^{acc} are taken from the 2002 PNN1 analysis [5]. The SETUP cuts are defined in Table 75.

Name of value	All runs	Prescale 163840	Prescale 131072
$K_{\pi 2}$ Events	144989	2973	141926
$< Prescale >$	131926	163840	131072
$KB_{LIVE} \times 10^{-12}$	1.79229	0.052475671	1.737988
$A_{K_{\pi 2},Br}$	0.3080 ± 0.0021	0.3136 ± 0.0049	0.3078 ± 0.0021
Br($K_{\pi 2}$)	0.2213 ± 0.0022	0.1905 ± 0.0051	0.2216 ± 0.0016

Table 72: $K_{\pi 2}$ branching fraction results for all runs and broken down by prescale factor.

19.5 The measured $K_{\pi 2}$ branching fraction

The value of $K_{\pi 2}$ branching fraction has been calculated using Equation 35,

$$BR(K_{\pi 2}) = \frac{191660 \times 10^5}{0.9383 \cdot 1.792 \times 10^{12} \cdot 0.3080 \cdot 0.78775 \cdot 0.774 \cdot 0.27428} \tag{38}$$

$$= 0.2213 \pm 0.0022 \tag{39}$$

and is within 6% of the PDG2007 [29] value 0.2092 ± 0.0012. The values of $f_s = 0.7740 \pm 0.0011$ (Eqn.21 of Ref. [5]) and of $\epsilon_{T \cdot 2 \cdot IC} = 0.9383 \pm 0.0027$ (derived from Table 17 of Ref. [5]) have been taken from the 2002 PNN1 analysis. Investigation of run-, prescale-factor- and rate-dependence of this modest discrepancy with the nominal branching fraction has been done.

The run dependence of $K_{\pi 2}$ branching fraction is shown in Fig.47 along with the run dependence of f_S determined from the $K_{\mu 2}$ monitor data for comparison [6]. Some indication of a modest run-dependence of the branching fraction and f_S is observed.

The calculation of $K_{\pi 2}$ branching fraction for runs with different prescale factors has been done using $A_{K_{\pi 2},Br}$ calculated for the runs with the given prescale factor. The results are shown on Table 72. There is a significant difference in the branching fraction determined for the two sets of prescale factors.

The rate-dependence is shown in Fig. 48 and Table 73. Rate is measured in millions of kaons per second. There is a clear-rate dependence in the branching fraction measurement.

Figure 49 plots the results from Table 73. The rate-dependence of the entire data sample is clear. The rate-dependence of the subset of data with prescaler 163840 is not consistent with the rate-dependence of the entire sample.

Table 74 shows the $K_{\pi 2}$ candidate event selection broken down by the two prescale factors. There are no glaring difference in event selection. Figure 50 shows the branching fraction versus run for the two prescale factors.

There is a clear rate dependence of the measured $K_{\pi 2}$ branching fraction. The range of variation in the measured branching fraction of $\sim$4.4% as a function of rate quantified in Table 73 does not account for the $\sim$5.8% overestimate of the average branching fraction in Eqn. 39. In addition there are some inconsistencies in the measured branching fraction for the two different prescale factors used in this analysis as well as indications of run-dependence. All these concerns lead us to assign a systematic uncertainty of $\pm$10% in the PNN2 acceptance.

[6]Thanks to Shaomin Chen for providing the f_S data from the 2002 PNN1 analysis.

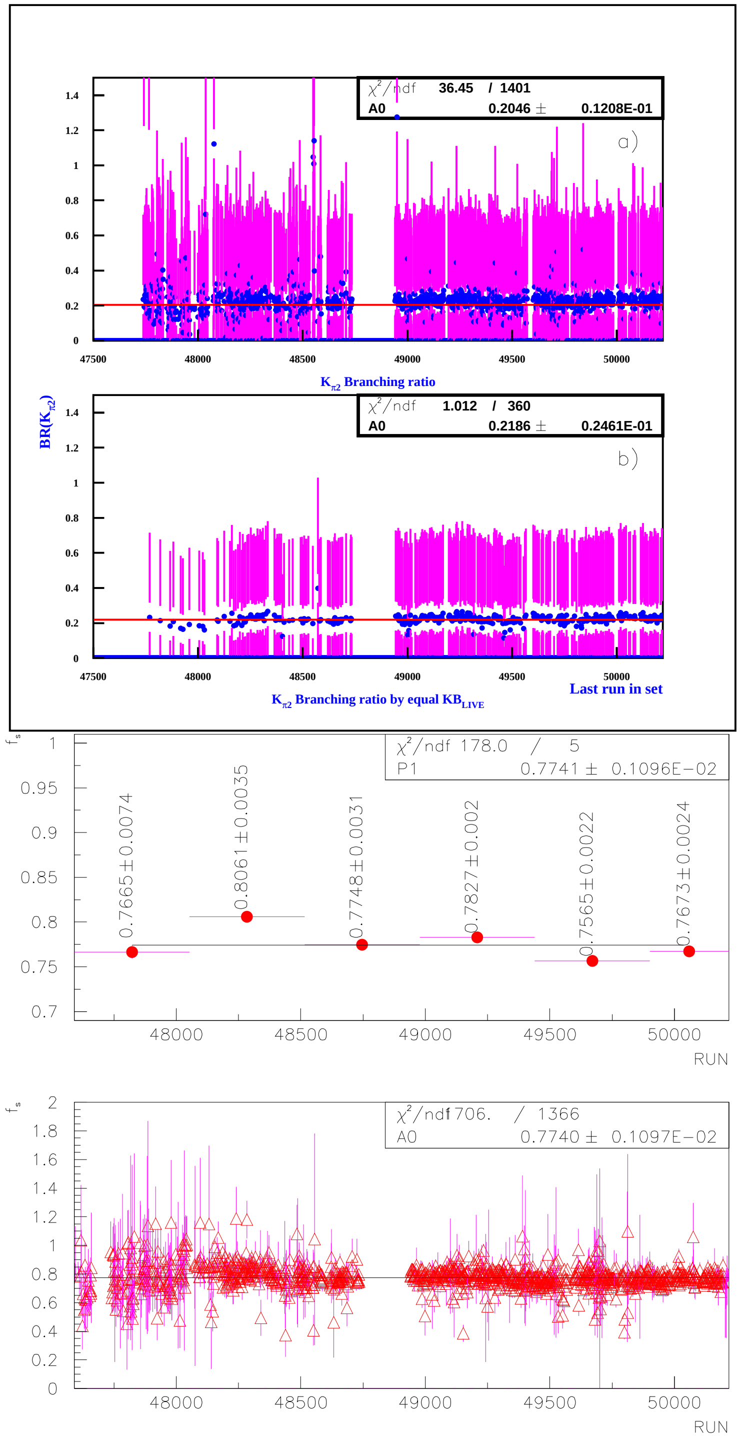

Figure 47: Top: The $K_{\pi2}$ branching fraction a) versus run number and b) versus last run in a block of runs defined by $\sum_{i=1}^{N_{\text{Spill}}} \frac{KBLIVE_i}{Prescale_i} \geq 3000$. Bottom: The f_S value versus run. The first point at upper plot corresponding to runs of $K_{\pi2}(1)$ monitor data with a prescale factor of 163840.

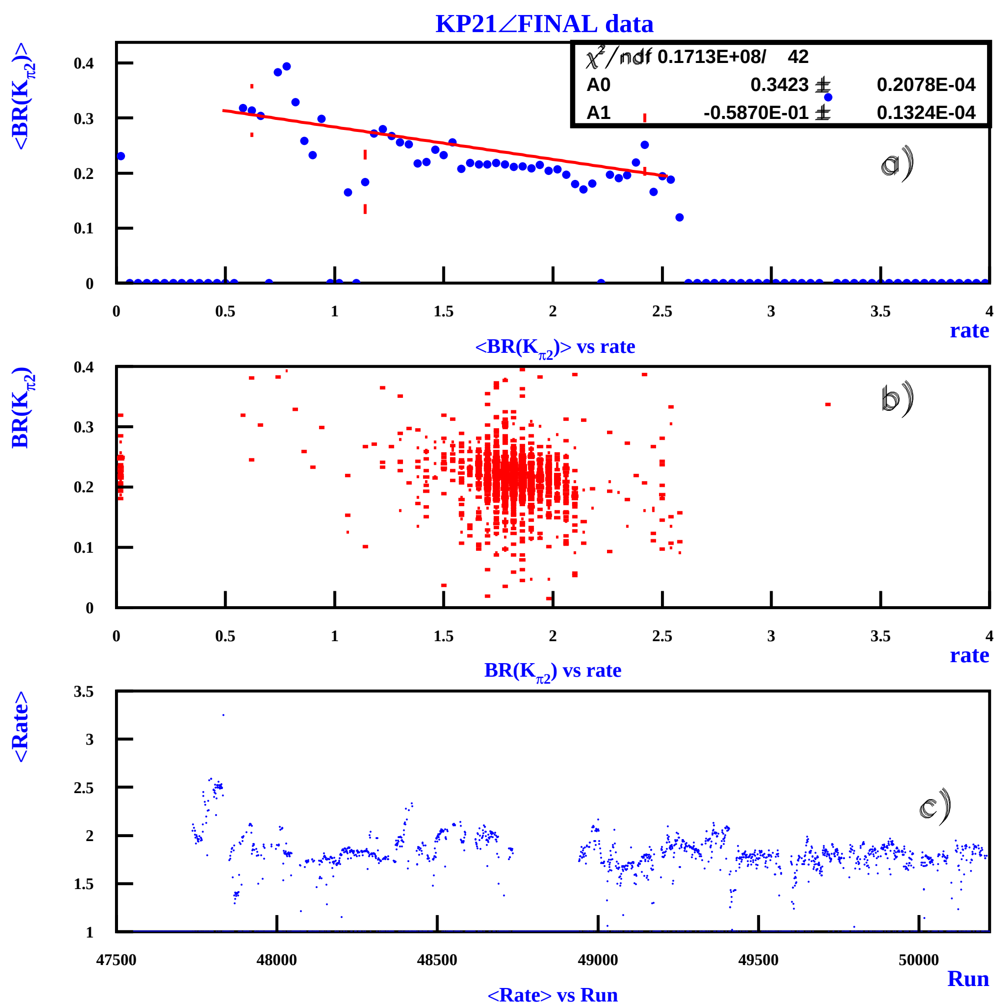

Figure 48: The $K_{\pi 2}$ branching fraction a) versus average rate and b) versus rate (scatter plot). c) shows the average rate versus run. Rate is measured in $K_{B,live}/T_{eff}$ (10^6/s).

All prescale factors	Rate $K_{B,live}/T_{eff}$ (10^6/s)				
Quantity	All	0.00-1.70	1.70-1.85	1.85-2.00	> 2.0
$K_{\pi 2}$ BR	0.2212	0.2284	0.2208	0.2194	0.2187
	$\pm$ 0.0022	$\pm$ 0.0025	$\pm$ 0.0023	$\pm$ 0.0023	$\pm$ 0.0024
$A_{K_{\pi 2},BR}$	0.3081	0.3248	0.3088	0.3034	0.2989
	$\pm$ 0.0021	$\pm$ 0.0026	$\pm$ 0.0023	$\pm$ 0.0023	$\pm$ 0.0025
$A_{RECO,BR}$	0.8597	0.8709	0.8608	0.8564	0.8524
	$\pm$ 0.0005	$\pm$ 0.0012	$\pm$ 0.0009	$\pm$ 0.0009	$\pm$ 0.0014
$A_{REST,BR}$	0.4321	0.4497	0.4326	0.4273	0.4228
	$\pm$ 0.0009	$\pm$ 0.0021	$\pm$ 0.0014	$\pm$ 0.0015	$\pm$ 0.0022
$KB_{LIVE} \times 10^{-12}$	1.792	0.280	0.639	0.594	0.279
Selected events	144989.	24716.	52010.	47141.	21116.
Selected events $\times PS \times 10^{-5}$	191660.	32602.	68366.	62050.	28635.
Trigger	878246.	138934.	312610.	290840.	135834.
Trigger $\times PS \times 10^{-5}$	1161090.	183250.	410936.	383023.	183845.
Events/Trigger	0.1651	0.1779	0.1664	0.1621	0.1555
Events$\times$ PS/Trigger$\times$ PS	0.1651	0.1779	0.1664	0.1620	0.1558
PS factor=163840	Rate $K_{B,live}/T_{eff}$ (10^6/s)				
Quantity	All	0.00-1.70	1.70-1.85	1.85-2.00	> 2.0
$K_{\pi 2}$ BR	0.1905	0.2115	0.1765	0.1812	0.2003
	$\pm$ 0.0051	$\pm$ 0.0077	$\pm$ 0.0065	$\pm$ 0.0058	$\pm$ 0.0068
$A_{K_{\pi 2},BR}$	0.3136	0.3462	0.3140	0.3126	0.2915
	$\pm$ 0.0049	$\pm$ 0.0105	$\pm$ 0.0099	$\pm$ 0.0082	$\pm$ 0.0084
$A_{RECO,BR}$	0.8538	0.8733	0.8484	0.8590	0.8375
	$\pm$ 0.0037	$\pm$ 0.0076	$\pm$ 0.0081	$\pm$ 0.0064	$\pm$ 0.0073
$A_{REST,BR}$	0.4429	0.4780	0.4464	0.4389	0.4198
	$\pm$ 0.0060	$\pm$ 0.0135	$\pm$ 0.0131	$\pm$ 0.0107	$\pm$ 0.0113
$KB_{LIVE} \times 10^{-12}$	0.052	0.009	0.012	0.017	0.014
Selected events	2973.	635.	621.	926.	791.
Selected events $\times PS \times 10^{-5}$	4871.	1040.	1017.	1517.	1296.
Trigger	18535.	3547.	3793.	5749.	5445.
Trigger $\times PS \times 10^{-5}$	30368.	5811.	6214.	9419.	8921.
Events/Trigger	0.1604	0.1790	0.1637	0.1611	0.1453
Events$\times$ PS/Trigger$\times$ PS	0.1604	0.1790	0.1637	0.1611	0.1453

Table 73: Measured rate-dependence of the $K_{\pi 2}$ branching fraction and factors entering in the branching fraction calculation for all data (top) and runs with the prescale factor 163840.

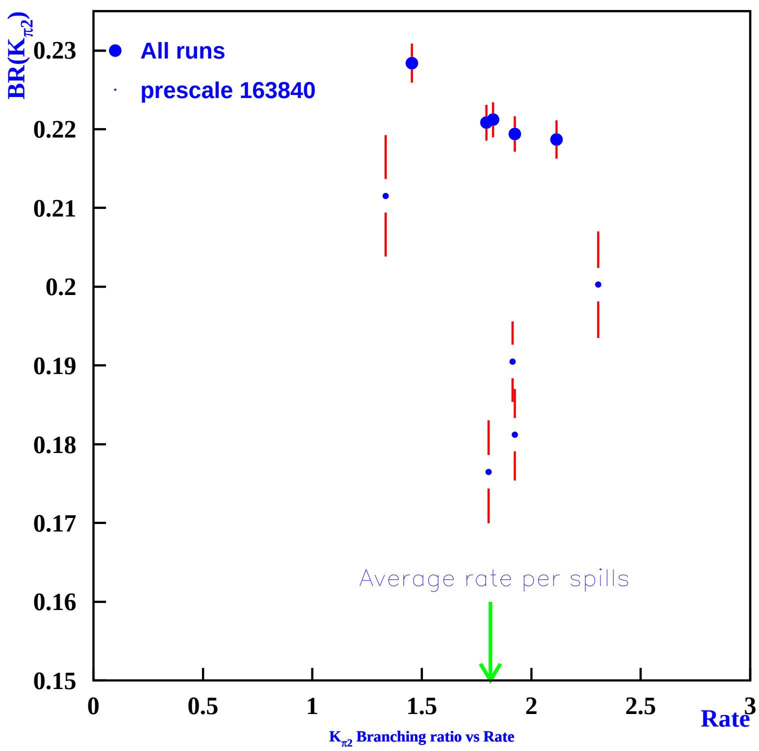

Figure 49: The $K_{\pi2}$ branching fraction versus rate for all runs (large points) and for runs with prescaler 163840 (small points). The arrow shows the average rate.

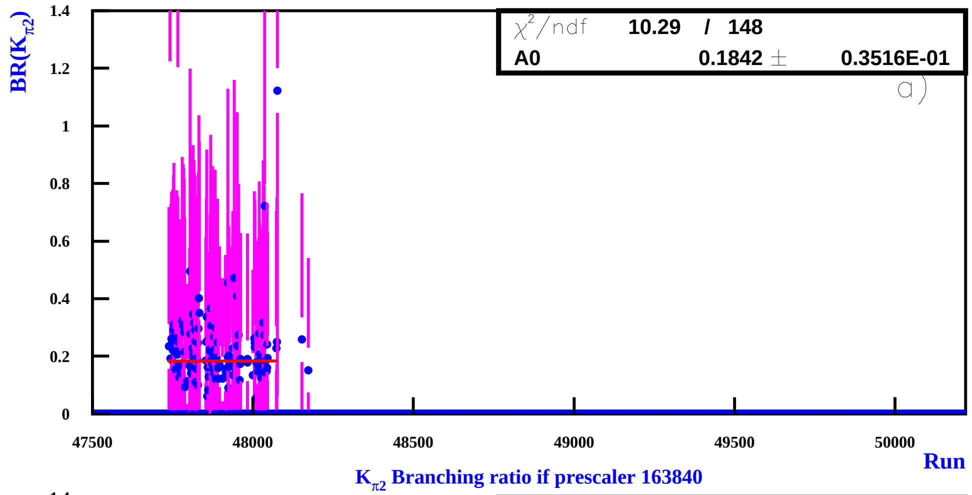

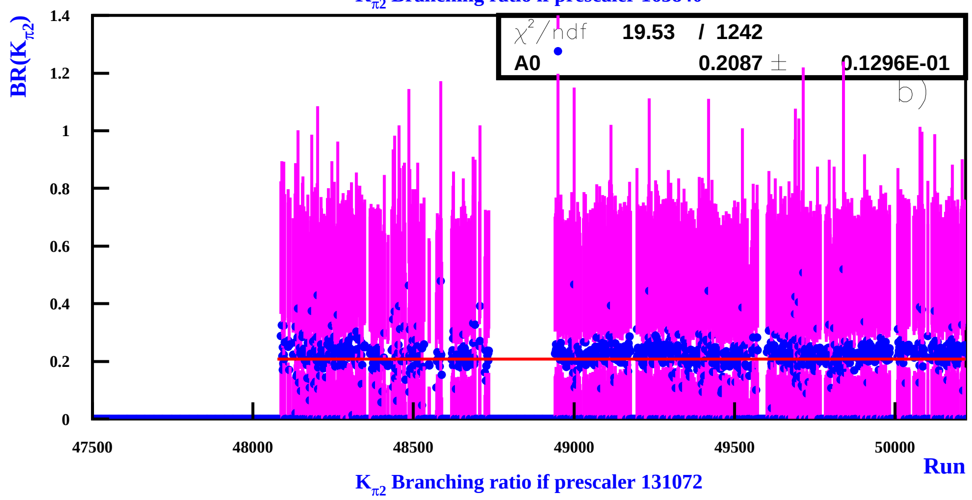

Figure 50: The $K_{\pi 2}$ branching fraction versus run number a) for runs with prescaler 163840 and b) for runs with prescaler 131072

19.6 UMC cut definitions

The following cuts have been used in the calculation of Monte Carlo kinematic and trigger acceptances for $K_{\pi 2}$ branching fraction measurement.

- **T•A** $\equiv$ **T•2**
- **Reach layer B** = `layv4` ≥ 6.
- $\overline{19_{ct}}$ μ-veto (described on p.207 of Ref. [4]).
- **UFATE**[7] requires that the pion stopped without decaying or interacting.

[7]UFATE, USTMED and USTOP_HEX are cuts based on UMC truth variables.

- **USTMED** requires that the pion stopped in the RS scintillator.
- **USTOP_HEX** The offline reconstructed and true stopping counters agree.
- **UTC/RANGE** The track reconstructed in UTC matches the track reconstructed in the Range Stack and Target [30]. For the PNN2 analysis, the **RDUTM** cut is used.
- **UTCQUAL** The UTCQUAL cut is described in Sec. 5.
- **TARGET** is SWATH CCD reconstruction cut. TARGET $\equiv$ ITGQUAL ≥ 2 in PNN1 and ITGQUAL ≥ 9 in PNN2.
- **KP2STOP** requires the stopping layer to be between layers 8 and 15 inclusive.
- **COS3D** Cut any event with a dip angle outside the effective detection region $|cos3d| < 0.5$.
- **KP2BOX** is a fixed cut corresponding to $\sim 3\sigma$ cuts in range, energy and momentum.

$$(199. < \mathrm{PTOT} < 215.) \cdot (28. < \mathrm{RTOT} < 35.) \cdot (100.5 < \mathrm{ETOT} < 115.) \qquad (40)$$

Cut & discrepancy	$N_{K_{\pi 21}}$	
	163840	131072
TRIGGER+Prescaler	18535	859195
BAD_STR -1.839%	18109(0.97702)	855246(0.99540)
RD_TRK 0.000%	18109(1.00000)	855246(1.00000)
TRKTIM 0.000%	18109(1.00000)	855246(1.00000)
RDUTM 0.000%	18109(1.00000)	855246(1.00000)
UTCQUAL -0.729%	15563(0.85941)	741238(0.86670)
TARGET+TGQUALT 0.643%	14390(0.92463)	680603(0.91820)
COS3D -0.804%	13510(0.93885)	644454(0.94689)
B4DEDX 0.247%	13136(0.97232)	625022(0.96985)
CPITRS 0.562%	12967(0.98713)	613466(0.98151)
CPITAIL 0.028%	12959(0.99938)	612914(0.99910)
ICBIT 0.011%	12955(0.99969)	612660(0.99959)
TIC -0.117%	12890(0.99498)	610302(0.99615)
TIMCON 0.068%	12775(0.99108)	604443(0.99040)
TGTCON 0.184%	12615(0.98748)	595759(0.98563)
DCBIT 3.939%	11243(0.89124)	507499(0.85185)
DELC -3.480%	9383(0.83456)	441201(0.86936)
CKTRS 0.076%	9094(0.96920)	427275(0.96844)
CKTAIL -0.284%	8804(0.96811)	414865(0.97096)
BWTRS -0.026%	8307(0.94355)	391554(0.94381)
RVUPV -0.624%	8070(0.97147)	382826(0.97771)
TARGF 0.431%	7673(0.95081)	362341(0.94649)
DTGTTP 0.004%	7673(1.00000)	362328(0.99996)
RTDIF 0.004%	7595(0.98983)	358630(0.98979)
TGQUALT 0.000%	7595(1.00000)	358630(1.00000)
PIGAP 0.239%	7519(0.98999)	354183(0.98760)
TGB4 1.425%	7090(0.94295)	328929(0.92870)
KIC -0.042%	6989(0.98576)	324383(0.98618)
TGGEO 0.635%	5811(0.83145)	267649(0.82510)
B4EKZ 0.488%	5374(0.92480)	246216(0.91992)
B4ETCON -0.027%	5349(0.99535)	245138(0.99562)
TGZFOOL -0.751%	5242(0.98000)	242075(0.98750)
PV_noBV 0.000%	5242(1.00000)	242075(1.00000)
IPIFLG -0.642%	3651(0.69649)	170158(0.70291)
KP2BOX -1.890%	2985(0.81758)	142334(0.83648)
KP2STOP -0.115%	2973(0.99598)	141926(0.99713)
RTOT40 0.000%	2973(1.00000)	141926(1.00000)
$N_{K_{\pi 2}}$ -0.479%	2973	141926

Table 74: $K_{\pi 2}$ candidate selection for runs with prescale 131072 and 163840.

$K_{\pi 2}$ SETUP	component cuts
$SETUP_{RD}$	TRIGGER, ICBIT, $t_{IC} - t_{Ck} > 5$ ns [8], B4DEDX, UTC, TARGET
$SETUP_{recon}$	TRIGGER, ICBIT, $t_{IC} - t_{Ck} > 5$ ns, B4DEDX, CPITRS, CPITAIL, CKTRS, CKTAIL, BWTRS, RVUPV, A_{RD} cuts,
$SETUP_{rest}$	TRIGGER, ICBIT, A_{RD} cuts,A_{recon} cuts, KP2BOX, KP2STOP, IPIFLG, COS3D.

Table 75: Setup cuts used for the $K_{\pi 2}$ acceptance measurements and event selection.

References

[1] M. Diwan, et. al. "PNN2 1/3 Analysis", "PNN2 2/3 Analysis", E787 Technical Notes **tn385**, **tn386**, 2001.

[2] Bipul Bhuyan, Ph. D thesis (2003).

[3] T. Junk, Nucl. Instrum. Meth. A **434**, 435 (1999).

[4] S. Chen *et al.*, "2002 pnn1 Data Analysis", E949, note K-034 (2003).

[5] S. Chen *et al.*, "Further 2002 pnn1 Data Analysis", E949, note K-038 (2004).

[6] K.Mizouchi, "Experimental Search for the Decay $\pi^0 \to \nu\bar{\nu}$", Ph.D. Thesis, January 2006.

[7] B.Bassalleck *et al.*, "Beam Instrumentation III What Was Built", E949 Technical Note K-021, 1 August 2001.

[8] I. Christidi, "Search for the rare decay $K^+ \to \pi^+\nu\bar{\nu}$ with $p_{\pi^+} < 199$ MeV/c", Ph.D. thesis, 2006

[9] Victorov, "Downstream Photon Veto Counter", E949 Technical Note K-015, 29 November 2000.

[10] Ilektra A. Christidi, "The Downstream Photon Veto", E949 Technical Note K-067, 1 February 2007.

[11] Zhe Wang, "P, E, R resolution in E949 pnn2 analysis", E949, note K-055 (2006).

[12] Tetsuro Sekiguchi, Ph. D thesis (2004).

[13] Benji Lewis, "A new Target Reconstruction and Target Scatter Algorithm", E949 Technical note k063, 17 November 2006.

[14] Vivek Jain, "Simulation of elastic scatters of pi+ in the target from Kp2 decays" E787 Technical note 375, 3 November 1999.

[15] W. M. Yao *et al.* [Particle Data Group], J. Phys. G **33**, 1 (2006).

[16] Correspondence with Kentarou.

[17] B. Lewis, "PNN2 1/3 Beam Background", E949 Technical Note **K-061**, 2006. Unpublished.

[18] C. Witzig, "pi- Absorption in the Range Stack", E787, note 278 (1994).

[19] http://thomasj.web.cern.ch/thomasj/searchlimits/ecl.html.

[20] http://www.hep.uiuc.edu/home/trj/cdfstats/mclimit_csm1/.

[21] R.M. Barnett *et al.* [Particle Data Group], Phys. Rev. D54 (1996) and earlier editions.

[22] B. Lewis, "Addition to Bad Runs List", E949 Technical Note **K-060**, 2006. Unpublished.

[23] V.V Anisimovsky *et al.* PRL 93, 031801 (2004).

[24] S. Adler *et al.* PRL 79, 2204 (1997).

[25] S. Adler *et al.* PRL 84, 3768 (2000).

[26] S. Adler *et al.* PRL 88, 041803 (2002).

[27] S. Adler *et al.* PLB 537, 211 (2002).

[28] S. Adler *et al.* PR D70, 037102 (2004).

[29] The 2007 off-year update of [15].

[30] Bipul Bhuyan, "Analysis of 1997 data in the pnn2 region", E787 Technical note 391 (2003).